Title
Construction and Preliminary HVS Tests of Pre-Cast Concrete Pavement Slabs

Authors
Kohler, Erwin R.
du Plessis, Louw
Theyse, Hechter

Publication Date
2008-06-01

Peer reviewed

January 2007

Research Report: UCPRC-RR-2006-10

Construction and Preliminary HVS Tests of Pre-Cast Concrete Pavement Slabs

Authors:
E. Kohler, L. du Plessis, and H. Theyse

Work Conducted as part of Partnered Pavement Research Center Strategic Plan Element No. 4.17: HVS testing of pre-cast PCC panels in District 8

PREPARED FOR:

California Department of Transportation
(Caltrans)
Division of Research and Innovation

PREPARED BY:

University of California
Pavement Research Center
UC Davis and Berkeley

DOCUMENT RETRIEVAL PAGE		RR No: UCPRC-RR-2006-10
Title: Construction and Preliminary HVS Tests of Pre-cast Concrete Pavement Slabs		
Authors: Erwin Kohler, Louw du Plessis, and Hechter Theyse		
Prepared for: Caltrans Division of Research and Innovation and Caltrans District 8	**FHWA No:** CA081087B	**Date**: January 2007
Strategic Plan Element No.: 4.17	**Status:** Final, approved	**Version** Stage 6

Abstract:

This report presents the details on the construction and preliminary load tests on an experimental pavement comprised of ten pre-cast slabs of the pavement known as the Super-Slab® System, installed at the intersection of I-15 and SR210, in San Bernardino County in southern California. The construction of the test section consisted of: (a) Construction of a cement-treated base (CTB), (b) Preparation of a sand bedding layer, (c) Placement of the pre-cast slabs, (d) Application of grout materials for the bedding and for the dowel/tie bars, (e) Diamond grinding the test pads, (f) Filling the joints, and (g) Construction of an asphalt concrete shoulder.

Subgrade evaluation was carried out with a dynamic cone penetrometer (DCP) and indicated a strong granular subgrade, with CBR (California Bearing Ratio) between 45 and 80. Average backcalculated elastic modulus for the CTB was about 2,200 MPa (tested on the pre-cast panels) and presented great variation. Subgrade modulus was 70 MPa (tested on CTB, consistent with results of testing on pre-cast panels). FWD testing showed deflections of 0.3 to 0.6 mm on the slabs, which after grouting were reduced to approximately 0.2 mm. The backcalculated elastic modulus of the concrete was found to be between 19,000 and 23,500 MPa (after grouting, averaging morning, and afternoon FWD data). Load Transfer Efficiency (LTE) values in the range of 5% to 40% were observed before grouting, and consistently near 100% after grouting, revealing that the grouting process mobilized the dowel bars so that they provided effective LTE. The materials used for the dowel grout and for the bedding grout showed flexural strengths at 28-days of 5.1 and 1.7 MPa, respectively.

The slabs were instrumented with displacement sensors (vertical and horizontal) and with thermocouples. Thermal deformations were collected, and revealed that the slab curl reduced from a range of ±1.5 mm before grouting to ±0.5 mm after grouting. The responses to traffic load also improved greatly after grouting. The wheel-induced deflections at the transverse joint decreased to one-quarter of the initial value at the standard load of 60kN (from about 1.0 mm to 0.25 mm). Rocking of the slabs, present before grouting, was also eliminated by grouting.

Two HVS tests were performed on the ungrouted slabs and indicated that the Super-Slab® System is able to withstand at least 86,500 ESALS in the ungrouted condition. This test was intended to simulate placement of the slabs without grouting during one nighttime closure, and then grouting the slabs during the next nighttime closure 24 hours later.

Keywords: Pre-cast concrete slabs, Super-Slab, Heavy Vehicle Simulator, HVS, Experimental pavement section, Thermal Curling, Pavement Responses, Accelerated Pavement Testing, Instrumented Slabs

Proposals for implementation:

Overnight opening to traffic in the ungrouted condition is acceptable for the Super-Slab system

Related documents:

UCPRC-TP-2005-01: HVS Test Plan (Strategic Plan Element 4.17), March 2005.
UCPRC-TM-2007-04: Interim Assessment of Expected Structural Life of Pre-Cast Concrete Pavement Slabs with HVS Testing

Signatures:

E. Kohler **1st Author**	J. Harvey **Technical Review**	D. Spinner **Editor**	J. Harvey **Principal Investigator**	M. Samadian **Caltrans Contract Manager**

DISCLAIMER

The contents of this report reflect the views of the authors who are responsible for the facts and accuracy of the data presented herein. The contents do not necessarily reflect the official views or policies of the State of California or the Federal Highway Administration. This report does not constitute a standard, specification, or regulation.

PROJECT OBJECTIVES

This project is responsive to the topics identified by Caltrans District 8 in its request to the Caltrans Pavement Standards Team (PST) for evaluation of the Super-Slab® System:

- The short-term objective is to determine failure mechanisms of the Super-Slab® panels and to answer a constructability issue regarding opening to traffic in the ungrouted condition.
- The long-term objective is to provide information to Caltrans to help determine how the performance of pre-cast panels compares to current Long-Life Pavement Rehabilitation Strategy (LLPRS) designs for jointed plain concrete pavements.

The project involves the evaluation of longitudinal and transverse joint behavior; measurement of load transfer efficiency; observations of possible joint deterioration; measurement of faulting, cracking, and settlement that may result from slab and cement-treated base (CTB) deterioration; estimation of expected service life of Super-Slab® pavement based on HVS test results; and comparison of Super-Slab® performance (expected service life) to HVS tests conducted at cast-in place jointed plain concrete slabs (SR14 at Palmdale).

EXECUTIVE SUMMARY

The California Department of Transportation (Caltrans) evaluated the use of the Super-Slab® System as a long-life rehabilitation strategy for concrete pavements using Heavy Vehicle Simulator (HVS) tests on a specially constructed experimental pavement in San Bernardino County. The Pavement Standards Team (PST) technical lead for this project was the METS Office of Rigid Pavements. The project originated in response to a request from Caltrans' District 8.

This report describes the construction process of the test sections (isolated arrangement of 5 by 2 slabs at the intersection of highways I-15 and SR210) and presents the detailed results of the preliminary short-duration performance tests.

Field Work Schedule

The overall schedule of the pavement construction and evaluation was:

- May 11, 2005 to June 8, 2005: Construction of test pavement, materials characterization, HVS thermal curl tests, HVS ungrouted load tests. (Documented in this report.)
- June 11, 2005 to September 20, 2005: HVS load test, dry condition, Section 597FD, (first of two sections).
- September 21, 2005 to February 24, 2006: HVS load test, dry condition, 598FD.
- February 24, 2006 to May 2, 2006: HVS load test, wet condition, 598FD.
- May 2, 2006 to August 30, 2006: HVS load test, wet condition, 597FD.

Construction

The construction of the Super-Slab® System consists of three main activities: the construction of the sand bedding layer, the precise placement of the pre-cast slabs, and the grouting of the slabs. The main steps followed in the construction of the actual experimental section are:

- *Construction of a cement-treated base (CTB)*, The Super-Slab® System will usually be placed on an existing CTB that may be in a fairly advanced state of damage. In the case of the HVS test sections, however, the pavement support was especially constructed.
- *Preparation of a sand bedding layer*. The function of the sand bedding layer is to provide an even support to the pre-cast slabs, thereby eliminating as far as possible the formation of voids between the pre-cast slabs and the support.

- *Placement of the pre-cast slabs*. The pre-cast slabs are placed strictly according to a predetermined grid. Although great care was exercised in preparing the bedding layer, the edges of adjacent slabs did not align perfectly, resulting in surface irregularities at the joints and corners.
- *Application of grout materials for the bedding and for the dowel/tie bars*. The grouting system consisted of a mechanical mixer with a piston pump and hoses with a customized fitting to inject the grout through holes in the slabs. The grouting of the dowel and tie-bars was done before the grouting of the bedding sand. A high-strength grout was used for the dowel and tie-bars. The grout for the bedding material was of a lower strength and was of a more liquid nature to ensure proper filling of any possible void between the slab and the support.
- *Diamond grinding the test pads*. Grinding of the surface to a level plane on the area of the test sections to be wheel trafficked (not the entire set of slabs, but just the loaded areas).
- *Filling the joints*. A backer rod was inserted into the joints, and a silicone seal was applied.
- *Asphalt concrete shoulder*. A temporary aggregate shoulder was replaced with an asphalt concrete shoulder.

Material Characterization

Subgrade strength evaluation was carried out with a Dynamic Cone Penetrometer (DCP), and the results indicated a fairly stiff granular subgrade, with a California Bearing Ratio (CBR) between 45 and 80. Testing with a Falling Weight Deflectometer (FWD) indicated deflections on the CTB of approximately 0.8mm under 40kN loads. Backcalculated elastic moduli from the deflection basins resulted on 200 to 600 MPa for the CTB while it was less than 14 days old and 50 to 100 MPa for the subgrade. FWD testing on the centers of the concrete slabs revealed maximum deflections of 0.3 to 0.6 mm, which after grouting were reduced to approximately 0.2 mm. The elastic modulus of the concrete was found to be between 19,000 and 23,500 MPa (after grouting, averaging morning and afternoon FWD data). The materials used for the dowel grout and for the bedding grout were tested on beams to determine their flexural strengths (modulus of rupture). At 28 days the results were 5.1 and 1.7 MPa, for the dowel and bedding grout, respectively (dowel grout being three times stronger than bedding grout).

Results of Preliminary Tests

The slabs were instrumented with displacement sensors and with thermocouples. Before any load was applied to the pavement, deformations of the slab caused by temperature changes were measured in the ungrouted and then in the grouted condition. This revealed that the slab's curl

at the corners was reduced from a range of ± 1.5 mm to a range of ± 0.5 mm by grouting the joints and under the slabs. Load Transfer Efficiency (LTE) values in the range of 5 to 40 percent were observed at the ungrouted transverse joints, with and average of about 16 percent. LTE was consistently close to 100 percent after grouting, revealing that the grouting process was effective in mobilizing the dowels to provide excellent LTE at the joints. LTE was measured with the FWD and with the sensors installed as part of the accelerated load testing with the HVS.

The responses to traffic load improved greatly after grouting. The deflections at the transverse joint were reduced by the grouting to one-quarter of the ungrouted value (from about 1.0 mm to 0.25 mm), meaning that the flexural stresses were also reduced. Rocking of the slab that occurred under the HVS wheel loading before grouting was eliminated.

Two HVS tests were performed on the ungrouted slabs to simulate the exposure of the ungrouted system to wheel loads. A total traffic of 86,500 ESALs was applied to each section over about 32 hours of HVS loading on each one, using a wheel load of 60kN. The results of this part of the experiment indicated that the Super-Slab® System is able to withstand that level of traffic in the ungrouted condition without observable or measurable damage.

TABLE OF CONTENTS

LIST OF FIGURES

LIST OF TABLES

ABBREVIATIONS USED IN THE TEXT

Average Daily Truck Traffic (ADTT)

California Department of Transportation (Caltrans)

Cement-treated base (CTB)

California Bearing Ratio (CBR)

Data Acquisition System (DAS)

Dynamic Cone Penetrometer (DCP)

Equivalent Single Axle Load (ESAL)

Falling Weight Deflectometer (FWD)

Heavy Vehicle Simulator (HVS)

Joint deflection measurement devices (JDMD)

Load Transfer Efficiency (LTE)

Long-Life Pavement Rehabilitation Strategies (LLPRS)

Layer Strength Diagram (LSD)

Multi-depth Deflectometer (MDD)

Partnered Pavement Research Center (PPRC)

Portland cement concrete (PCC)

Table 1: SI* (Modern Metric) Conversion Factors

APPROXIMATE CONVERSIONS TO SI UNITS				
Symbol	**Convert From**	**Multiply By**	**Convert To**	**Symbol**
LENGTH				
in	inches	25.4	millimeters	mm
ft	feet	0.305	meters	m
AREA				
in^2	square inches	645.2	square millimeters	mm^2
ft^2	square feet	0.093	square meters	m2
VOLUME				
ft^3	cubic feet	0.028	cubic meters	m^3
MASS				
lb	pounds	0.454	kilograms	kg
TEMPERATURE (exact degrees)				
°F	Fahrenheit	5 (F-32)/9 or (F-32)/1.8	Celsius	C
FORCE and PRESSURE or STRESS				
lbf	poundforce	4.45	newtons	N
lbf/in^2	poundforce/square inch	6.89	kilopascals	kPa
APPROXIMATE CONVERSIONS FROM SI UNITS				
Symbol	**Convert From**	**Multiply By**	**Convert To**	**Symbol**
LENGTH				
mm	millimeters	0.039	inches	in
m	meters	3.28	feet	ft
AREA				
mm^2	square millimeters	0.0016	square inches	in^2
m^2	square meters	10.764	square feet	ft^2
VOLUME				
m^3	cubic meters	35.314	cubic feet	ft^3
MASS				
kg	kilograms	2.202	pounds	lb
TEMPERATURE (exact degrees)				
C	Celsius	1.8C+32	Fahrenheit	F
FORCE and PRESSURE or STRESS				
N	newtons	0.225	poundforce	lbf
kPa	kilopascals	0.145	poundforce/square inch	lbf/in^2

*SI is the symbol for the International System of Units. Appropriate rounding should be made to comply with Section 4 of ASTM E380. (Revised March 2003)

1. INTRODUCTION

The California Department of Transportation (Caltrans) evaluated the use of the Super-Slab® System (Super-Slab®) as a long-life rehabilitation strategy for concrete pavements. A document previously prepared by the University of California Pavement Research Center (UCPRC) (1) outlines the evaluation strategy proposed by Caltrans District 8 to assess suitability of the pre-cast slab system. Besides the test plan, that document includes brief overviews of Caltrans' Long-Life Pavement Rehabilitation Strategies (LLPRS) and of the Super-Slab® System.

The District's draft Evaluation Plan identified four objectives in its pilot program. The first three objectives focus on evaluation of a trial project. They were to evaluate (1) design and contract preparation requirements, (2) biddability of the Super-Slab® Pavement pay item, and (3) constructability. The fourth objective includes Heavy Vehicle Simulator (HVS) testing to evaluate the long-term performance of the Super-Slab® System.

In January 2005, in response to the request from District 8, the Caltrans Pavement Standards Team (PST) asked the Division of Research and Innovation (DRI) to direct the UCPRC to perform HVS testing and associated testing and analysis on a test section with Super-Slab® Pavement pre-cast panels through the Partnered Pavement Research Center (PPRC) contract managed by DRI. The PST technical lead for this project was the METS Office of Rigid Pavements. The scope of work included the following[1]:

1. Construction of test sections by the manufacturer.
2. Characterization of the pavement structure and materials.
3. Preliminary, short duration HVS testing of the pre-cast slab system, under the following conditions:
    a. HVS testing of the slabs previous to the grouting (dowel bar slots in the joints and bedding grout under the slab) to evaluate staged construction. The thinking is that during a night closure some slabs would be placed in one closure and opened to traffic with the joints ungrouted, followed by grouting of the joints in another closure. The plan called for this testing to be performed without addition of water to the pavement.

[1] Construction (item 1), material characterization (item 2), and preliminary HVS testing (item 3a) are the subjects of this report. They were communicated to Caltrans in a provisional document submitted in August 2005 under title "Interim Report. HVS Testing of Super-Slab® at the Junction of Highways I-15 and SR210."

b. HVS testing of the slabs after grouting, in the dry condition and including the application of very high loads to provide early results after a short duration of testing.

c. HVS testing of the slabs under dry and wet conditions using a less aggressive loading schedule to evaluate longer-term performance[2].

The overall schedule of the construction of the test sections, and testing performed on them is shown in Table 2.

Table 2. Chronology of Construction and All Testing on Pre-Cast Panel Test Sections

Date	Operation	Document in Which Results are Presented
May 11, 2005	Construction of underlying structure	This report
May 20, 2005	FWD testing on underlying structure	
May 24, 2005	Placement of pre-cast slabs	
May 25 and 31, 2005	FWD testing on slabs, ungrouted	
May 27 and 28, 2005	Thermal curl test on 597FDUG	
May 29 and 30, 2005	Load test on 597FDUG	
May 30 and 31, 2005	Load test on 598FDUG	
June 3, 2005	FWD testing on slabs, after grouting	
June 7 and June 8, 2005	Thermal curl test 598FDTC	
June 11 to September 20, 2005	HVS load test, dry condition, 597FD	Tech Memo Reference (2) and Research Report Reference (3)
September 21, 2005 to February 24, 2006	HVS load test, dry condition, 598FD	Research Report Reference (3)
February 24 to May 2, 2006	HVS load test, wet condition, 598FD	
May 8, 2006	FWD testing at 598FD	
May 2 to August 30, 2006	HVS load test, wet condition, 597FD	

This report describes the construction process of the test sections and presents detailed results of the preliminary short-duration performance tests originally summarized in Reference (2). These tests were performed on two HVS test sections, numbered 597 and 598 in the PPRC HVS database, under ungrouted and grouted conditions. The results included in this report, as well as those included in references (2) and (3), are indicated in Table 2.

[2] Results of longer-term tests (item 4) have been communicated to Caltrans through presentations, and will be formally documented in a detailed report currently being prepared (3).

The HVS test sections were constructed at the interchange of Interstate I-15 and State Route (SR) 210 in San Bernardino County. The location of the test section is presented in Figure 1.

The test results presented in this document include:

- Thermal curl tests performed on the slabs before grouting of the slabs and joints;
- Load tests on the slabs before grouting of the joints and slabs;
- Thermal curl tests after grouting of the joints and slabs; and
- Initial load tests on Section 597FD slabs after grouting of the slabs and joints to provide preliminary results to the District. (Longer-duration load tests performed afterward are documented in Reference [3]).

(a) State level

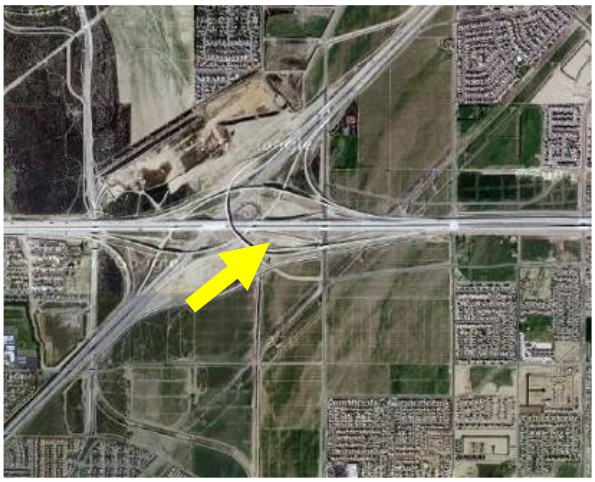

(b) Intersection level

(a) City level

Figure 1. Location of the test sections at the interchange of highways I-15 and State Route 210 in San Bernardino County, CA.

2. CONSTRUCTION OF THE TEST SECTIONS

This chapter provides an overview of the process followed during the construction of the HVS test sections, including:

- Construction of the ten test slabs, arranged in a two-by-five slab grid;
- Analysis of the subgrade prior to construction of the cemented-base layer using Dynamic Cone Penetrometer (DCP) data;
- Structural evaluation of the Super-Slab® System using Falling Weight Deflectometer (FWD) data measured after construction and prior to HVS loading; and
- Analysis of laboratory data from the concrete used during the manufacture of the concrete slabs.

2.1 Construction Process of the Super-Slab® Test Grid

The Super-Slab® System is intended as a rapid replacement option for damaged concrete pavements. Individual slabs or a whole section of the pavement may be replaced by the Super-Slab® System. This implies that the Super-Slab® System will usually be placed on an existing cement-treated base (CTB) that may be in a fairly advanced state of damage. In the case of the HVS test sections, however, the underlying pavement structure had to be built because the test sections were not constructed on an existing, damaged pavement. The construction process therefore started with the preparation of the subgrade and the construction of a CTB in the general area shown in Figure 2. The thickness of the CTB was 4 inches, and its surface was relatively uneven (see Figure 3).

Figure 2. General area for the construction of the Super-Slab® System test grid before construction.

Figure 3. Texture of the completed CTB prior to construction of the Super-Slab® System.

Construction of the Super-Slab® System consists of four main steps:

1. Construction of the sand bedding layer,
2. Placement of the pre-cast slabs,
3. Grouting of the slabs and joints, and
4. Joint preparation and grinding.

2.1.1. Construction of the Sand Bedding Layer

The function of the sand bedding layer is to provide very even support to the precast slabs thereby eliminating the formation of voids between the slabs and support to the maximum extent possible. After spreading the sand on top of the CTB, the sand is wetted, compacted, and bladed repeatedly to very tight profile tolerances. Figure 4 shows the compaction and blading of the sand with a hand-propelled grader running on two rails to ensure an even surface. The thickness of the bedding layer varied from about 6 mm to as much as 18 mm in spots since the surface of the CTB was not even. The average thickness was 9 to 10 mm. The material used was stone sand with the gradation indicated in Table 3. Fineness modulus was 2.84.

Table 3. Gradation of the Stone Sand Used in Bedding Layer

Sieve No.	Sieve Size (mm)	Percent Passing by Weight
3/8	9.5	100.0
4	4.75	98.4
8	2.36	80.7
16	1.18	63.9
30	0.600	46.2
50	0.600	20.7
100	0.150	6.6
200	0.075	0.0

(a) Compaction of the sand bedding layer.

(b) Precision blading of the sand bedding layer.

Figure 4. Construction of the sand bedding layer.

2.1.2. Placement of the Pre-Cast Slabs

After completion of the construction of the sand bedding layer, the exact corner locations of the slabs are marked on the surface of the sand. The pre-cast slabs are placed strictly according to this predetermined grid and not with a constant gap width. This is done to prevent creep of the slabs which could result in the last of the pre-cast slabs butting up against an existing slab when a section of pavement is replaced. Figure 5 shows the markings for the placement of the pre-cast slabs.

Figure 5. Precise setting out of the corner locations of the pre-cast slabs.

Figure 6 shows certain details of the pre-cast slabs. Figure 6(a) shows the epoxy-coated dowel bars cast into one end of the 4.572 m (15 ft) long by 3.962 m (13 ft) wide by 220 mm (9 in.) thick slabs at the time of manufacture. Figure 6(b) shows the dove-tailed recesses on one of the transverse edges of the slab that accept the dowel bars on the opposing end of the adjacent slab, the foam strip on the longitudinal edge of the slab that confines the bedding grout, and the bedding grout channel that runs underneath the slab. Figure 6(c) shows the female end of the tie bars cast into the longitudinal edge of the slab that accepts the male ends of the tie bars as shown in Figure 6(d).

(a) Epoxy-coated dowel bars cast into the transverse edge of the slabs.

(b) Dowel-bar recesses and bedding grout confinement strip.

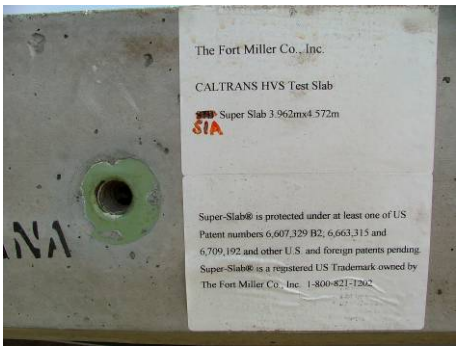

(c) Female end of the tie-bars cast into the longitudinal edge of the slab.

(d) Male-to-female connection of the tie-bars.

Figure 6. Details of the pre-cast slabs.

The pre-cast slabs arrived on site on flat-bed trucks and were lifted and lowered into place with a crane as shown in Figure 7. The tie bars were then screwed into the longitudinal edge of the slab connecting to the adjacent lane and the adjacent slab placed as shown in Figure 8.

(a) Lifting of the slab from the flat-bed.

(b) Precise placement of the slab.

Figure 7. Placement of the pre-cast slabs.

(a) Fixing the tie bars on the longitudinal edge.

(b) Placement of the slab on the adjacent lane.

Figure 8. Fixing the tie bars and placement of the slab on the adjacent lane.

The dowel bars and the transverse joint were then sprayed with a bond-breaker as shown in Figure 9 and the placement of the slabs continued. Although great care was exercised in preparing the bedding layer, the edges of adjacent slabs did not have perfect vertical alignment, resulting in surface irregularities at the joints and corners as shown in Figure 10.

Figure 9. Spraying of the dowel bars with a bond-breaker.

Figure 10. Misalignment of adjacent slabs causing surface irregularities.

Once all the slabs of the HVS test sections were in place, plastic spacers were driven into the joints between the ungrouted slabs to prevent their movement, and the outer edges of the joints were sealed using expanding foam to prevent ingress of material into the joint (as shown in Figure 11). Figure 11(a) also clearly shows the grout holes for the dowel bars on the transverse joint and the tie bars on the longitudinal joint. The construction team then continued with the construction of a temporary aggregate shoulder around the perimeter of the five-by-two grid of pre-cast slabs.

(a) Plastic spacers being driven into the joints between the ungrouted slabs.

(b) Expanding foam used for sealing of the outer edges of the joints to prevent ingress of material into the joint.

Figure 11. Final work on the joints between the ungrouted slabs.

2.1.3. Grouting of the Slabs and Joints

On a normal replacement project, the ungrouted slabs would be exposed to traffic for a day before the grouting continued during the next nighttime closure. The ungrouted slabs were therefore instrumented and tested with the HVS before grouting continued. (The details of the instrumentation and testing are presented in Section 3.2.) After completion of the ungrouted tests, the grouting of the slabs continued.

The fast-setting grout used in the grouting process required that the mix water be cooled before mixing. Ice blocks were placed in the mix water to cool it. The grouting system consisted of a mechanical mixer with a piston pump and hoses with customized fittings to inject the grout into the grout holes in the slabs as shown in Figure 12.

(a) Mechanical mixer and piston pump.

(b) Hose with fitting for injecting the grout.

Figure 12. Basic components of the grouting equipment.

The grouting of the dowels and tie bars at the joints was completed before the grouting of the bedding sand. A high-strength grout was used for the dowels and tie bars. The injection fitting was placed into one of the grout holes and the grout was pumped into the cavity until it started to flow from the hole on the other end of the dowel and tie-bar cavities, as shown in Figure 13. The excess grout was scraped off before it set.

(a) Filling of the dowel and tie-bar cavities with grout.

(b) Removal of excess grout.

Figure 13. The grouting of the dowel and tie-bar cavities.

Once the grouting of the dowel and tie-bar cavities was completed, the grouting of the bedding material commenced. The grout for the bedding material was of a lower strength than the grout used for the dowel and tie-bar cavities and was more like a fluid than a paste to ensure proper filling of any possible void between the slab and the support. The bedding grout was applied in a manner similar to the dowel and tie-bar grout but with the addition of a fitting placed in the exit hole of the bedding grout, as shown in Figure 14.

(a) Injection of the bedding grout.

(b) Excess bedding grout pouring from the exit hole.

Figure 14. The grouting of the bedding material.

2.1.4. Joint Preparation and Grinding

The construction process was concluded by cutting of the joints to a constant width, grinding of the surface to a level plane, filling the joints with a joint backer as shown in Figure 15, and sealing the joints. The construction team then continued with removal of the temporary aggregate shoulder and its replacement with an asphalt concrete shoulder.

(a) Level grinding of the surface.

(b) High-density foam strip installed in the joints.

Figure 15. Finishing details of the surface and joints.

2.2 Dynamic Cone Penetrometer Analysis

The DCP is used to evaluate the structural strength of the unbound layers in a pavement system through the measurement of the shear resistance of a standard cone pushed vertically into the pavement under the influence of a standard falling weight (4, 5).

The field DCP data collection took place on May 6, 2005, on the undisturbed *in situ* soil before the removal of any vegetation or subgrade preparation. A testing area 22.9-m long and 7.3-m wide (74 ft by 24 ft) was identified as the area where the Super-Slab® test pavement would be constructed. In order to characterize the structural strength of the subgrade in this area, eight DCP tests were done on the *in situ* soil at the locations indicated in Figure 16. Four DCP tests (4.6 m apart) were done in two rows, 7.3 m apart for a total of eight DCP measurements. The first row was toward the northern end of the testing area with holes marked 2N, 4N, 6N, and 8 N. The holes on the southern end were marked 1S, 3S, 5S, and 7S.

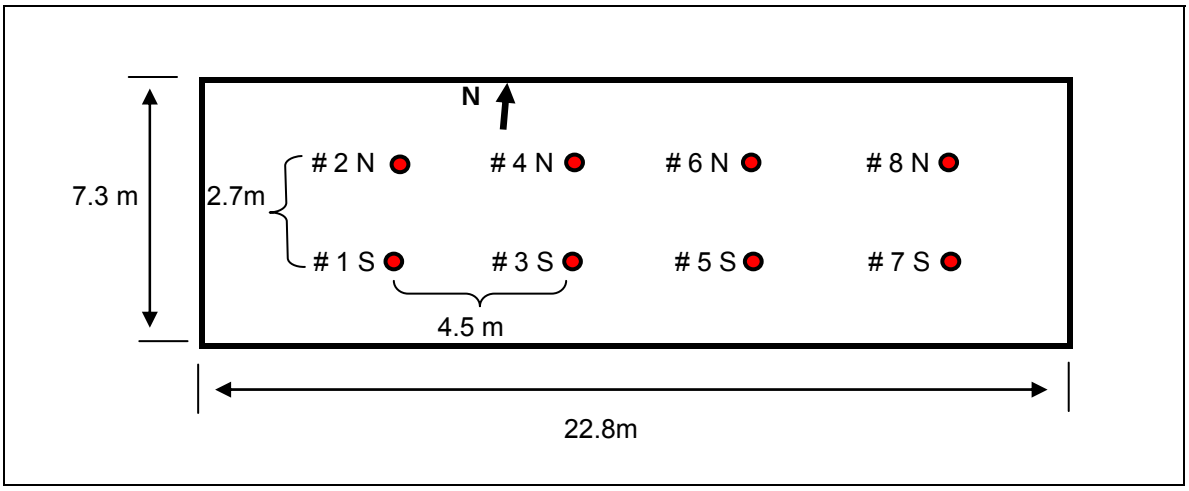

Figure 16. DCP positions at the Super-Slab® test pavement area.

The subgrade at the location of the HVS test site consists of a sandy material with a fair amount of stones embedded in the soil. These stones made penetration with the DCP very difficult and only three of the eight DCP tests could be completed with the rod penetrating to the its full length of 800 mm (2.6 ft). Five of the eight tests were stopped early because of very low or zero penetration even after successive blows with the hammer.

Figure 17 shows the DCP layer strength diagram (LSD) for the combined data of the DCP tests done on the northern side of the test site. Although the DCP did not always penetrate to the full depth of 800 mm the LSD clearly show that the top 200 mm (0.65 ft) of the subgrade generally had a relatively high penetration rate of approximately 30 mm/blow (0.1 ft/blow). Below 200 mm depth, the penetration rate decreased to between 2 and 4 mm/blow (0.0065 and 0.013 ft/blow) which is very low for a pavement subgrade. These low penetration rates, combined with the fact that the DCP did not always penetrate 800 mm, indicate a stony subgrade.

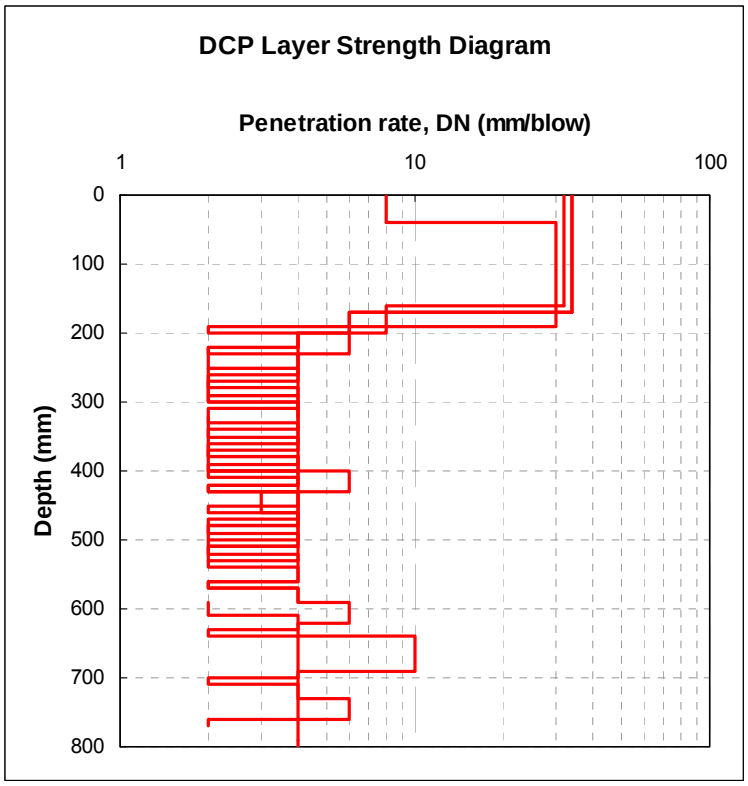

Figure 17. DCP layer strength diagram for the test locations on the northern side of the site.

Figure 18 shows the LSD for the combined data of the DCP tests done on the southern side of the test site. Although the thickness of the top layer with the high penetration rate is only about half of the thickness of this layer on the northern side, the general trend in the data is very similar to the trend observed on the northern side of the site.

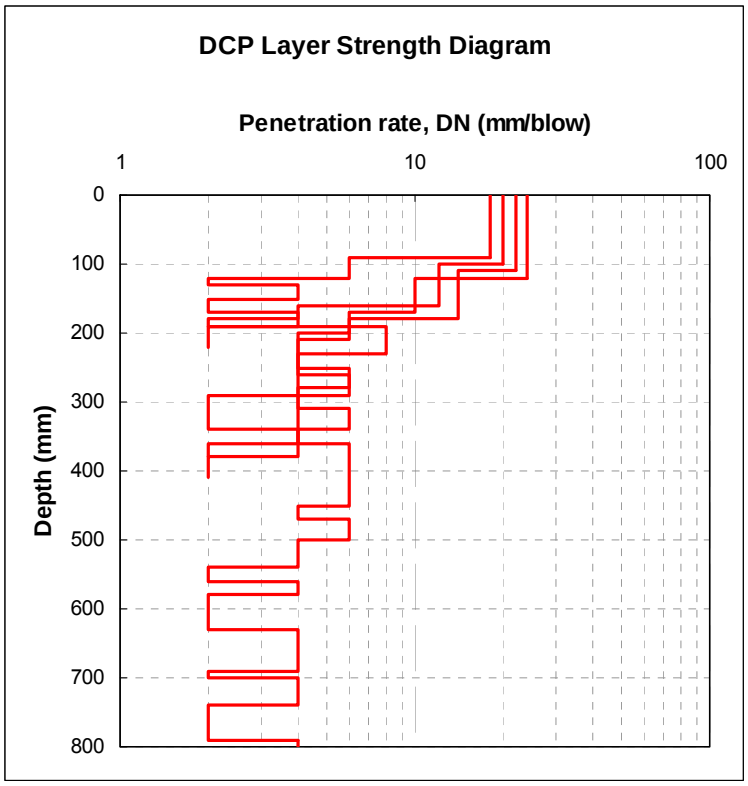

Figure 18. DCP layer strength diagram for the test locations on the southern side of the site.

Table 4 summarizes the DCP results. The table shows the number of blows to penetrate to maximum depth, the average penetration rates in mm/blow calculated for the upper portion of the subgrade [about 100 mm (0.32 ft) for the test locations on the southern side and 200 mm (0.64 ft) for those on the northern side] as well as the average penetration rate for the portion of the subgrade below the upper layer to the maximum depth of penetration.

Table 4. Summary of the Subgrade DCP Results

DCP Test Location	Maximum Penetration Depth (mm)	Number of Blows to Maximum Penetration Depth	Penetration Rate (mm/blow)	
			Upper Portion	Lower Portion
1 S	840	200	22	3.7
3 S	410	75	24	4.1
5 S	380	85	20	3.5
7 S	220	55	18	2.4
2 N	500	125	19	2.7
4 N	530	110	20	4.1
6 N	770	200	20	3.0
8 N	840	200	20	3.4
Average			20.4	3.3

The results displayed in Table 4 are indicative of a fairly strong subgrade for the portion of the subgrade below the upper layer. Penetration rates of below 6 mm/blow are indicative of layers consisting of good quality natural gravel often used as subbase material. Using well-established correlations (2, 5) the *in-situ* CBR of the subgrade calculated using through the DCP data is between 45 and 80 which is significantly higher than the norm for subgrades, and indicates a granular material.

Based on the results obtained by the DCP analysis it is concluded that the subgrade at the site where the Super-Slab® test section was constructed has sufficient bearing capacity to carry the expected loads. If well protected through the design of a proper upper structure, the subgrade at this testing area should not be the cause of any early unexpected failures under the influence of repetitive loading.

It should be borne in mind that the presence of stones embedded in the subgrade has a significant influence on the DCP results and all conclusions based on DCP data should be handled with caution.

2.3 FWD Surveys and Data Analysis

Falling Weight Deflectometer tests (FWD) were conducted at the test site:

- To determine the structural strength of the substructure (base and subgrade). This was done through FWD testing on the cement-treated base (CTB) prior to the placement of the concrete slabs;
- To assess the integrity of the joints before and after grouting was done based on the Load Transfer Efficiency (LTE) at the joints;
- To investigate the effects of temperature on LTE through a comparison between FWD data collection during the hottest part of the day and data collected during the night;
- To determine the stiffness of the various layers of the complete structure, including the concrete slabs.

To achieve this, a Heavy Weight Deflectometer (HWD) was used. This equipment is essentially the same as an FWD but with the capability for heavier loads than standard FWDs. The HWD is normally used for the evaluation of strong concrete pavements such as airfields and was used at the test site. For clarity the acronym “FWD” will be used throughout this report although the data was collected with an HWD.

FWD surveys were done early in the morning, before sunrise, at low surface temperatures and were repeated in the afternoons when the surface temperature was hotter. FWD testing was performed at four stages of construction:

1. On May 20, 2005, on top of the cement-treated base;
2. On May 25, 2005, on the ungrouted slabs before the arrival of the HVS;
3. On May 31, 2005, on the ungrouted slabs not obscured by the HVS after the arrival of the HVS; and
4. On June 3, 2005, after all concrete joints had been grouted, and prior to the start of HVS testing.

FWD testing on the CTB prior to the placement of the Super-Slab® test grid was done as detailed in Figure 19. Row A is the southern side with Station 0 toward the western end of the testing slabs, and with stationing increasing eastward.

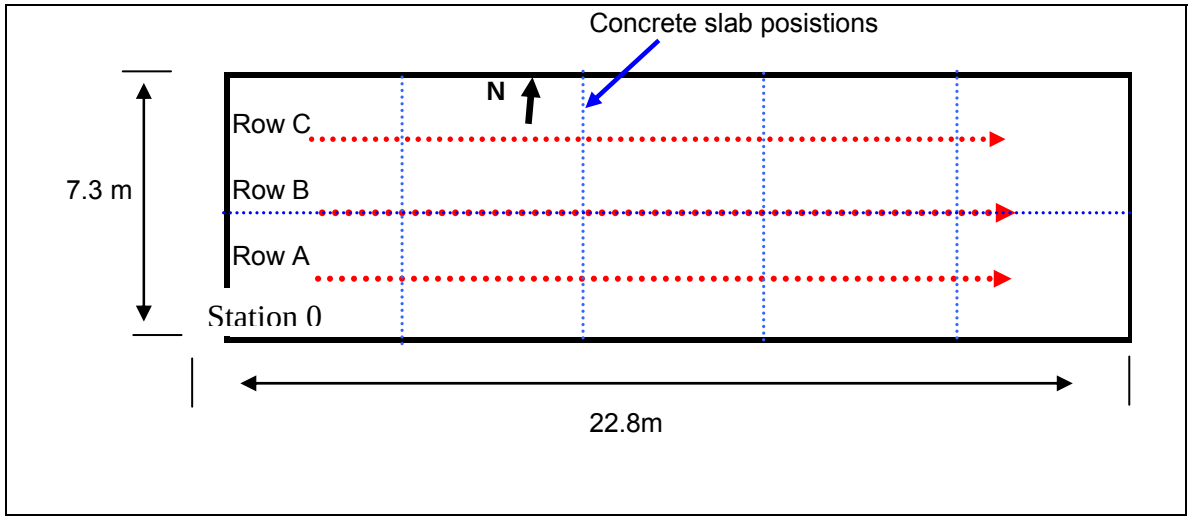

Figure 19. FWD survey rows on the base prior to Super-Slab® placement.

Figure 20 shows the FWD deflection data collected on the CTB prior to the placement of the concrete slabs. The figure shows three graphs: the first is the FWD deflections normalized for a 40kN load, the second graph shows the backcalculated stiffness values of the CTB layer, and the last graph shows the backcalculated stiffness values of the subgrade.

Although the deflections seem high [on the order of 0.8 mm (2,000 mils)] it should be borne in mind that the results were obtained with the FWD placed directly on top of the CTB layer.

The backcalculated stiffness values for the CTB typically ranged between 200 and 600 MPa (29,000 and 87,000 psi) and are somewhat lower than what would be expected from a newly

constructed layer without exposure to any traffic. The FWD survey on the CTB was done on May 20, 2005, while the DCP tests on the subgrade were done on May 6, 2005. The CTB had been constructed less than 14 days prior to FWD testing and would not yet have reached maximum strength. The subgrade stiffness is within the range of values expected for a subgrade material, ranging from about 50 to 100 MPa (7,250 and 14,500 psi), with a few points in the range of 200 MPa. These results are presented in Table 5.

Table 5. Backcalculated Moduli from Deflections Measured on Top of CTB

Layer	Representative Value (MPa)	Typical Range (MPa)
Cement-treated base (CTB)	400	200 and 600
Subgrade (SG)	70	50 to 100

Figure 21 shows the FWD data collection points on each of the ten concrete slabs after placement. The measurements done at the corners and along the edges of the slab were used to calculate LTE across the joints (transverse as well as longitudinally), whereas the center-slab deflection serves as an indication of the total structural strength of the complete pavement system. LTE was measured twice, on what would be the approaching and the leaving sides of the joints if the pavement were open to traffic, so that results from a given “upper corner” are at the same location as the “lower corner” of the subsequent slab, the difference being that the load is on the opposite side of the joint.

All FWD data recording locations on all 10 slabs are shown in Figure 22. The data showing the LTE values for the data from both rows A and C can be seen in Figure 23 to Figure 26. Row B was not done after the placement of the slabs as this row fell exactly on the longitudinal joint of the slabs (see Figure 19).

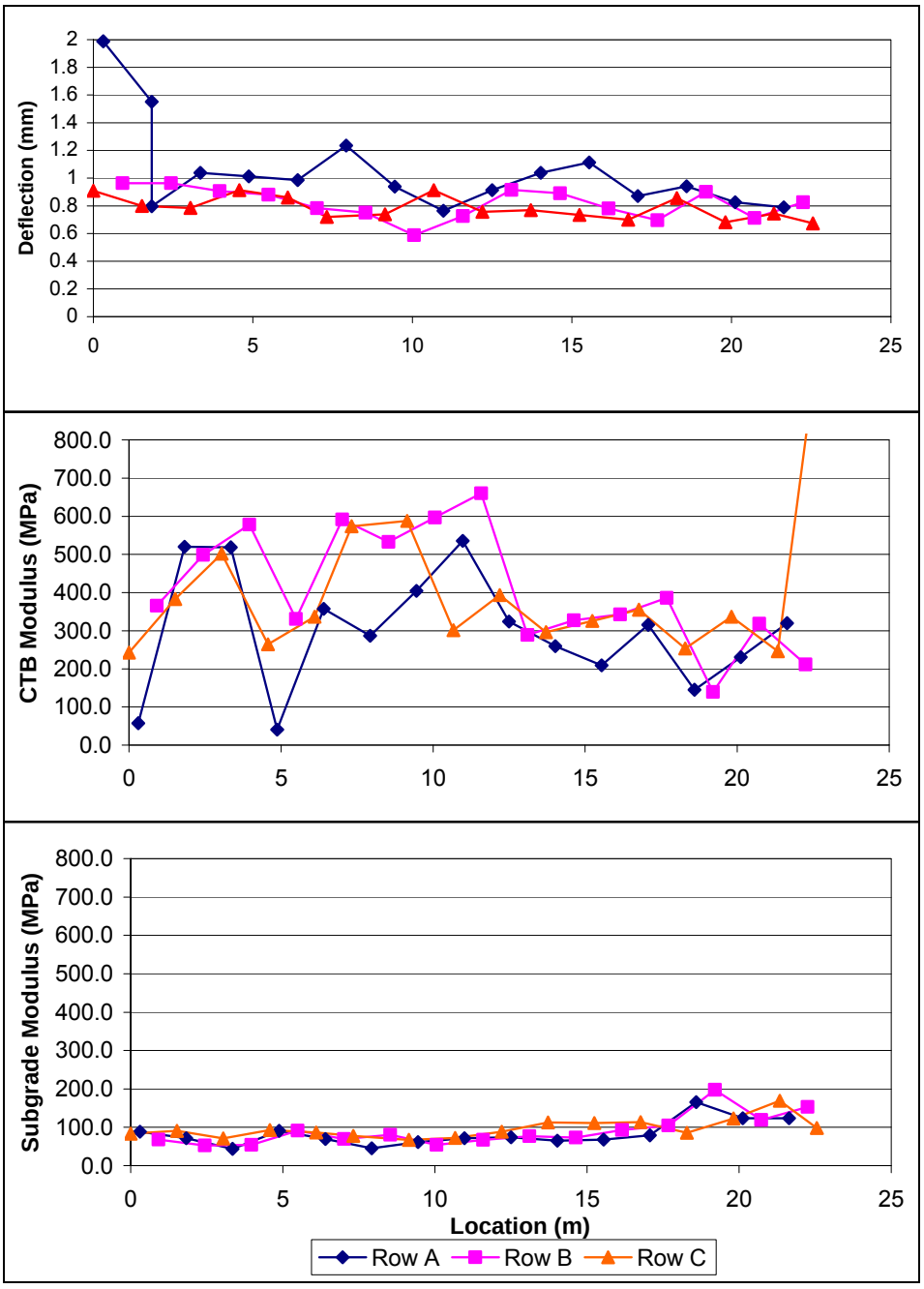

Figure 20. FWD data collected on the CTB layer.

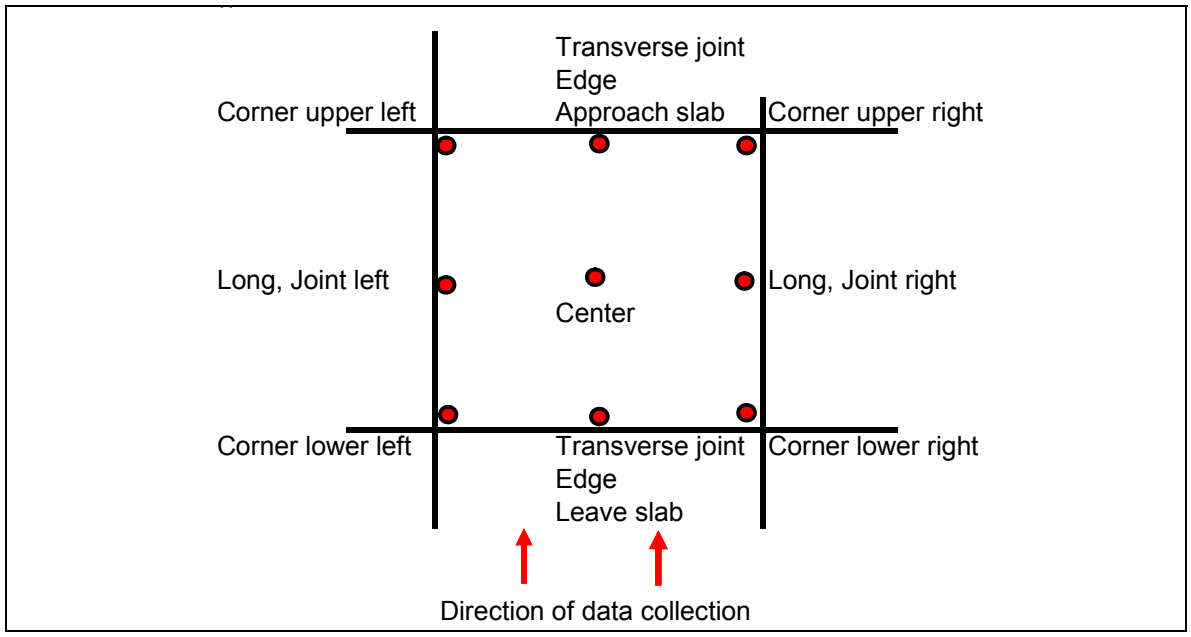

Figure 21. FWD test locations on each Super-Slab® slab.

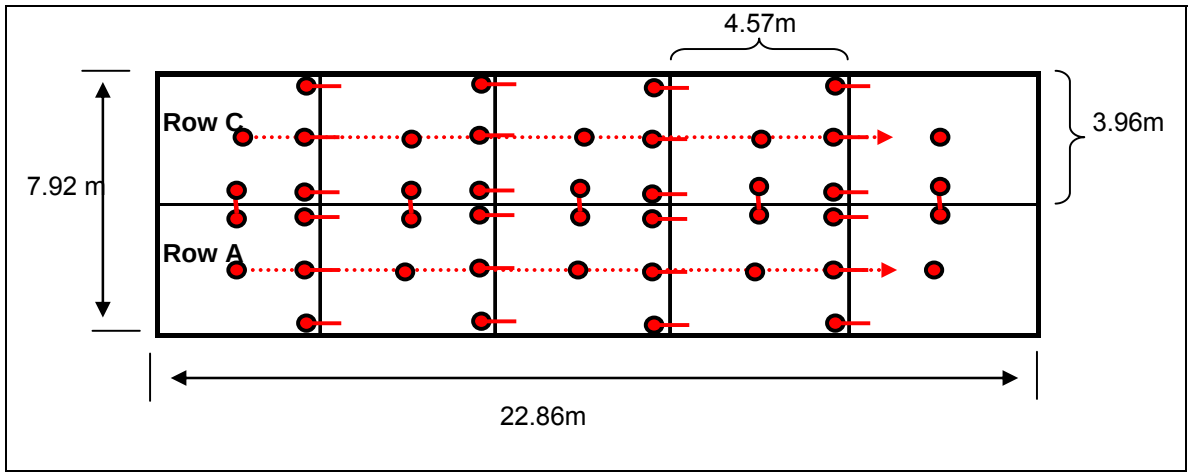

Figure 22. FWD data collection points on the concrete slabs.

The LTE values are significantly higher after grouting than before. It is obvious that there is little load transfer prior to the grouting, with LTE values in the range of 5 to 40 percent, and an average of 16 percent. These values are low, but reveal some LTE through the support layer, as the dowels are loose and the faces of the joint are not in contact. Trafficking with the HVS on the ungrouted slabs did not cause a reduction in LTE (which was not high, as explained). Regardless of the level of LTE in the ungrouted condition, the grouting caused load transfer to increase to close to 100 percent. This illustrates that most of the LTE in the completed system was transmitted through the grout and dowels. Table 6 shows the average and the range of the measured LTE. The results

come from 32 tests with eight transverse joints evaluated in four positions (eight tests for the "after HVS" dataset).

Table 6. Measured Load Transfer Efficiency Before and After Grouting, Morning and Afternoon

	A.M.		P.M.	
LTE (%)	**Average**	**Range**	**Average**	**Range**
Ungrouted	16	4 to 40	39	8 to 83
UG after HVS	16	6 to 25	67	55 to 79
Grouted	100	92 to 104	98	91 to 102

The effect of temperature on LTE is clearly visible. The average surface temperature recorded during FWD data collection during the daytime was 41°C (106°F) and during the nighttime it was 21°C (70°F). During nighttime, the edges tend to curl upward due to slab contraction and a negative temperature differential in the concrete (the surface being colder than the bottom). This curling effect reduces the load transfer by reducing slab contact with the base at the joints and corners, which reduces load transfer through the underlying layers. The opposite happens during daytime when the slabs expand, which causes an increase in load transfer. These temperature effects were less visible after grouting, which illustrates the effectiveness of the steel dowels and the grouting in restricting relative vertical movement across the joints even under the influence of temperature changes.

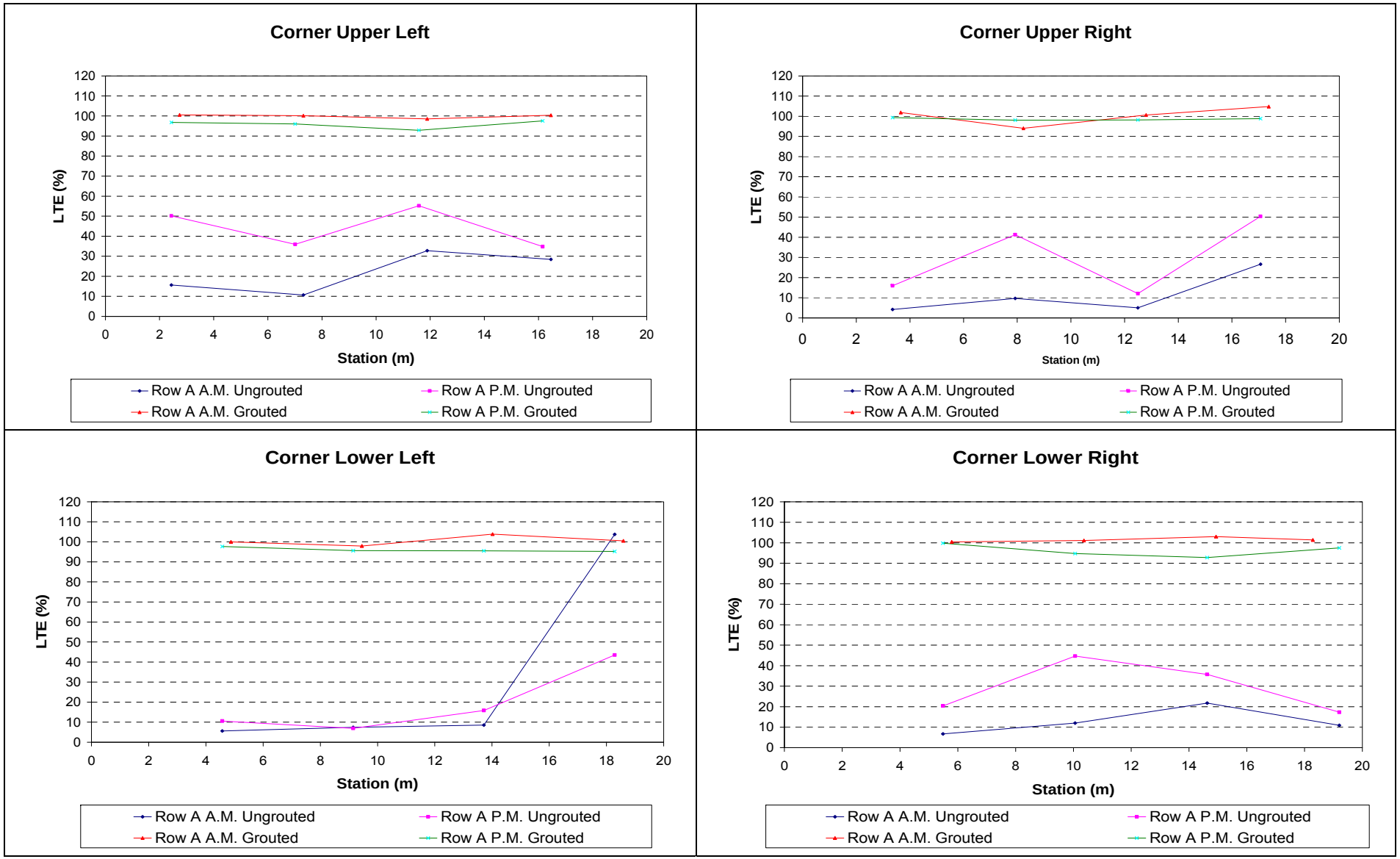

Figure 23. Transverse joint LTE data from the corners of the slabs: Row A.

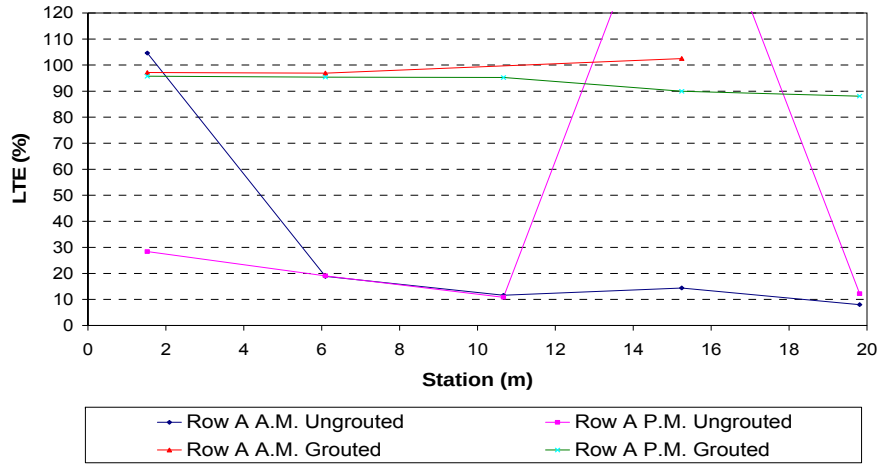

No data : AC shoulder on the right side.

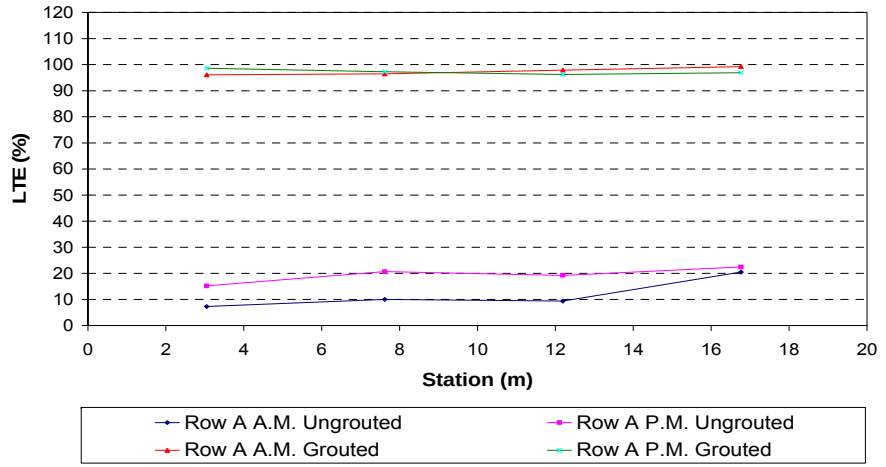

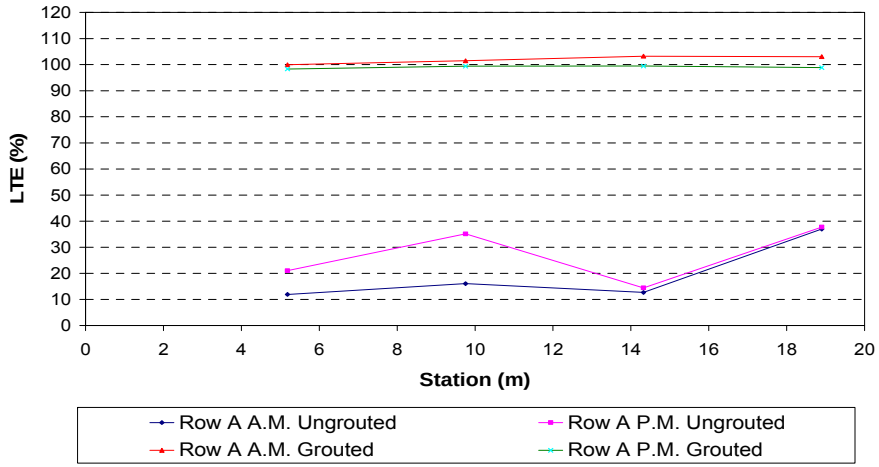

Figure 24. LTE data from mid-slab edge positions: Row A.

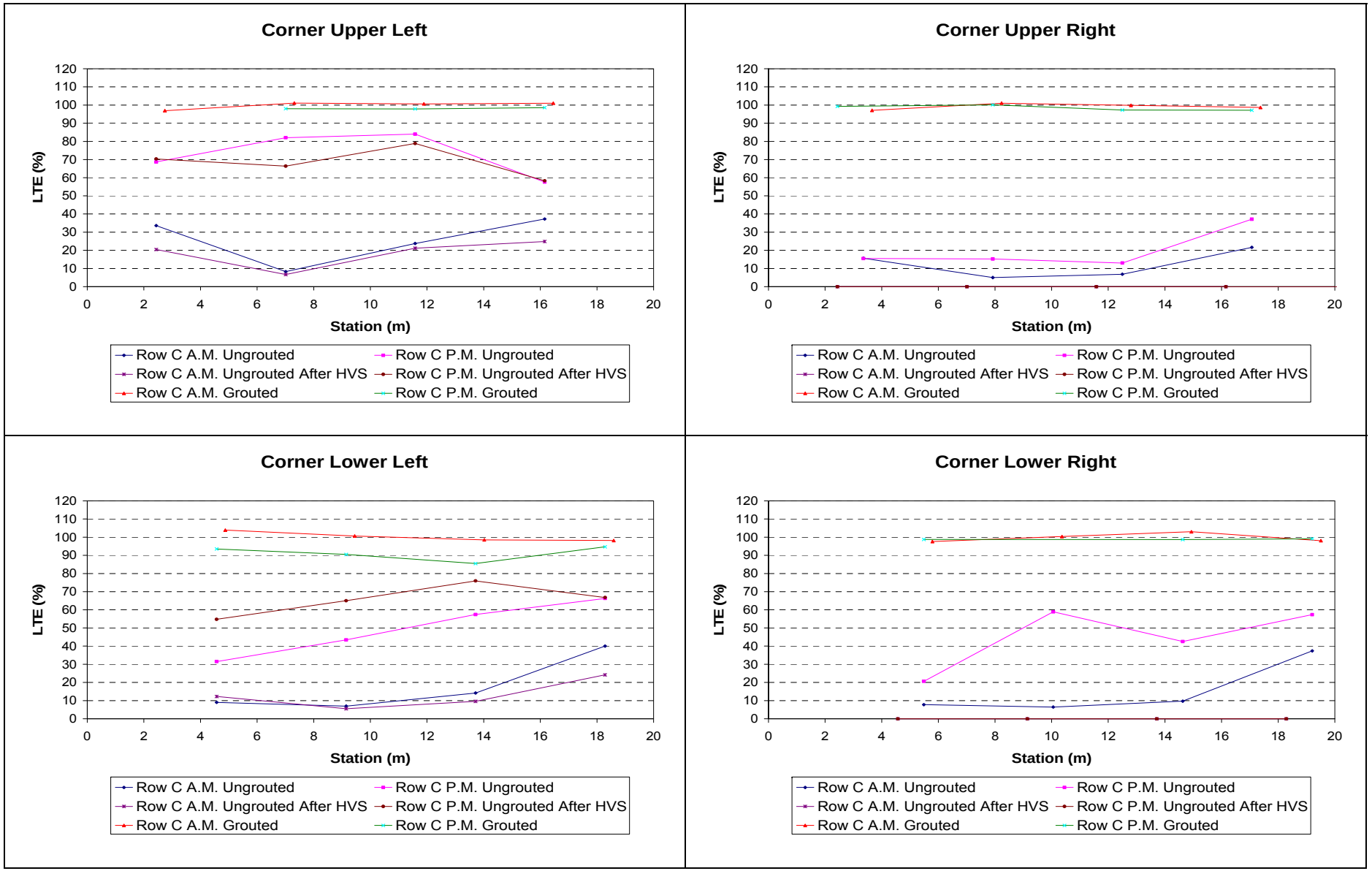

Figure 25. Transverse joint LTE data from the corners of the slabs: Row C.

No data: AC shoulder on left side.

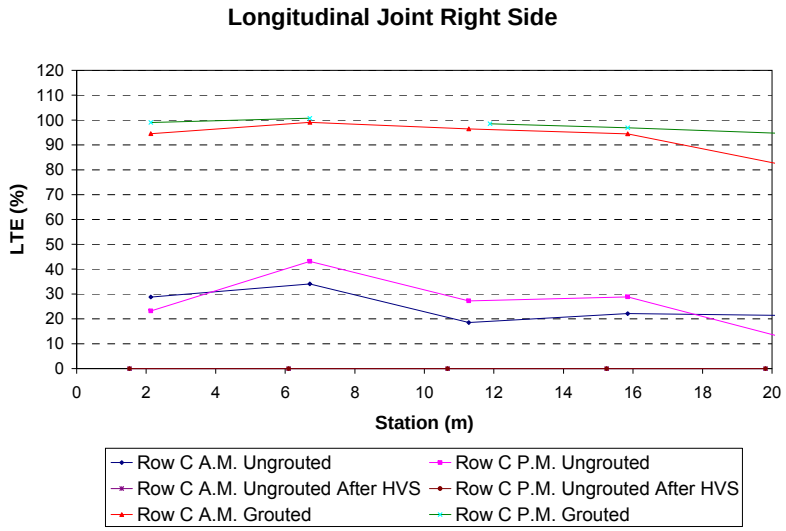

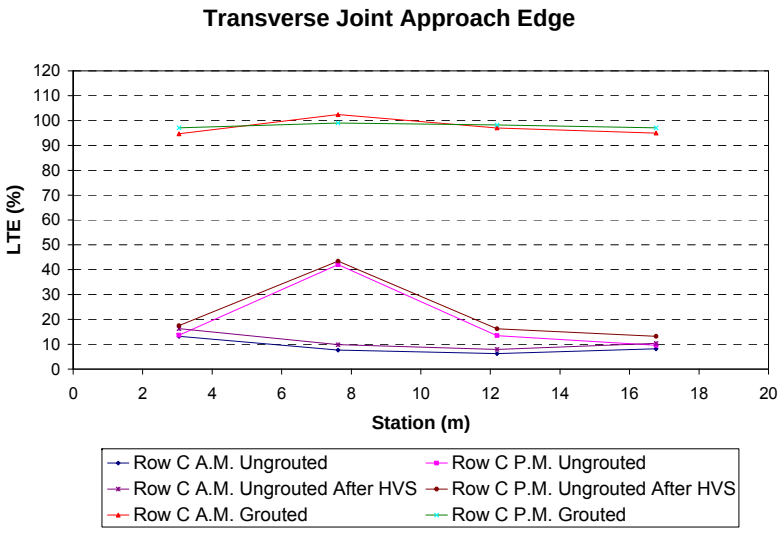

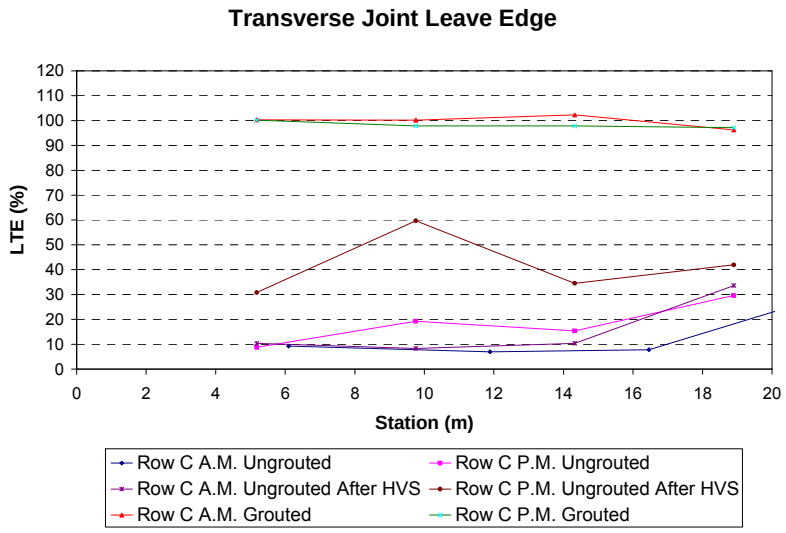

Figure 26. LTE data from the mid-slab edge positions: Row C.

Surface deflections were recorded with the FWD at the center of each slab as shown in Figure 21 and Figure 22. These data are shown in Figure 27.

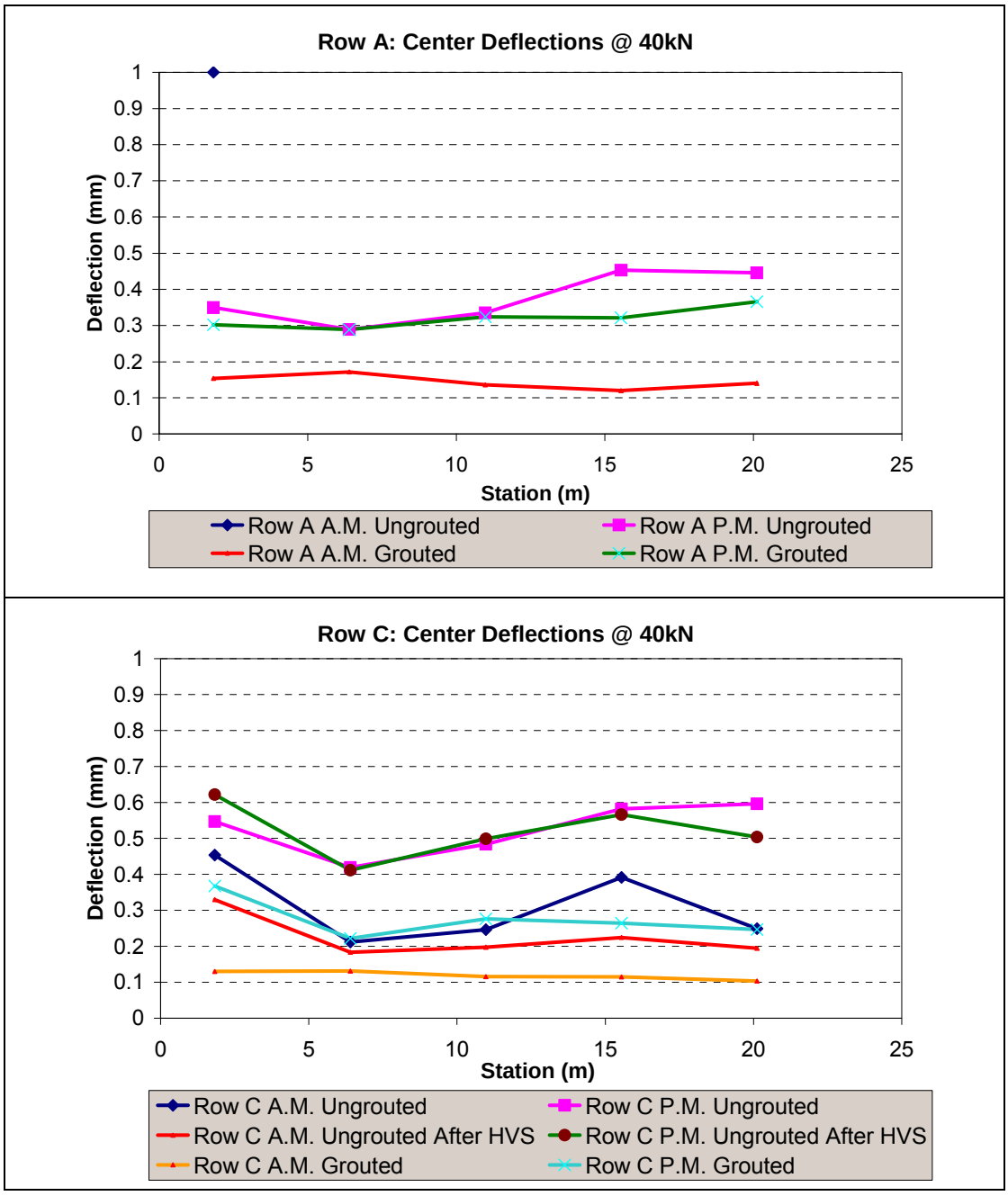

Figure 27. FWD 40kN deflection data.

The deflections vary as expected with temperature. The daytime temperature differential caused the slabs to curl slightly downward which resulted in higher center deflections when compared to the nighttime measurements. The grouting caused increased load transfer between slabs which caused the deflections after grouting to be lower than those recorded before grouting. Statistical summaries of the peak deflections measured at the center of the slabs can be seen in Table 7 for three testing stages: (i) ungrouted slab, not yet trafficked, (ii) ungrouted slabs after applying 86,500 ESALs with the HVS, and (iii) after grouting of the joints and slabs. The average, sample standard deviations, and coefficient of variations for the various cases are shown in the table. The information presented was compiled from only five slabs per row and due to the small sample size the derived statistical parameters should be interpreted with caution, although they are included here to assist in the interpretation of the results.

Table 7. FWD Deflections Measured at Slab Centers on Top of Pre-Cast Slabs

Deflection		Ungrouted		Ungrouted after HVS		Grouted	
Row	**Parameter**	**A.M.**	**P.M.**	**A.M.**	**P.M.**	**A.M.**	**P.M.**
A	Ave (mm)	0.199	0.375	n/a	n/a	0.144	0.321
	STD (mm)	0.025	0.072	n/a	n/a	0.019	0.029
	Coef of Var (%)	12.6	19.2	n/a	n/a	13.5	9.1
C	Ave (mm)	0.311	0.375	0.226	0.52	0.119	0.275
	STD (mm)	0.106	0.072	0.06	0.079	0.012	0.056
	Coef of Var (%)	34.1	19.2	26.5	15.2	9.7	20.2

The following observations regarding the peak FWD deflections are made:

- The influence of the day-night temperature variation on the deflection measurements is significant. Lower center slab deflections were recorded in the early mornings (slabs curled upward) in comparison to those recorded in the afternoon (slabs curled downward). This is expected because the afternoon curling tends to reduce the contact stress between the slab and the base caused by gravity and the mass of the slab.
- The maximum center slab deflections were recorded on the ungrouted slabs in the afternoon where the deflections varied between 0.375 and 0.525 mm (14.8 and 21 mils.) These values are high for newly placed slabs, but are explained by the fact that the slabs were unconnected (ungrouted) during time of testing, because of possible voids between slab and the sand layer, and temperature effects.
- The influence of the grouting is clearly visible where the average deflections showed a significant drop after the grouting in comparison with before grouting. Deflections varied between 0.119 and 0.321 mm (4.7 and 12.6 mils), which is what is to be expected from an untrafficked new pavement.

- Although limited to a small sample size, the variation in the data is less after grouting than before. The sections behave more uniformly from a structural standpoint after grouting than before.

The backcalculated moduli for the concrete, the cemented base, and the subgrade are presented in Figure 28. The backcalculations were performed using the Elmod© 5 software at three testing stages: (i) ungrouted slab, not yet trafficked, (ii) ungrouted slabs after applying 86,500 ESALs with the HVS, and (iii) after grouting of the joints and under the slabs. In each case the deflection data were collected in the early morning at low temperature and also in the afternoon at a higher temperature. Table 9 shows the average backcalculated moduli for each row of slabs (rows A and C), for the various layers, and under the different conditions (time of day and testing stage). Results at individual locations are presented in Figure 29 to Figure 31. The results shown in Figure 28 are the average of all test locations. The morning data is considered to be provide more reliable results because the testing is at the center of the slab, which is in contact with the under layers when the temperature differential is negative (colder on the surface of the slab).

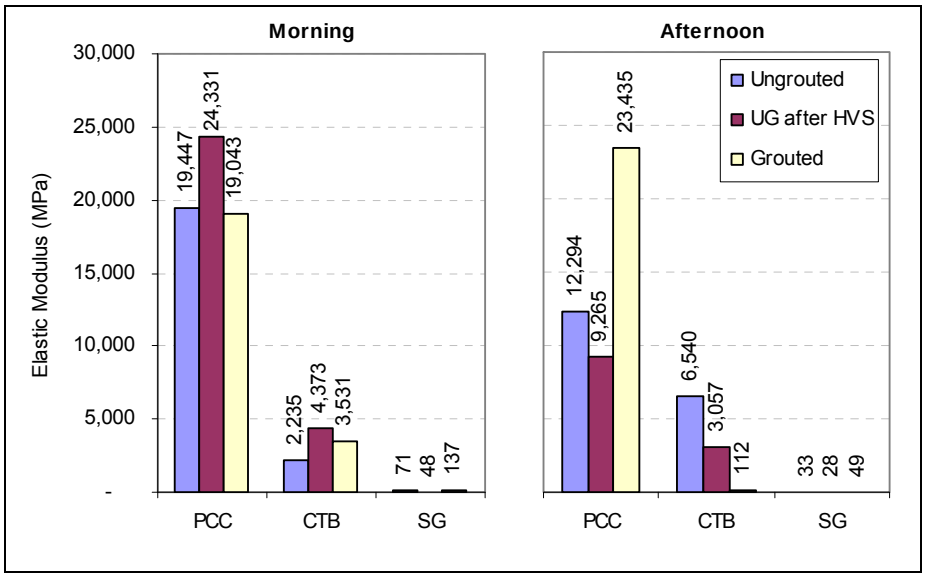

Figure 28. Backcalculated elastic moduli for the concrete, the cemented base, and the subgrade, obtained from morning and afternoon deflection data.

Table 8 presents the values considered representative of the materials comprising the three structural layers of the pavement system.

Table 8. Backcalculated Moduli from Deflections Measured on Top of Pre-Cast Slabs

Layer	Representative value (MPa)	Typical Range (MPa)
Portland cement concrete (PCC) pre-cast slabs	19,500	5,000 to 30,000
Cement-treated base (CTB)	2,200	1,000 to 8,000
Subgrade (SG)	70	20 to 120

The subgrade modulus is consistent with what was obtained from deflection testing directly on the newly constructed base (as opposed to these results obtained from deflection testing on top of the pre-cast panels). The CTB modulus obtained previously, when the material was up to 14 days old, increased to a more reasonable value, but in the lower range of what would be expected for a cement-treated base. The testing after grouting took place when the CTB was approaching 28 days.

Table 9. Detailed results of Backcalculation from Deflections Measured on Top of Pre—Cast Slabs

Average Moduli (MPa)		Ungrouted		Ungrouted after HVS		Grouted	
Row	Layer	A.M.	P.M.	A.M.	P.M.	A.M.	P.M.
A	PCC	31,000	14,200	n/a	n/a	16,900	21,700
	CTB	2,983	3,155	n/a	n/a	3,288	35
	SG	75	43	n/a	n/a	126	50
C	PCC	12,000	12,125	26,438	8,175	16,750	23,875
	CTB	4,467	10,633	5,775	9,000	4,513	20
	SG	74	27	48	28	136	50

The backcalculation results from deflection taken before grouting should be interpreted with caution. At that stage the slabs were not properly connected and slab rocking could be the cause of the high degree of variation in the data as seen in the graphs. The data after grouting are more consistent and in agreement with what are expected values. As seen in the tables and graphs, there is significant variation within and between the various data sets. As explained before, the effect of the ungrouted (not connected) slabs on the variation in surface deflections is amplified during the backcalculation process. A significant amount of scatter is visible in the graphs. After grouting the trends are more consistent with a lower degree of variation between the various slabs.

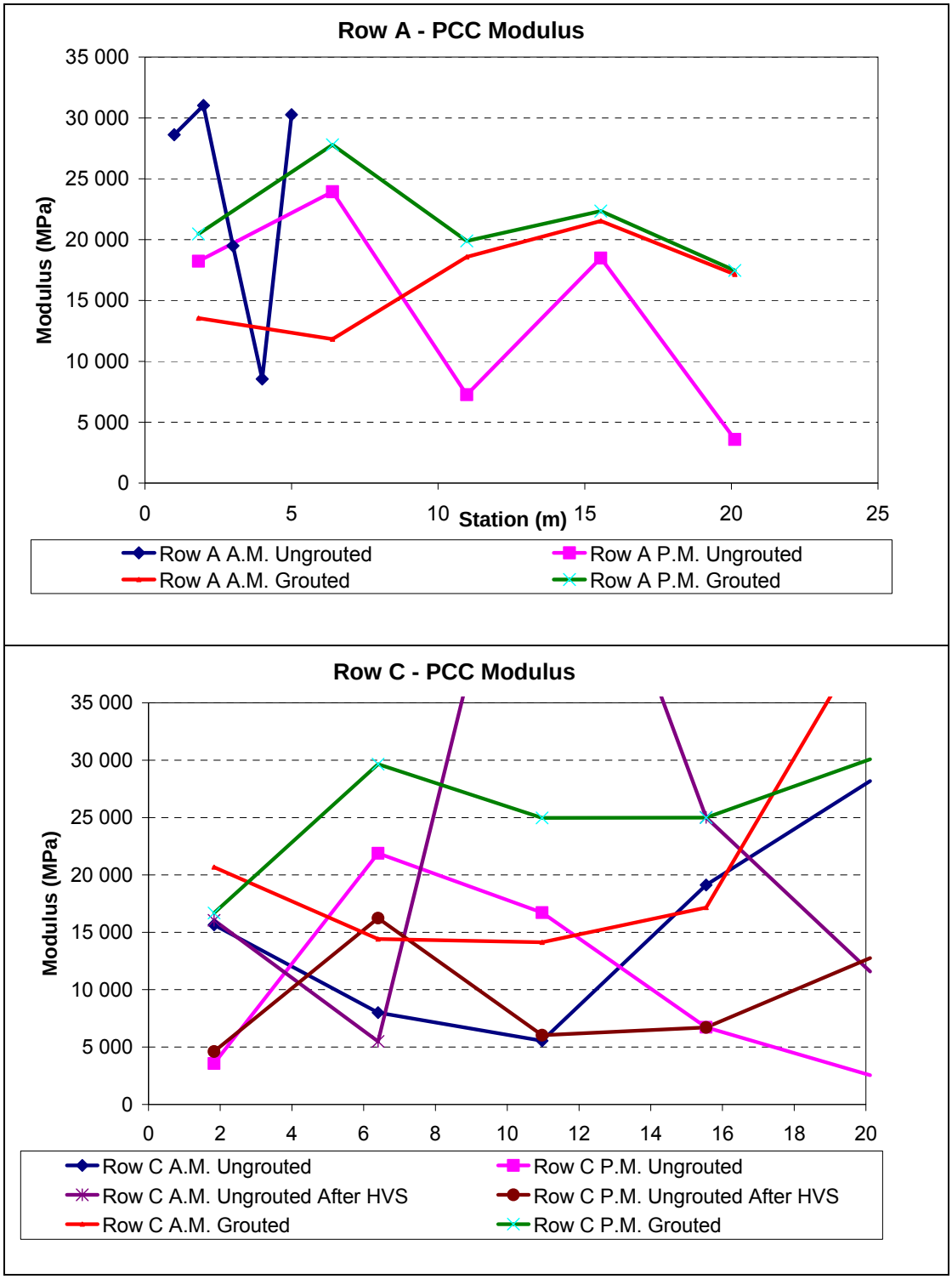

Figure 29. Backcalculated stiffness of concrete layer.

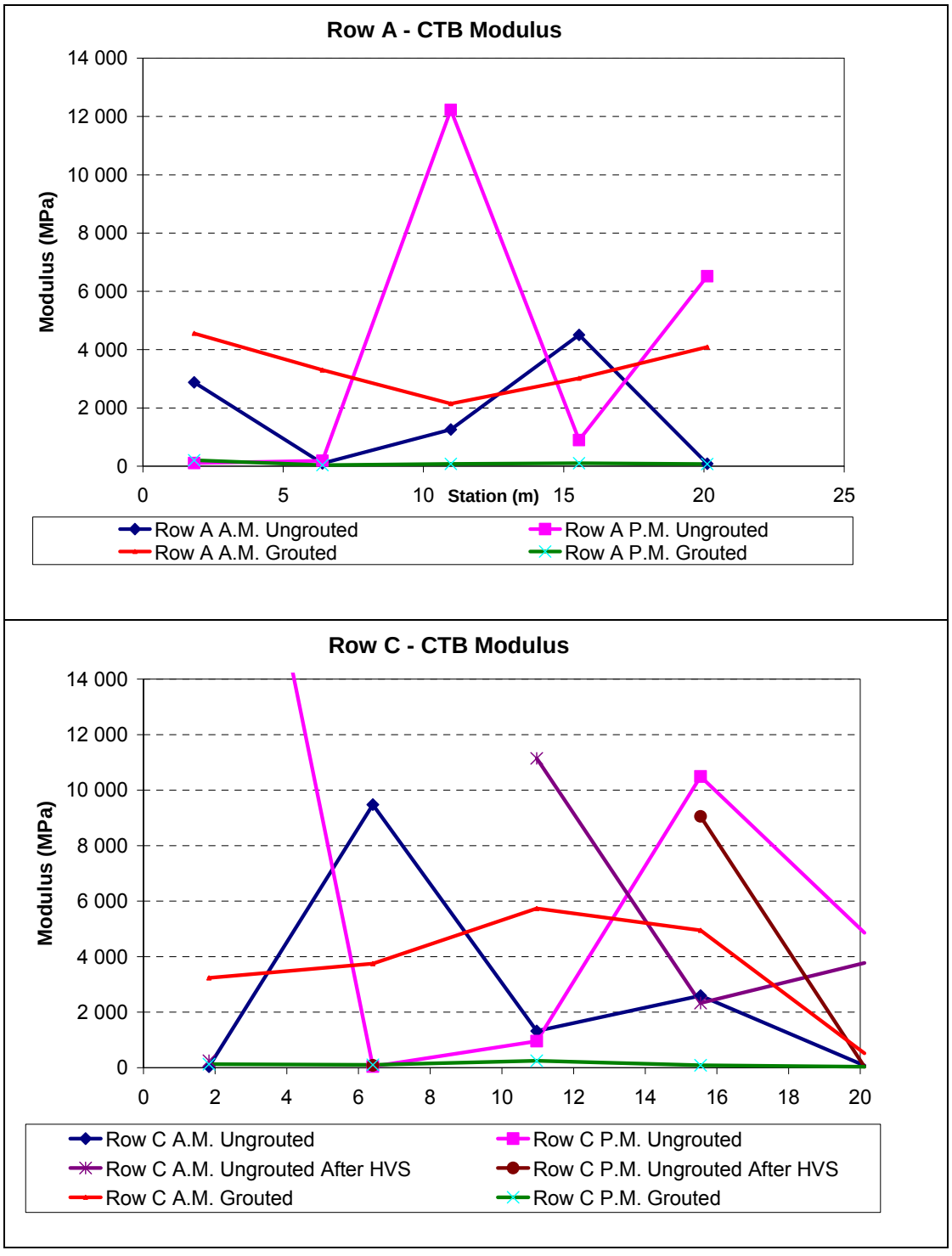

Figure 30. Backcalculated stiffness of CTB layer.

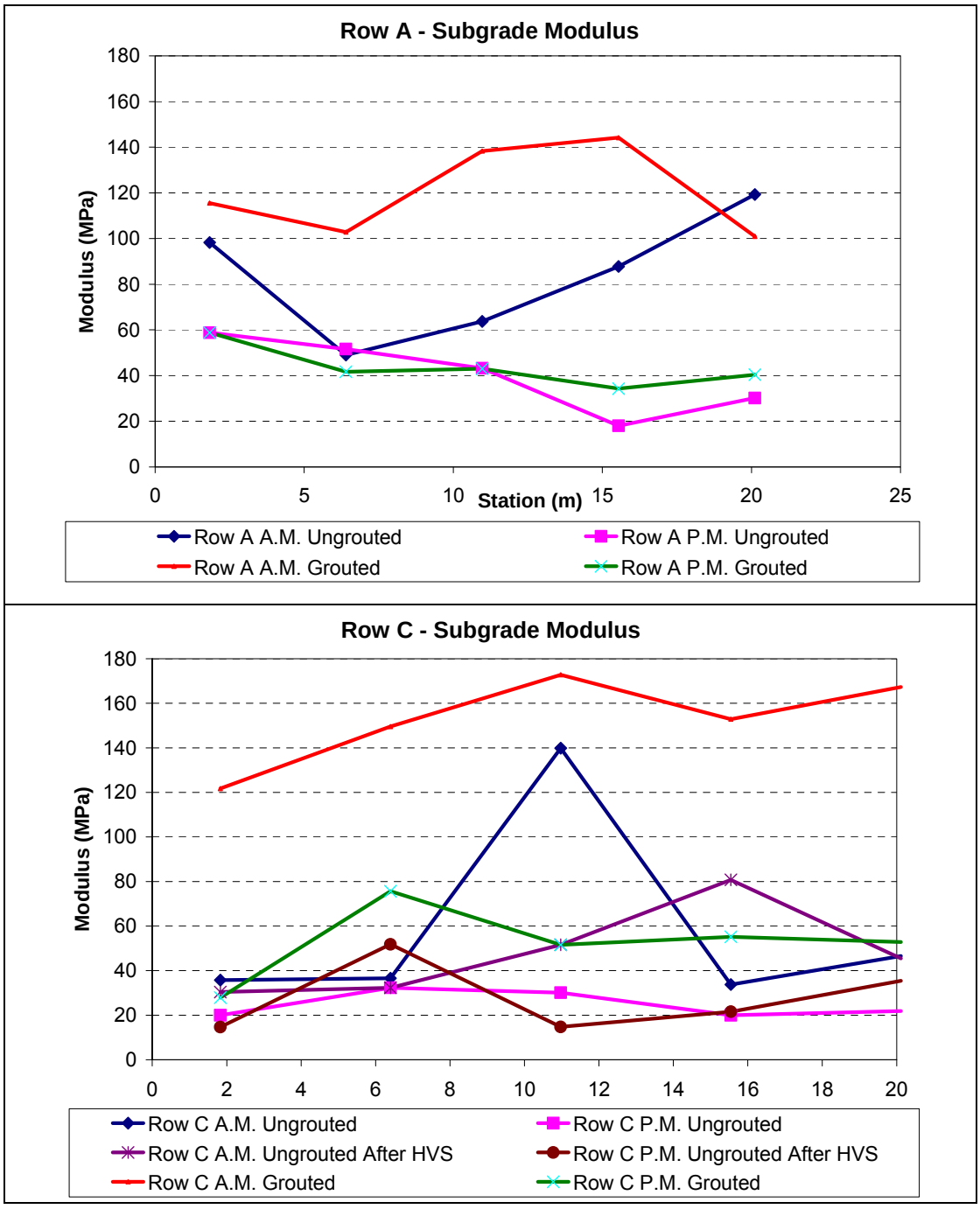

Figure 31. Backcalculated stiffness of subgrade.

2.4 Laboratory Test Results

Beams of 150 by 150 by 450 mm (6 by 6 by 18 in.) were cast from the dowel and bedding grouts at the time of grouting. These beams were tested after one, fourteen, and twenty-eight days curing to determine the modulus of rupture. Table 10 summarizes the modulus of rupture results which are plotted in Figure 32 for the dowel grout and in Figure 33 for

the bedding grout. It can be seen that the bedding grout is considerably weaker than the dowel grout, and that the dowel grout has strength similar to that of concrete slabs.

Table 10. Modulus of Rupture (MPa) Results for the Dowel and Bedding Grout

Dowel Grout			Bedding Grout		
Curing Age (days)			Curing Age (days)		
1	14	28	1	14	28
3.06	3.89	5.29	1.09	1.21	1.88
3.94	4.52	5.07	1.19	1.21	1.51
		5.04	0.87	1.23	
3.5*	4.2*	5.1*	1.1*	1.2*	1.7*

* Average modulus of rupture.

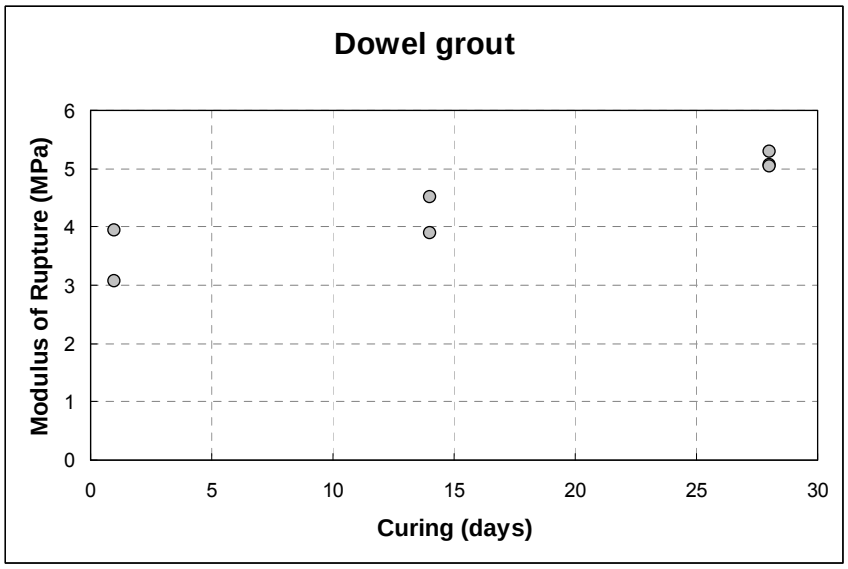

Figure 32. Dowel grout modulus of rupture plotted against curing time.

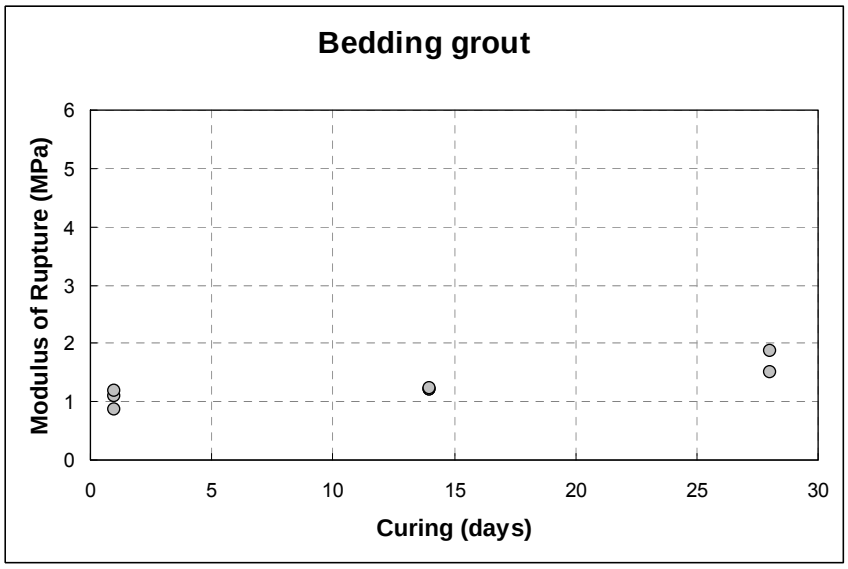

Figure 33. Bedding grout modulus of rupture plotted against curing time.

3. TEST SECTIONS NOMENCLATURE AND INSTRUMENTATION

3.1 Test Nomenclature

As mentioned earlier, a test grid consisting of two lanes each with five pre-cast slabs was constructed for this experiment. Two test sections were established, one on the north side and one on the south side. These two test sections were designated 597FD and 598FD, according to the convention for all HVS tests performed by the UCPRC[3]. Throughout this report these two test sections are referred to as Test 597FD and Test 598FD. Two specific phases of the experiment were labeled with two extra letters to indicate "thermal curling" (TC), and "ungrouted" (UG). This system of nomenclature is consistent with the global HVS database used by the HVS International Alliance.

Figure 34 shows approximately at scale the length of the HVS with respect to the test grid. Two joints were studied in each section. The approximate area of the pavement trafficked with the HVS wheel at each section is also shown.

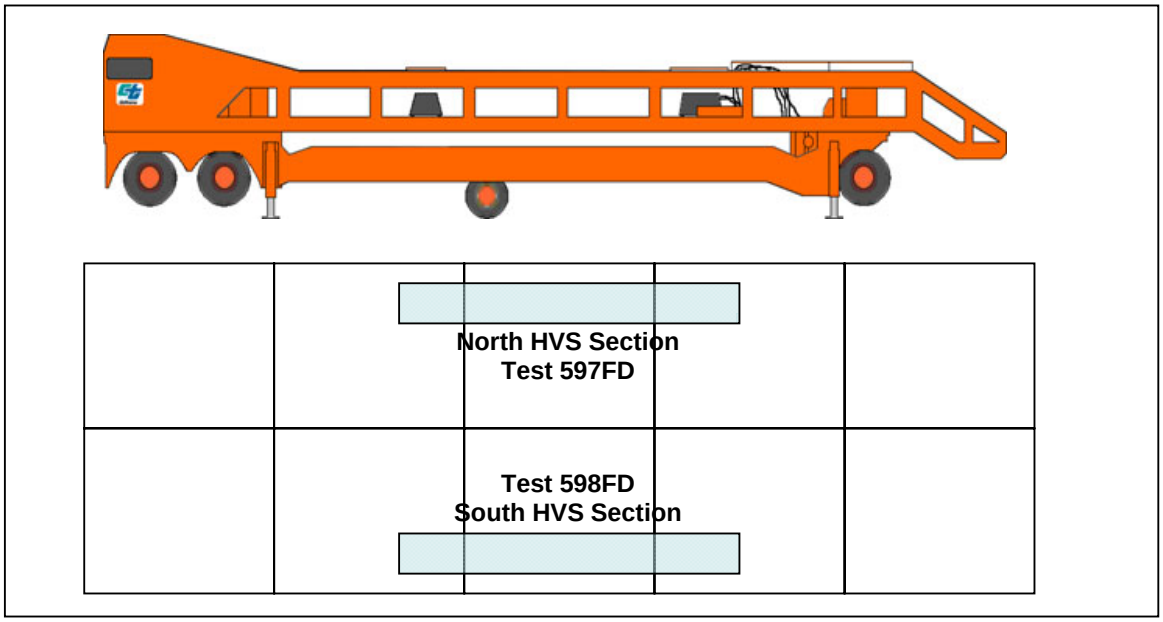

Figure 34. Schematic of the positioning of the HVS and trafficked areas in tests 597FD and 598FD.

[3] The abbreviations FD and RF attached to test section numbers 597 and 598 refer to testing performed under "field" conditions and at the Richmond Field Station, respectively.

(a) 597FD test (b) 598FD test

Figure 35. Photographs of HVS2 during Tests 597FD and 598FD.

3.2 Instrumentation

This section provides an overview of all the instrumentation locations on both lanes of the test grid of pre-cast slabs. Not all the instruments were used at the same time; the instrumentation detail of each HVS test is provided in the sections relating to each specific HVS test. The instrumentation is concentrated mostly on the center column of slabs in the five-by-two grid. Therefore, standing on the southern longitudinal edge of the slabs looking north and numbering the slabs from left to right starting at the top, left-hand corner most of the instrument locations are on slabs 3 and 8 as shown in Figure 36. The symbol "J" is used to indicate vertical joint-deflection measurement devices (JDMD) and the symbol "H" is used to indicate horizontal joint-deflection measurement devices. JDMDs are linear displacement measurement devices that have reference rods anchored away from the slabs, and measure absolute vertical deformations. Horizontal JDMDs are mounted across joints and measure relative opening and closing of the joint (the sensors do not identify the contribution of the individual slabs to the total deformation).

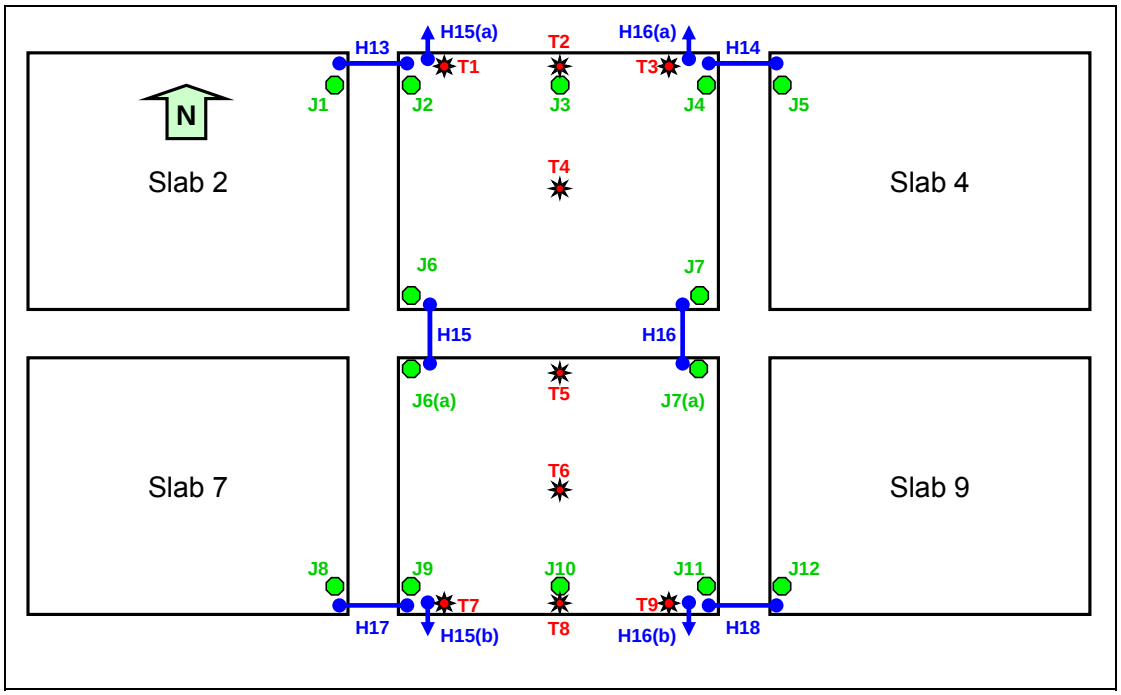

Figure 36. Complete set of thermocouple and JDMD locations.

Thermocouples, indicated by the symbol "T" in Figure 36, were installed at depths of 10, 60, 110, 160, and 210 mm in the 220-mm thick slabs.

Multi-depth Deflectometers (MDDs) are vertical displacement measurement devices installed in the slab. Each module in an MDD is anchored at a different depth in the pavement. To install a MDD, a 38-mm (1.5-in.) hole is first drilled through the pavement. A metal anchor rod is inserted into the hole and embedded in concrete several meters below the pavement. Gauges are anchored to the sides of the hole at different depths in the pavement, with the metal rod passing through them. MDDs were installed close to the location of vertical JDMDs 1, 2, 4, 5, 8, 9, 11, and 12. The MDD modules were installed in the top-cap as close to the surface as possible, at 230 mm (9 in) depth at the top of the CTB, at 380 mm (15 in) depth at the bottom of the CTB, and at 680 mm (27 in)depth in the subgrade. All the MDDs and vertical JDMDs were anchored at a depth of 3 m. Some of the sensor anchors can be seen in Figure 38, where the wheel trafficked and the diamond ground areas are shown. Figure 38 shows examples of installed JDMDs and MDDs. Figure 39 illustrates the JDMD instrumentation at the two joints and at mid-slab for Test 598FD.

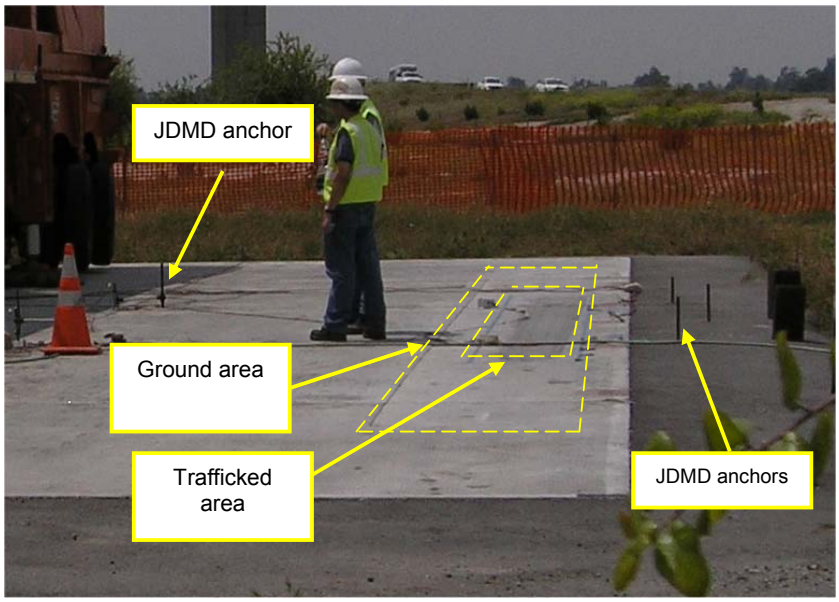

Figure 37. Trafficked test area and some JDMD anchors for Test 597FD.

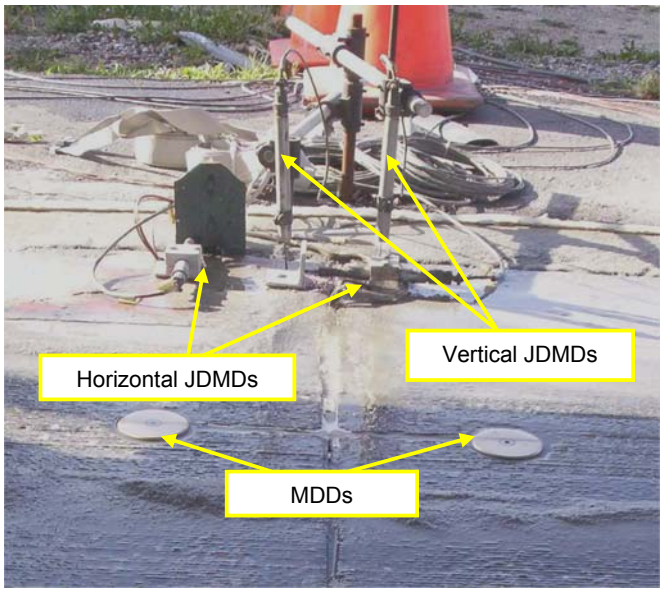

Figure 38. Examples of JDMDs and MDDs.

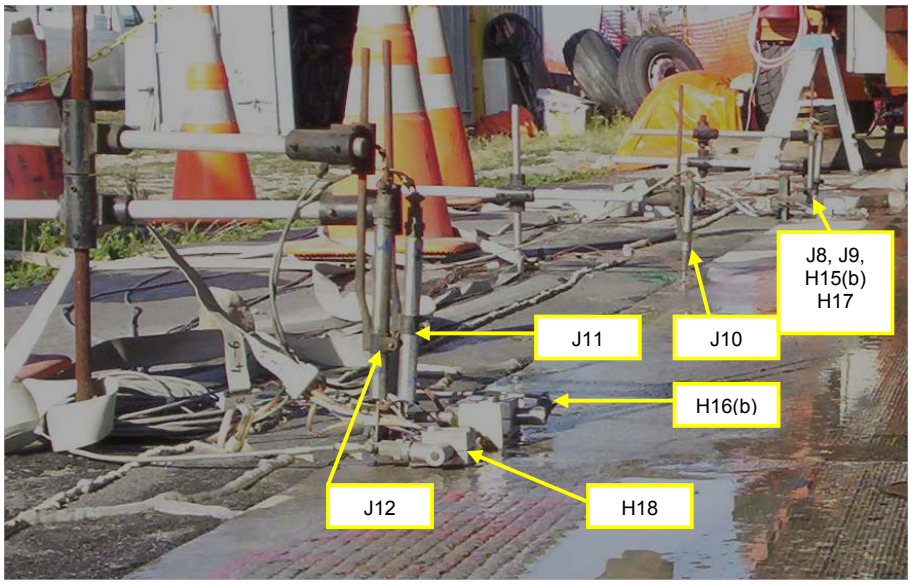

Figure 39. Photograph of JDMDs for Test 598FD.

4. TESTS PERFORMED BEFORE GROUTING

4.1 Thermal Curl Test 597FDTC

Before the HVS was placed on the test slabs, the thermal curl of the ungrouted slabs was tracked over a 24-hour period from 14h00 (2 p.m.) on May 27, 2005, to 14h00 on May 28, 2005, without any loading being applied to the slabs. The instruments monitored on an hourly basis during this time period are shown in Figure 40.

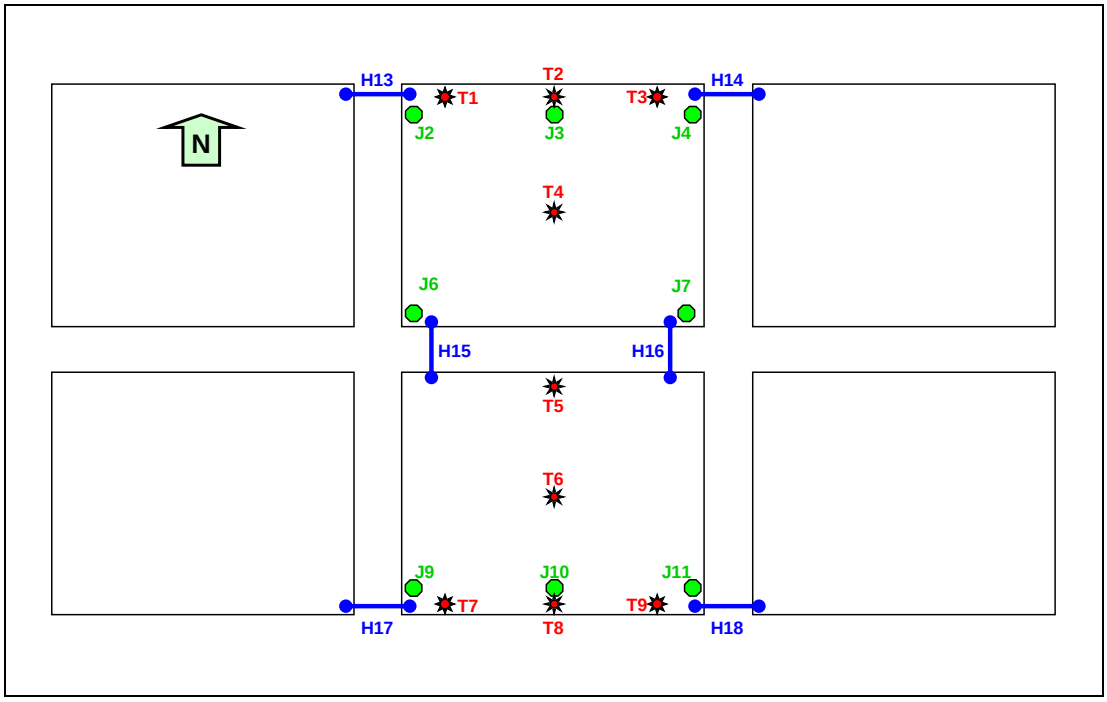

Figure 40. Thermocouples and JDMDs monitored during the thermal curl test on the ungrouted slabs.

The average slab temperature and temperature gradient were calculated from the temperature data recorded at five depths for each of the thermocouples shown in Figure 40. The average slab temperature is shown in Figure 41 and the temperature gradient in Figure 42. The JDMDs can only measure the relative movement of the slab since the start of the test with no indication of the neutral position of the slab. An assumption therefore had to be made that the slabs were in a neutral position at the time the temperature gradient was zero. This occurred on two occasions, between 18h00 and 19h00 on May 27, 2005, and between 09h00 and 10h00 on May 28, 2005. The JDMD readings at 10h00 on May 28, 2005, were therefore assumed to represent the neutral position of the slab and all other measurements were adjusted relative to the measurement taken at this time.

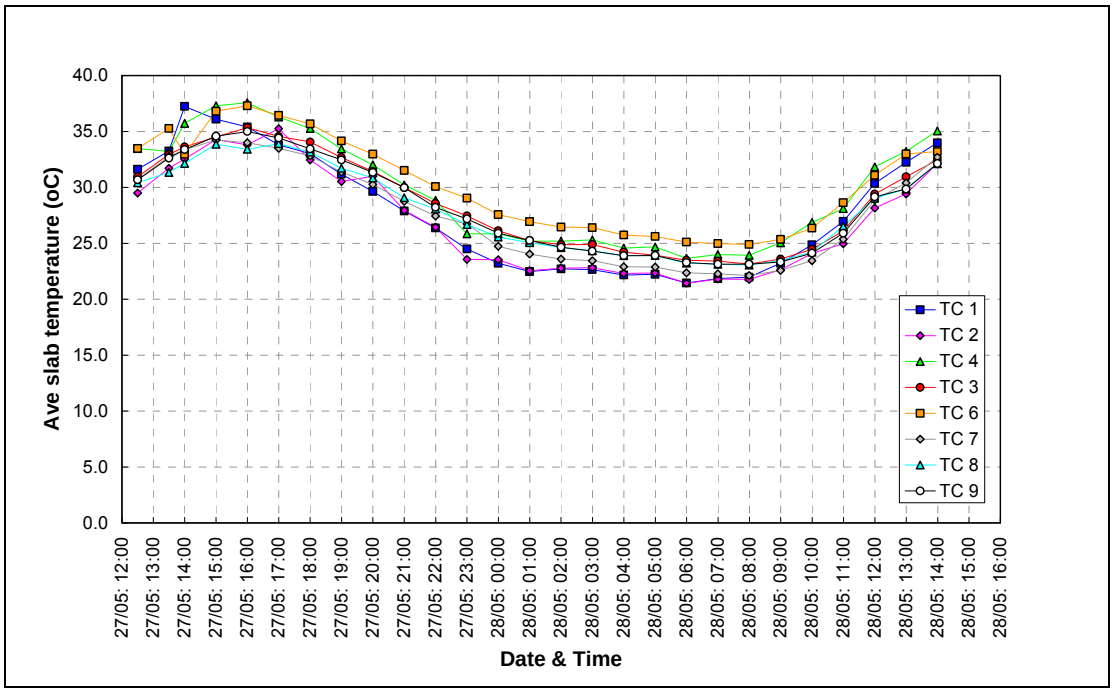

Figure 41. Average slab temperature during the ungrouted thermal curl test.

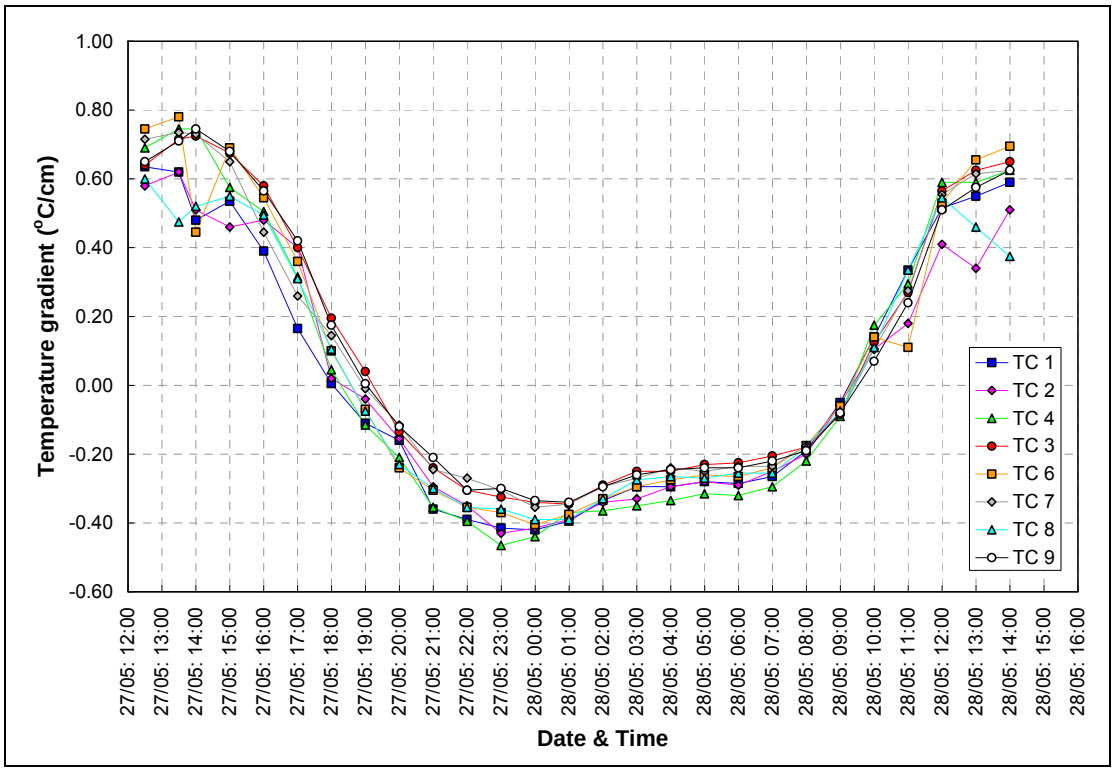

Figure 42. Temperature gradient during the ungrouted thermal curl test.

Figure 43 shows the relative movement (in terms of the previously determined neutral position) of the all the vertical JDMDs shown in Figure 40 at the corners of the slabs. As expected, the corners of the slabs curled upward during nighttime when the slabs had a negative

temperature gradient (warmer at the bottom than at the top of the slab). Figure 44 shows the adjusted joint activity recorded by the horizontal JDMDs. Again, as expected the joints closed up at the higher temperatures during daytime. The highest vertical movement occurred at JDMD 6 with a range from 1.5 mm downward to 1.5 mm upward (3 mm total) and the smallest movement occurred at JDMD 4 with a range from 0.5 mm downward to 0.5 mm upward (1 mm total). The range of joint opening and closing was from 0.2 mm to -0.8 mm giving a total joint activity of 1 mm.

In an effort to determine the relationship between temperature gradient and vertical curl, the adjusted JDMD readings were plotted with the temperature gradient data. Figure 45 shows a typical example of the adjusted vertical movement at JDMD 9 plotted with the temperature gradient calculated from the temperature data for the closest thermocouple, TC7. It is apparent that the vertical curl is correlated to the temperature gradient.

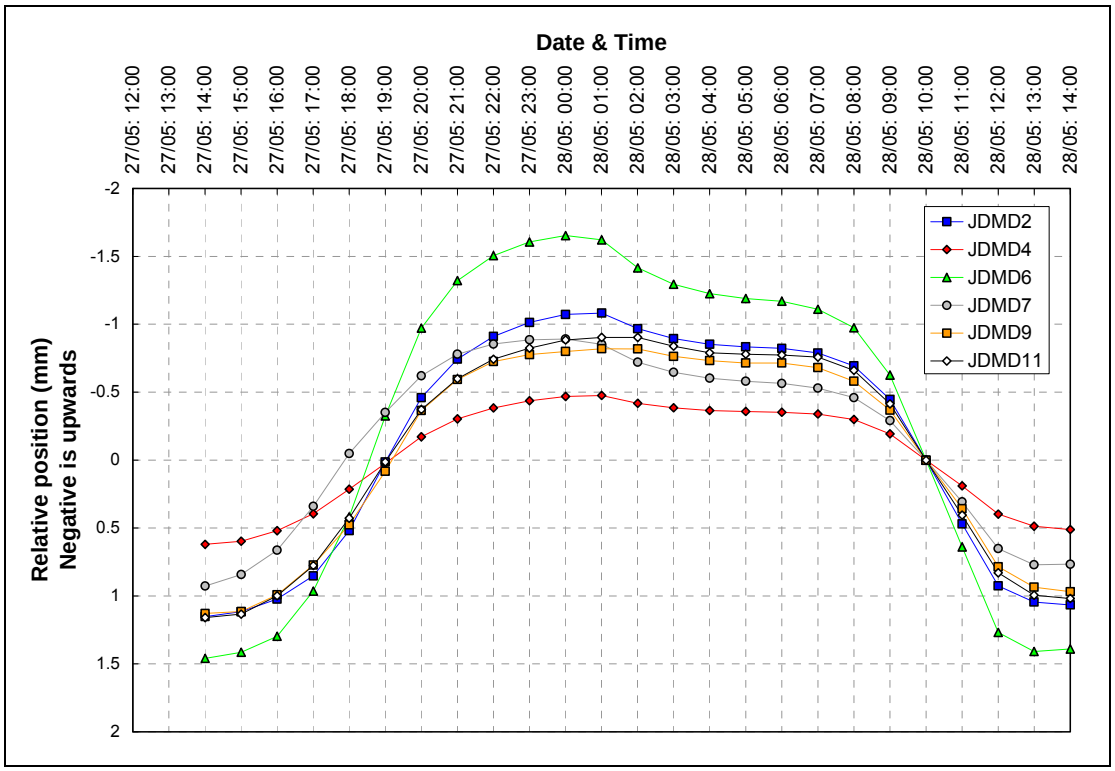

Figure 43. Adjusted vertical movement of the slab corners during the ungrouted thermal curl test.

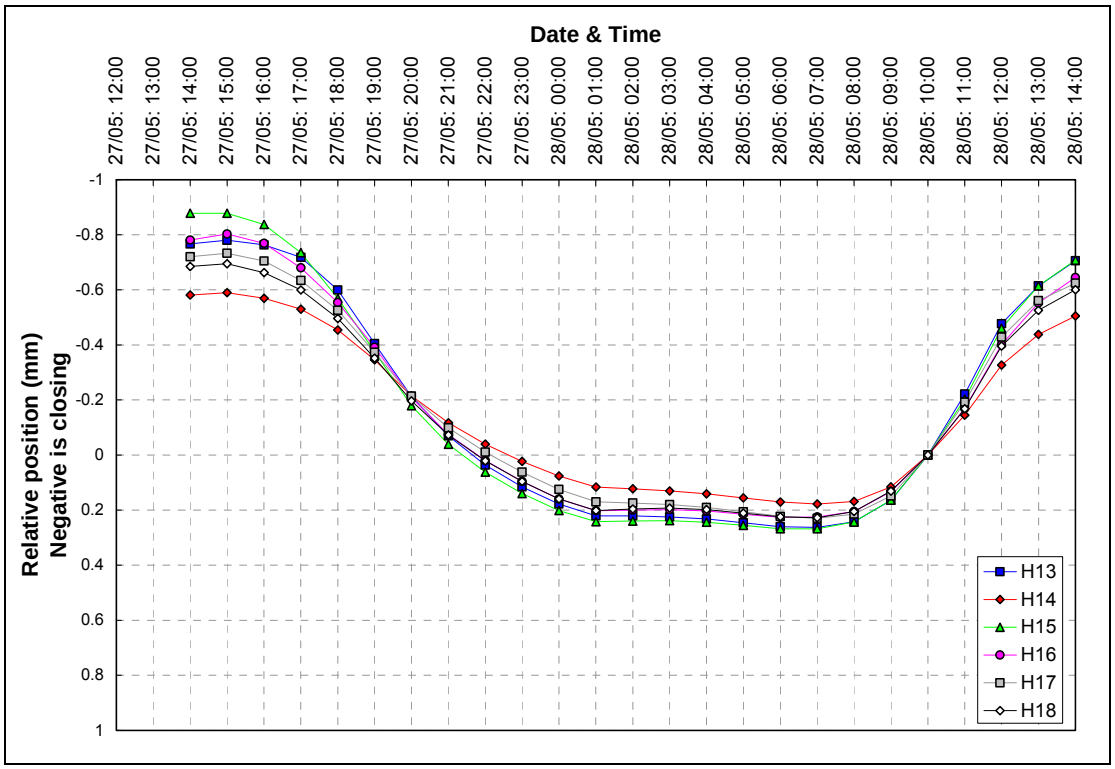

Figure 44. Adjusted horizontal joint activity during the ungrouted thermal curl test.

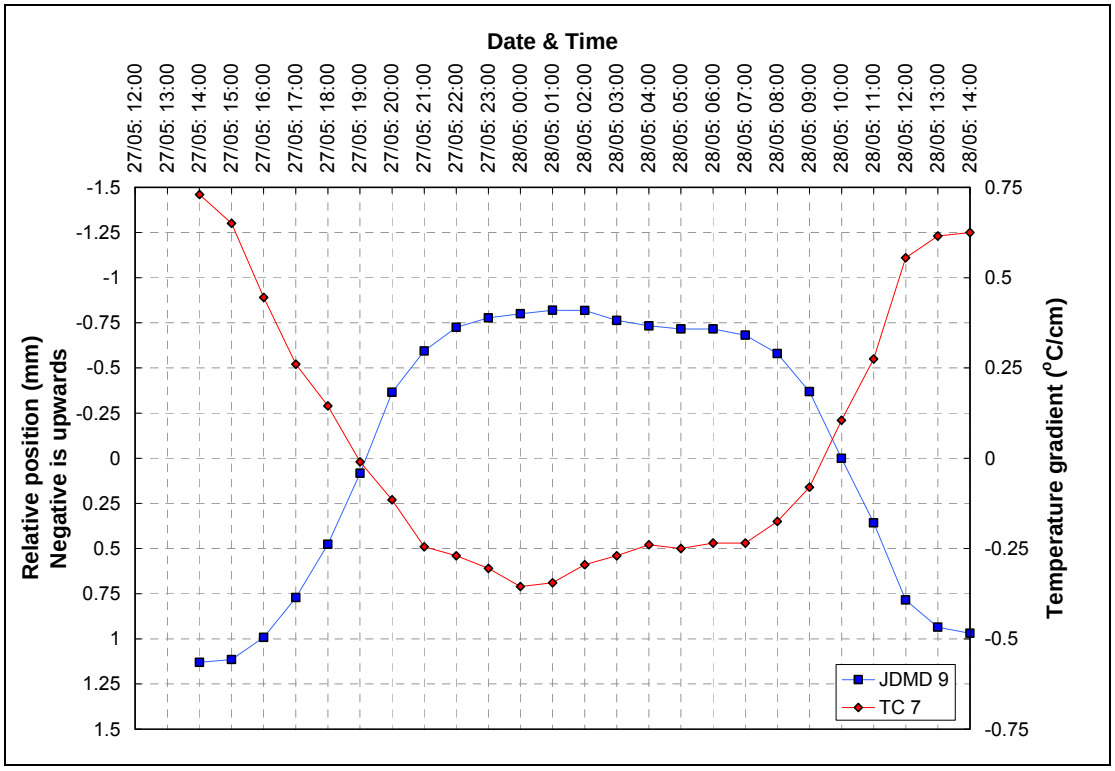

Figure 45. Example of the relationship between the temperature gradient and vertical movement of the slab corners.

This correlation was explored further by plotting the adjusted vertical corner movement against the temperature gradient for the JDMDs with thermocouples in close proximity. The results from this process are shown in Figure 46.

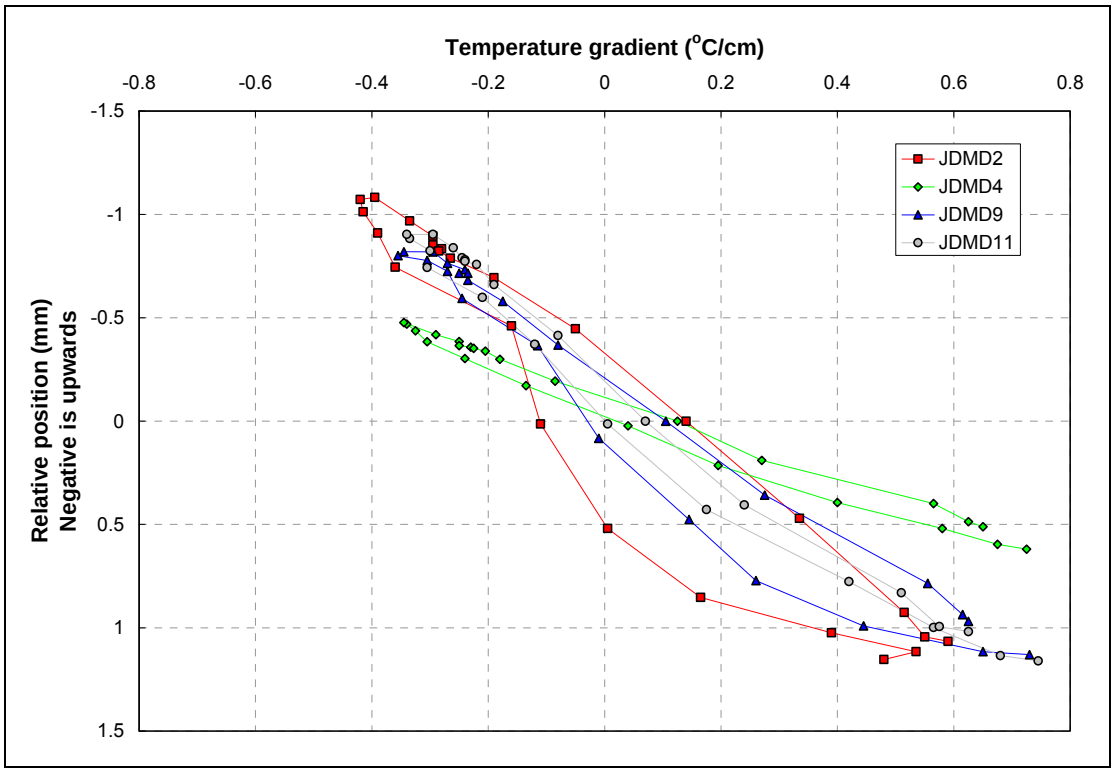

Figure 46. The correlation between the temperature gradient and vertical movement of the slab corners.

The response at JDMD 4 seems to be more constrained than at the other JDMDs with 1 mm less total movement at JDMD 4 over the same range of temperature gradient experienced by the other slab corners, and it is simply an indication of small asymmetric deformations that could be caused by a difference in support conditions, small geometric differences in the slab, or non-uniform joint width. JDMD 4 and 11 were located on the doweled side of their respective slabs, while JDMD 2 and 9 were on the slotted side of the slabs. This could have resulted in a reduced range of vertical movement at JDMD 4 and 11 compared to JDMD 2 and 9. However, only JDMD 4 experienced less movement.

A similar analysis was done for the horizontal joint activity by plotting the horizontal deformation (opening and closing of the joint) against temperature gradient as shown in Figure 47. Temperature gradient is primarily responsible for rotation of the joint faces, although it is also an indirect measure of average temperature in the slab. This is the likely reason for the apparent nonlinearity of the relation between deformation and temperature gradient. Horizontal joint activity was also plotted against the temperature recorded by the surface thermocouple sensors.

The result from this process is shown in Figure 48 and yields a much more linear correlation between the two parameters.

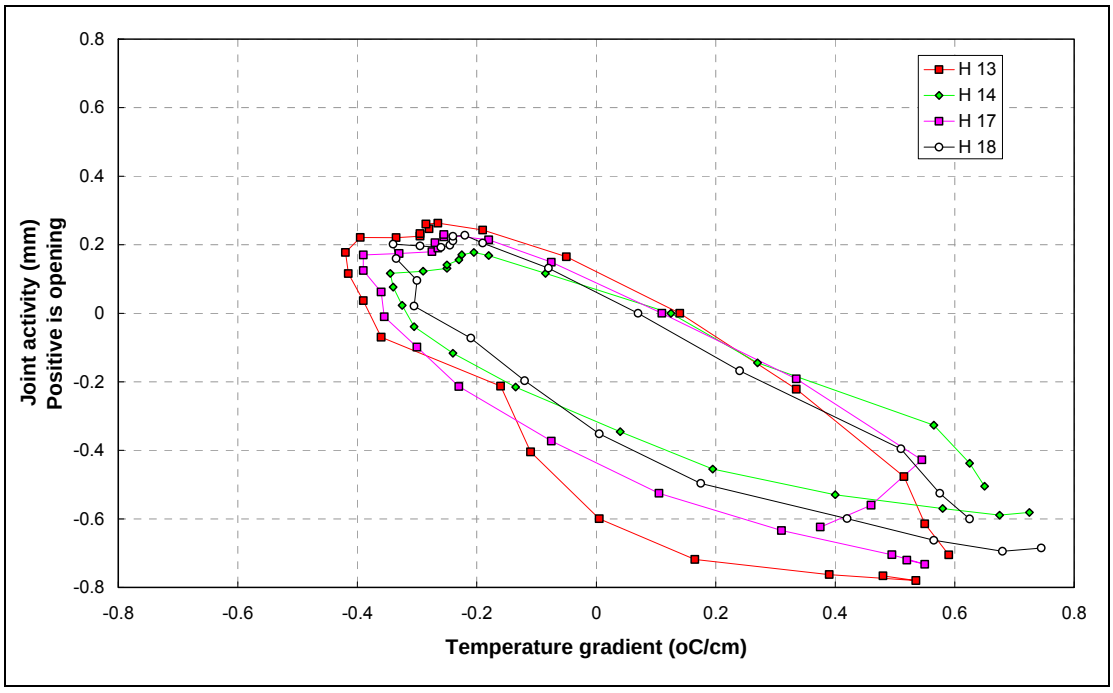

Figure 47. The correlation between temperature gradient and horizontal joint activity

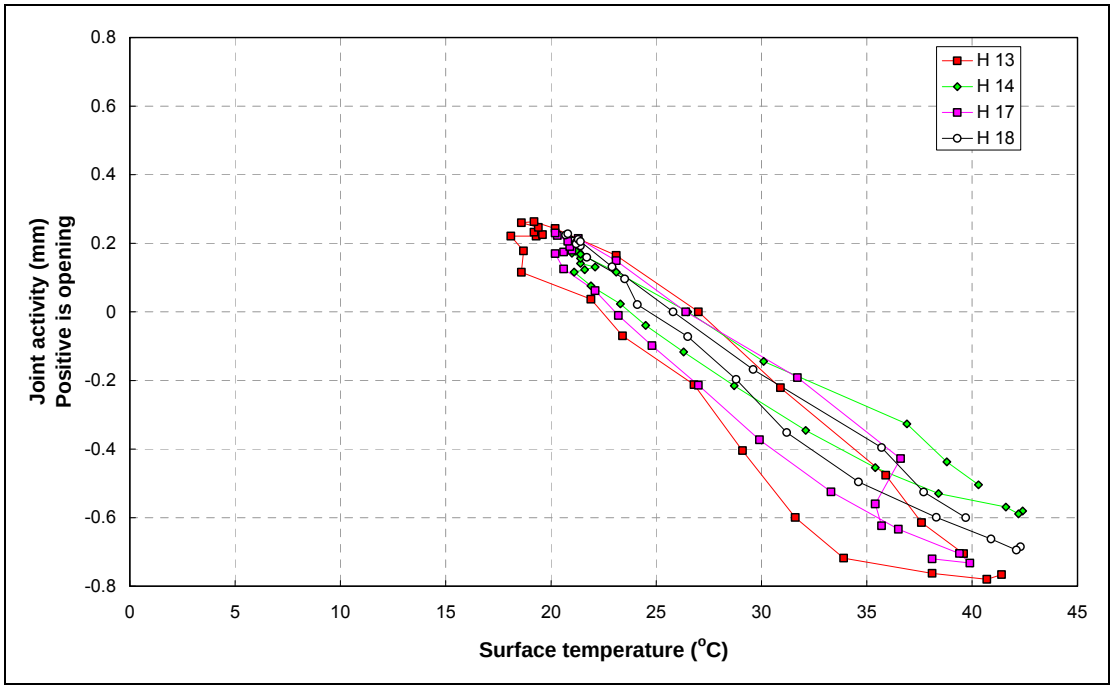

Figure 48. The correlation between the surface temperature and horizontal joint activity.

In summary the following observations are made regarding the ungrouted thermal curl test:

- The vertical curl at the corners of the unrestrained slabs varied over a range from 1 mm at JDMD 4 to 3 mm at JDMD 6 for a temperature gradient ranging from -0.4°C/cm to +0.8°C/cm (temperature differential top to bottom of -9°C to +17°C);
- The horizontal joint activity had a total movement of 1 mm for a surface temperature range from approximately 20°C to 40°C;
- There is a strong linear correlation between the temperature gradient and the vertical movement at the slab corners caused by thermal curl; and
- There is a strong linear correlation between the surface temperature and horizontal joint activity.

4.2 Ungrouted Load Tests Background

Two HVS tests were performed on the ungrouted slabs to simulate the exposure of the ungrouted Super-Slab® System to traffic from the time of placement to the time of grouting which normally occurs during the next nighttime closure. These tests were performed on the central three slabs of each row of the five-by-two grid to ensure that both lanes were exposed to the same loading conditions in the ungrouted state. In addition to the thermal movement, the resilient deflection of the ungrouted slabs was also recorded in sets of three load cycles taken at hourly intervals during these tests.

The traffic loading for the ungrouted tests was determined from an Average Daily Truck Traffic (ADTT) count of 6,767 for the southbound direction of I-15 in 2000 as provided by Caltrans District 8 and the assumption that the contractor would be able to get back to the site to grout it the next night after placement of the slabs. The ADTT of 6,767 was compounded to the year 2005 with a 3 percent growth rate per annum giving an ADTT of 7,853 for 2005. Eighty percent of the truck traffic was assumed to run on the slow lane giving 6,282 trucks per day on the outer truck lane. Given a period of 16 out of 24 hours that the ungrouted pavement will be open to traffic, a further 33 percent reduction was applied to this number resulting in 4,146 trucks in the outer truck lane from one nighttime closure to the next. Assuming 3.8 ESALs per truck, a total of 15,756 ESALs had to be applied. The unidirectional production rate of the HVS is 500 repetitions per hour, therefore requiring 31.5 hours of testing. The duration of the ungrouted tests was therefore set at a minimum of 32 hours to achieve the required traffic loading. The traffic load for the ungrouted tests was planned to be a 40 kN half-axle load, the equivalent of an ESAL, but because of a systematic error in the calibration of the HVS wheel load, the actual wheel load was 60 kN, resulting in the equivalent of approximately 86,500 ESALs being applied to each section during the ungrouted tests.

4.3 Load Test 597FDUG

Figure 49 shows the instrumentation layout for the first ungrouted test, 597FDUG which started at 06h06 on May29, 2005, and ended at 17h27 on May 30, 2005, at 16,002 repetitions of a 60-kN load applied in unidirectional mode from the cabin to the tow-end of the HVS (from west to east or from left to right in terms of the layout shown in Figure 49).

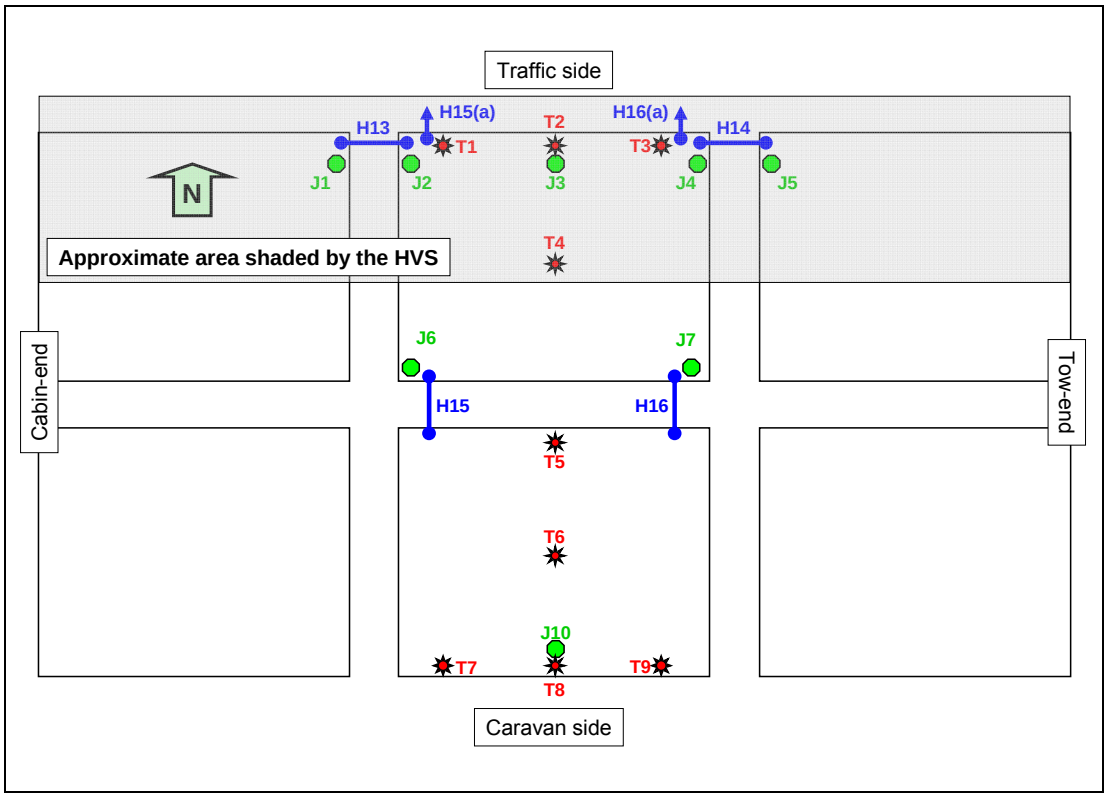

Figure 49. Thermocouples and JDMDs monitored during the first ungrouted test, 597FDUG.

The average slab temperature and temperature gradient were calculated from the temperature data recorded at the five depths for each of the thermocouples shown in Figure 49. The average slab temperature is shown in Figure 50 and the temperature gradient in Figure 51. The temperature moved in a narrow band between 20 and 25°C (67 and 75°F) for most of the test and only exceeded 25°C from 11h00 on May 30, 2005, at a few of the thermocouple locations. The shading effect of the shadow of the HVS on the test section is apparent from the temperature data, with thermocouples 1 to 4 having a lower temperature and temperature gradient after 11h00 on May 30, 2005, than the exposed thermocouples (TCs 5 to 9). The time of zero temperature gradient is also different for the shielded and exposed thermocouples. The exposed thermocouples reached a zero temperature gradient at 11h00 on May 29, 2005, and the shielded thermocouples only reached a zero temperature gradient at 12h00 on May 30, 2005.

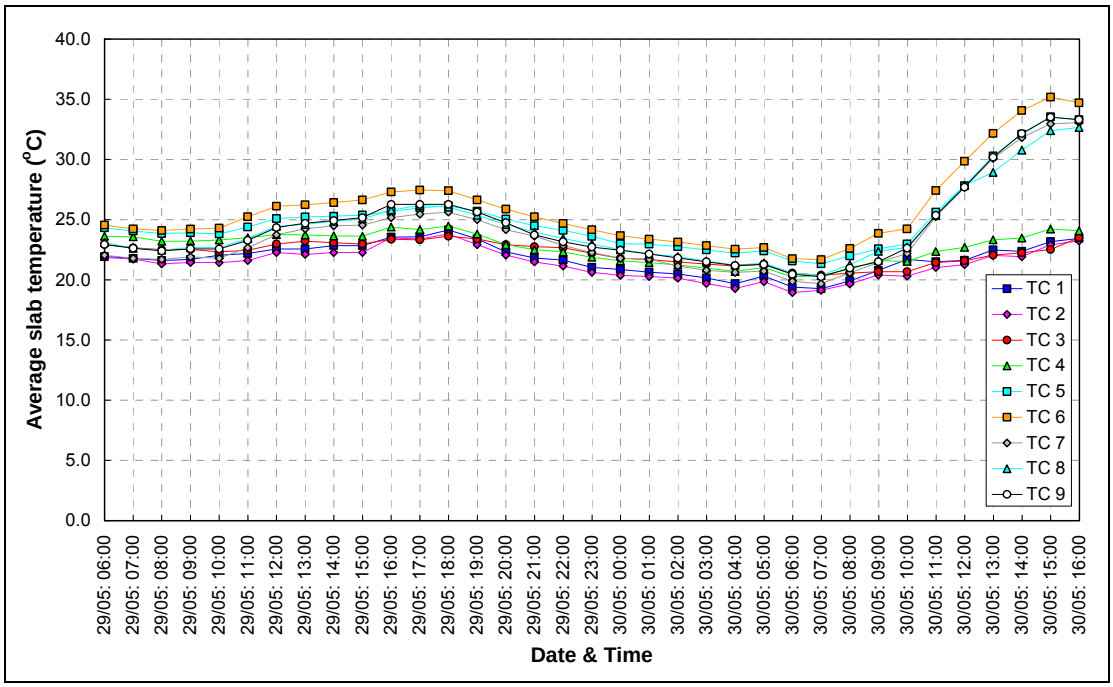

Figure 50. Average slab temperature during the ungrouted test, 597FDUG.

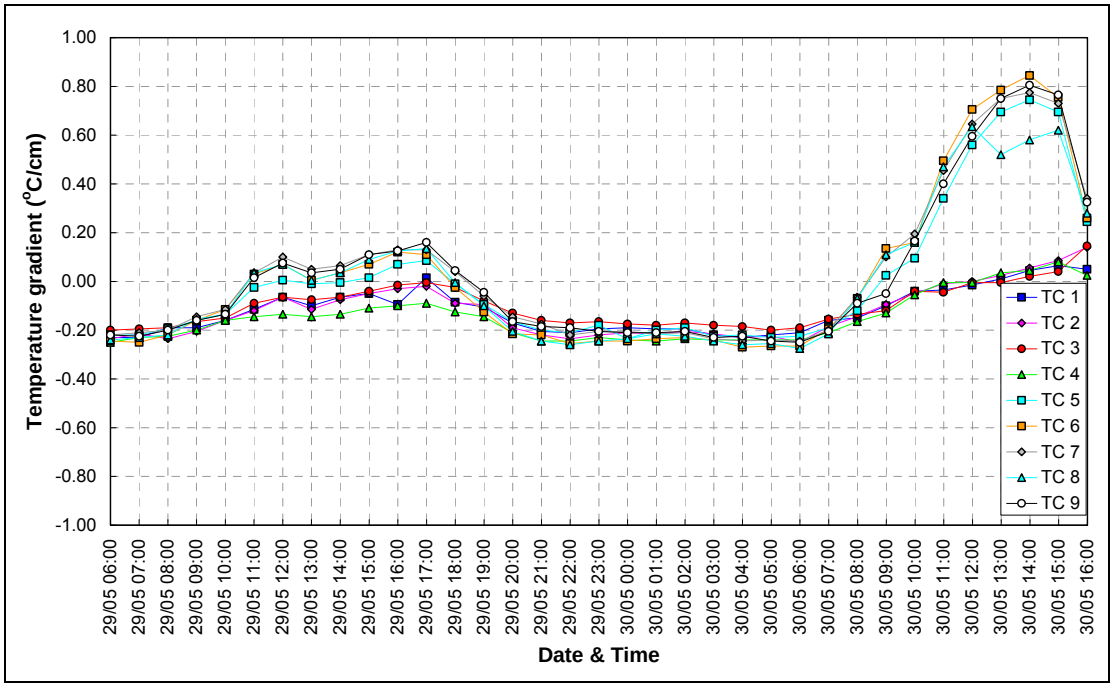

Figure 51. Temperature gradient during the ungrouted test, 597FDUG.

The JDMD readings at 11h00 on May 29, 2005, were therefore assumed to represent the neutral position for the vertical JDMDs 1 to 5 and horizontal JDMDs 13, 14, 15(a), and 16(a) (sensor location shown in Figure 49). The JDMD readings at 12h00 on May 30, 2005, were

assumed to represent the neutral position for the vertical JDMDs 6, 7, and 10, and horizontal JDMDs 15 and 16.

Two types of displacement measurements were taken with the JDMDs: the transient thermal curl of the slabs and the resilient load related deflection. The transient thermal curl of the slabs represents the unloaded condition of the slabs and slowly changes with time as the temperature conditions change while the resilient deflection rapidly increases and rebounds as the wheel passes over a specific point on the pavement.

4.3.1 Thermal Curl Response

Figure 52 and Figure 53 show the transient thermal curl behavior of the slabs during the ungrouted load test 597FDUG in terms of the vertical corner positions and joint activity. Figure 54 and Figure 55 show the difference in the temperature gradient and thermal curl of a slab corner shielded by the HVS compared to an exposed corner. Regardless of these differences, the thermal curl of the shielded and exposed slab corners are determined by the temperature gradient as illustrated by Figure 56 for the shielded corners and Figure 57 for the exposed corners. The relationship between transverse and longitudinal joint thermal curl activity and surface temperature is shown in Figure 58 for the transverse joints and Figure 59 for the longitudinal joints.

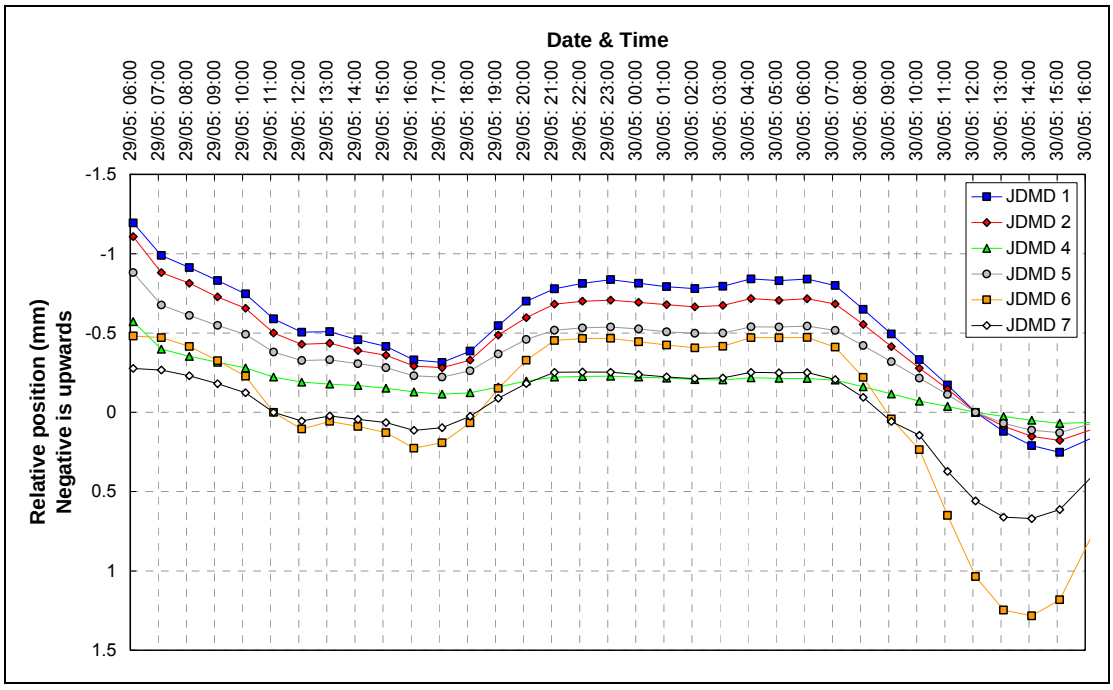

Figure 52. Adjusted thermal curl vertical position of the slab corners during the ungrouted load test, 597FDUG.

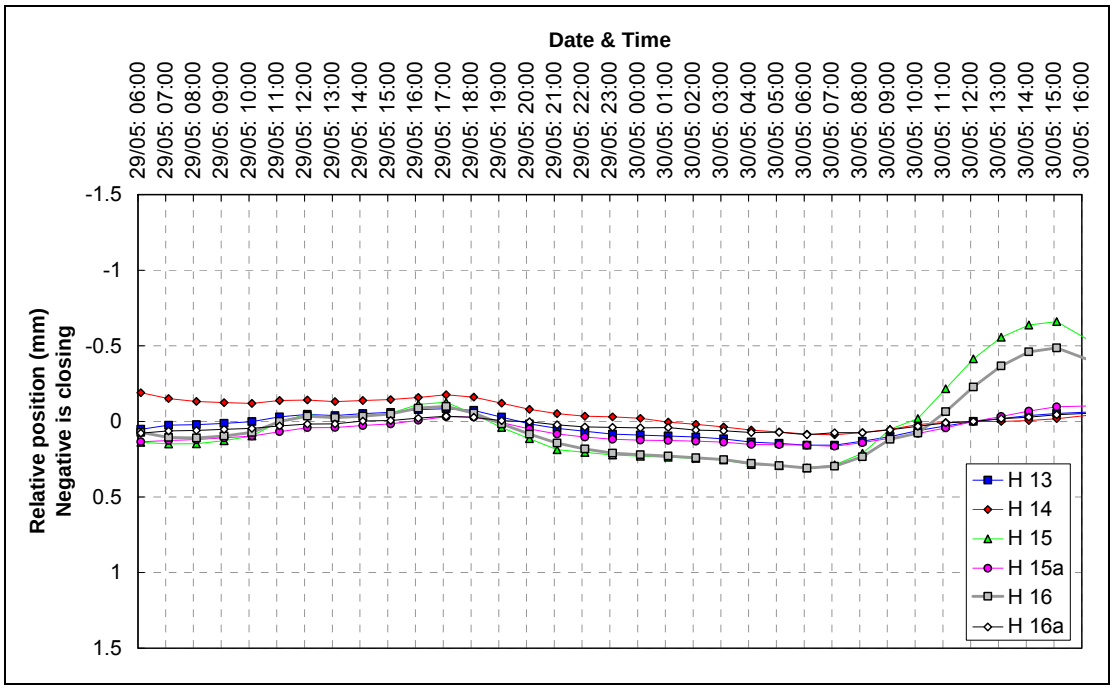

Figure 53. Adjusted thermal curl horizontal joint activity during the ungrouted load test, 597FDUG.

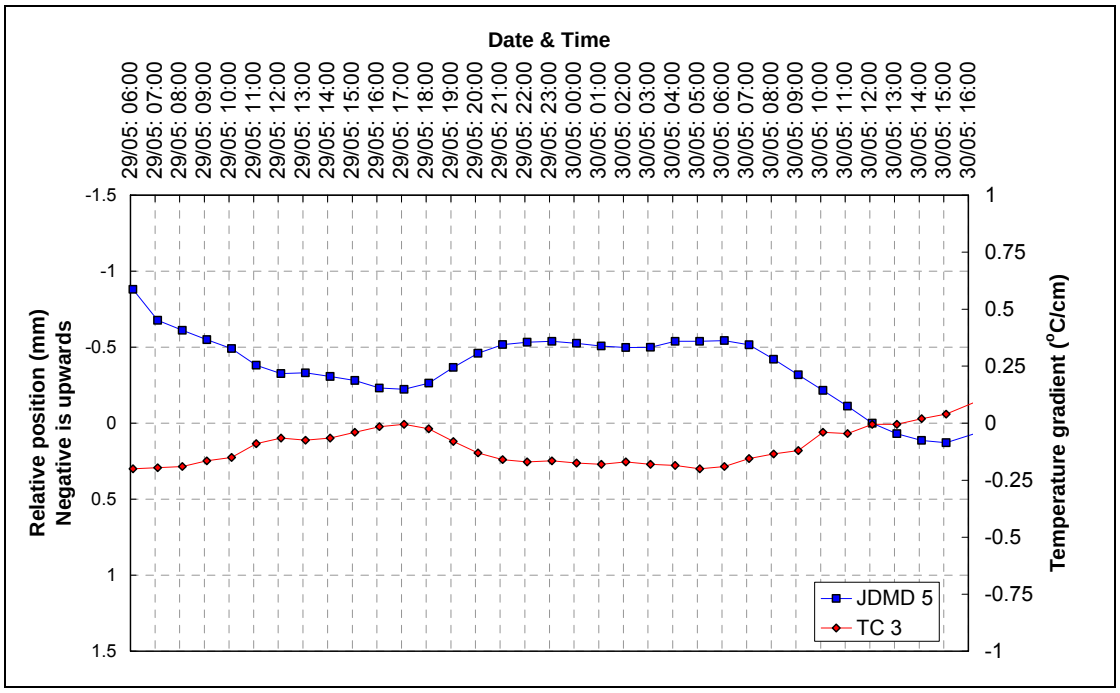

Figure 54. Adjusted thermal curl vertical position and temperature gradient for a shielded slab corner during the ungrouted load test, 597FDUG.

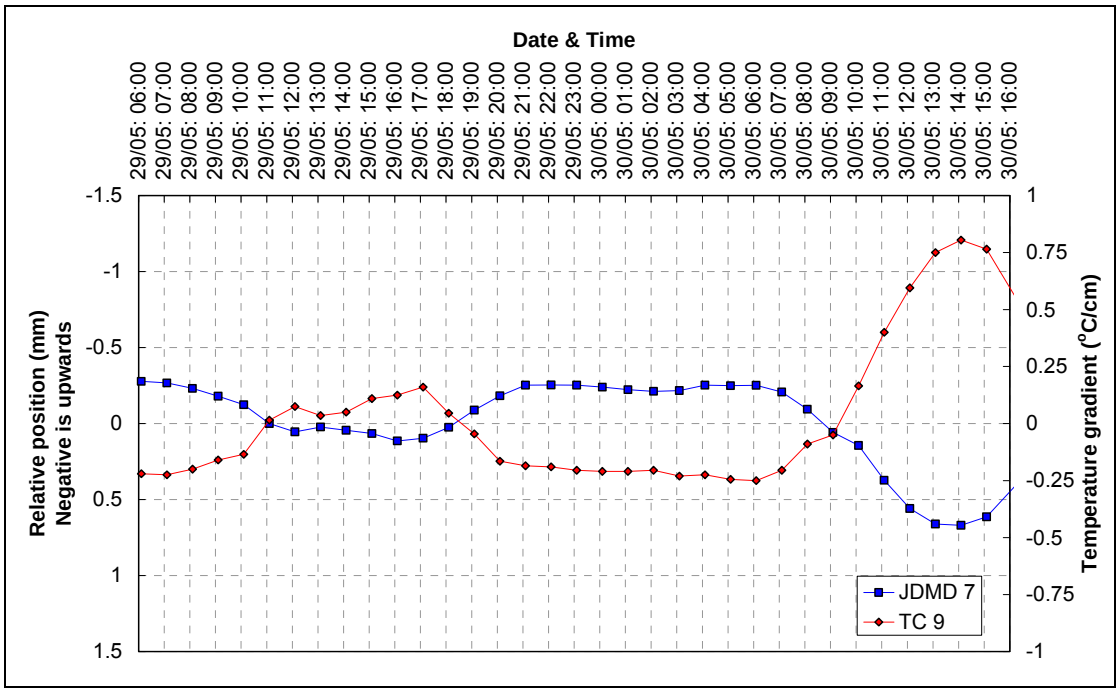

Figure 55. Adjusted thermal curl vertical position and temperature gradient for an exposed slab corner during the ungrouted load test, 597FDUG.

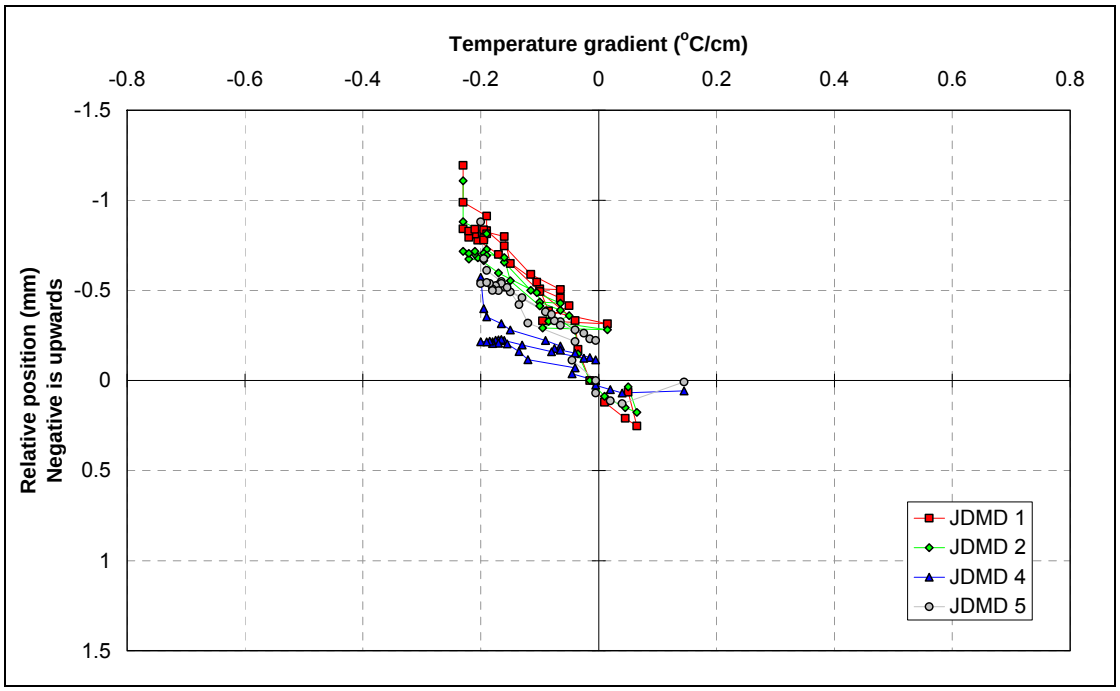

Figure 56. Relationship between thermal curl and temperature gradient for the shielded slab corners during the ungrouted load test, 597FDUG.

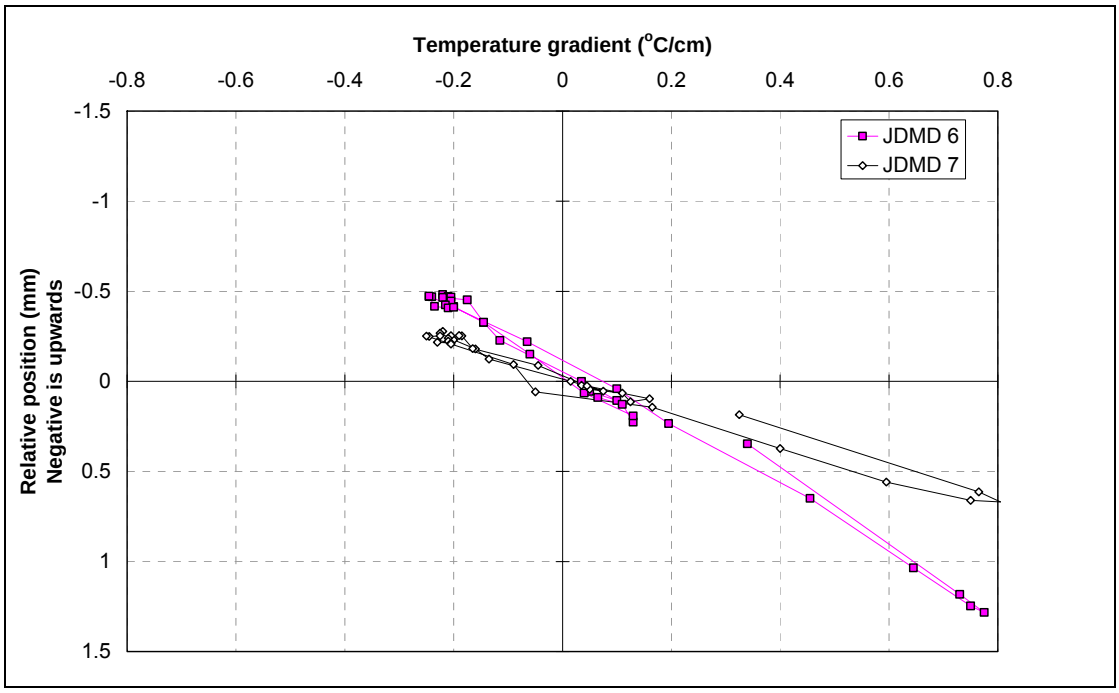

Figure 57. Relationship between thermal curl and temperature gradient for the exposed slab corners during the ungrouted load test, 597FDUG.

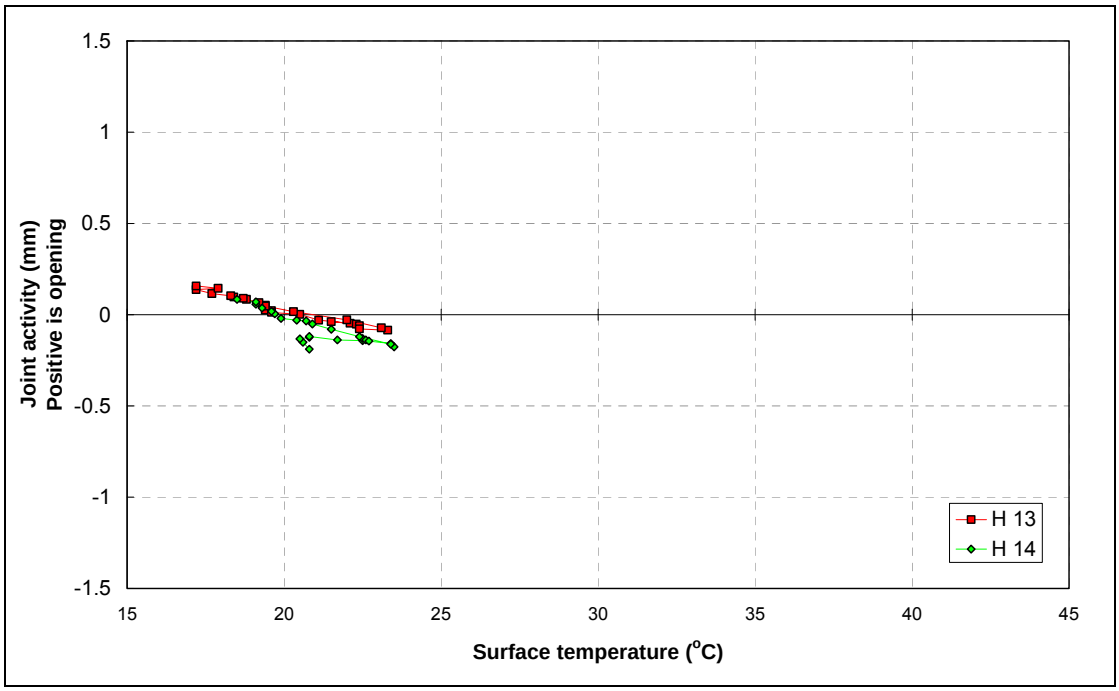

Figure 58. Relationship between transverse joint horizontal deformation caused by thermal curl activity and surface temperature during the ungrouted load test, 597FDUG.

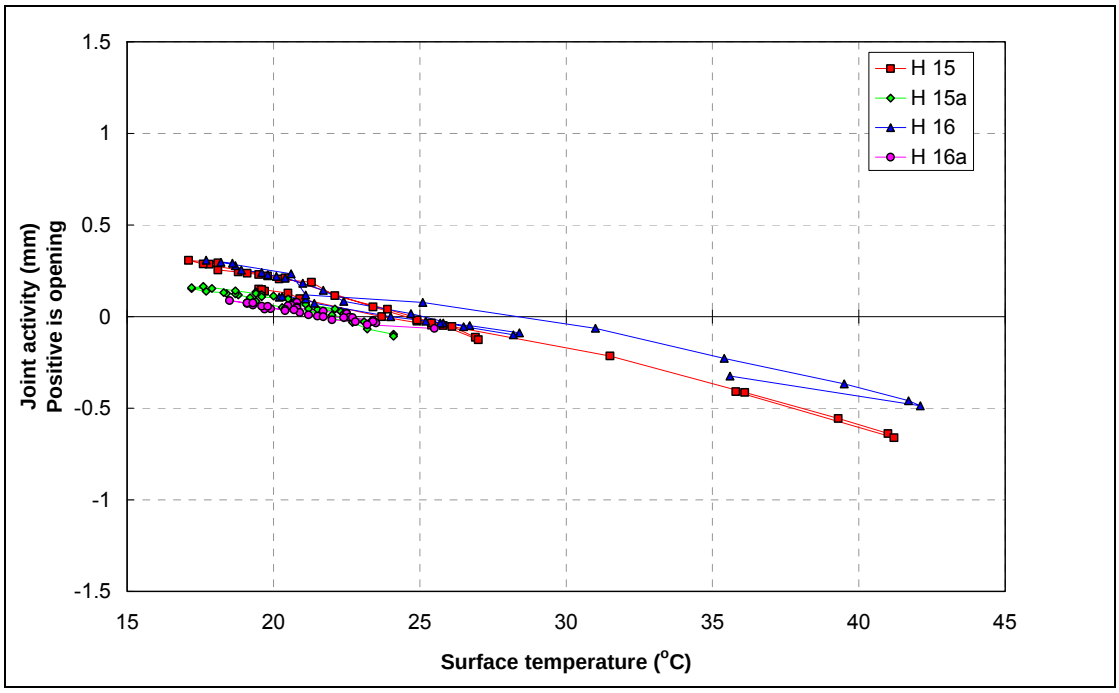

Figure 59. Relationship between longitudinal joint horizontal deformation caused by thermal curl activity and surface temperature during the ungrouted load test, 597FDUG.

4.3.2 Resilient Deflection Response

Figure 60 and Figure 61 show the vertical deflection influence lines for the first and second joints, respectively, on Test 597FDUG at the end of the HVS test. The response at the first joint is symmetrical with an equal amount of resilient vertical deflection of almost 1 mm at the two corners on either side of the joint. There is very little load transfer at the joint with the deflection recorded by JDMD 1 immediately rebounding to zero as the wheel leaves the approach slab. The influence line for JDMD 2 shows that the slab rocked around its transverse axis and the corner at JDMD 2 lifted by about 0.1 mm when the wheel was at the far end of the slab. The response was similar at the second joint where JDMDs 4 and 5 were installed. However, the corner where JDMD 4 was installed is either better supported or the slab is stiffer there than at the other corners as its deflection was significantly lower.

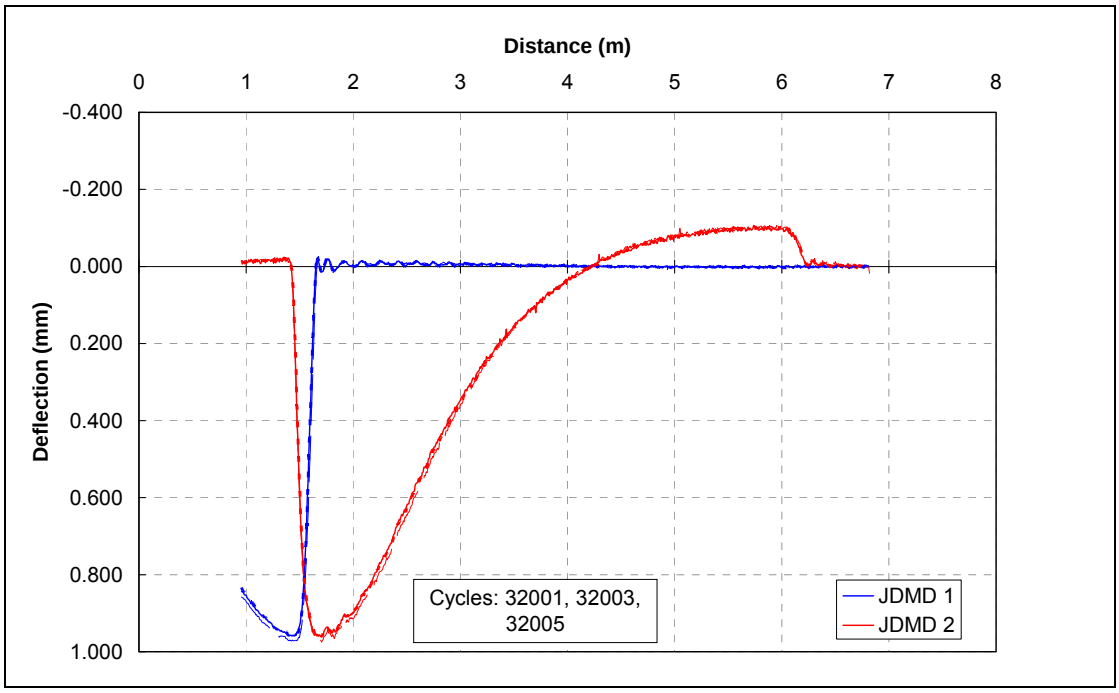

Figure 60. Resilient vertical corner deflection influence lines for the first joint on the ungrouted load test, 597FDUG.

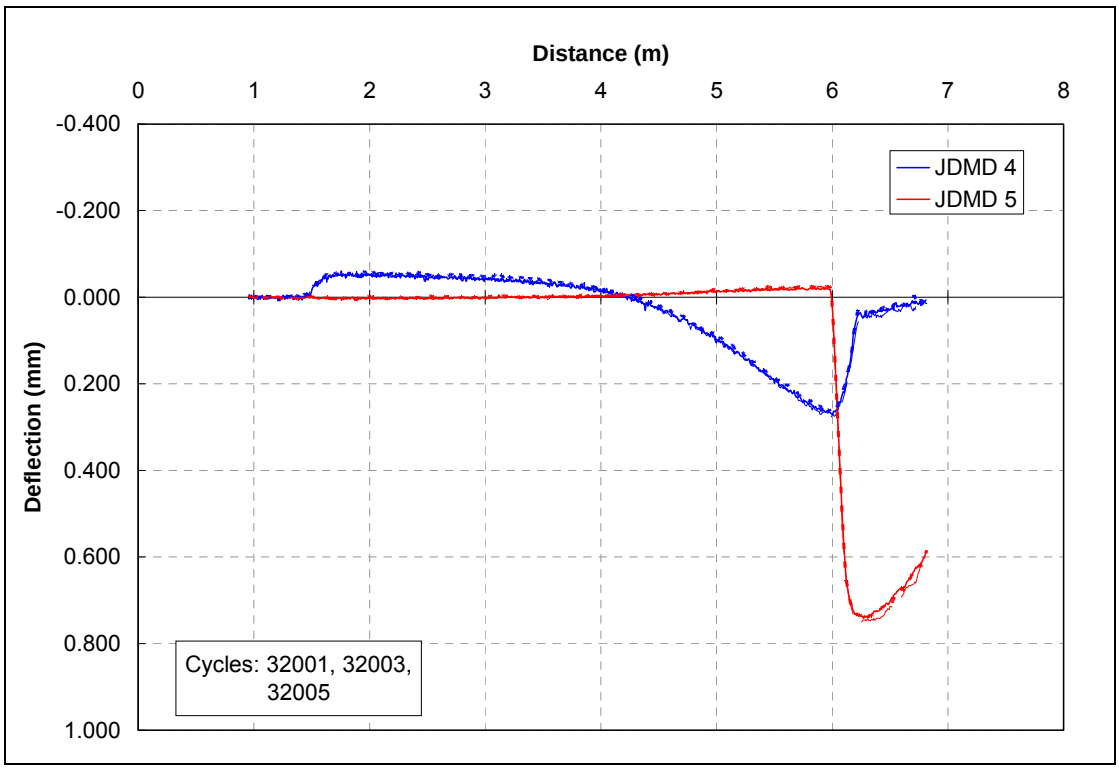

Figure 61. Resilient vertical corner deflection influence lines for the second joint on the ungrouted load test, 597FDUG.

The vertical deflection influence lines from JDMDs 6 and 7 installed at the untrafficked corners of the test slab also showed that the slab rocked around its transverse axis, with the response at JDMD 6 being synchronized with the response of JDMD 2 and JDMD 7 with JDMD 4 as is shown in Figure 62. The vertical mid-slab deflection influence lines plotted in Figure 63 show that even the mid-slab position on the trafficked slab (JDMD 3) lifted slightly when the wheel load was at either edge of the slab. There was, however, no load transfer to the far side of the untrafficked slab (JDMD 10).

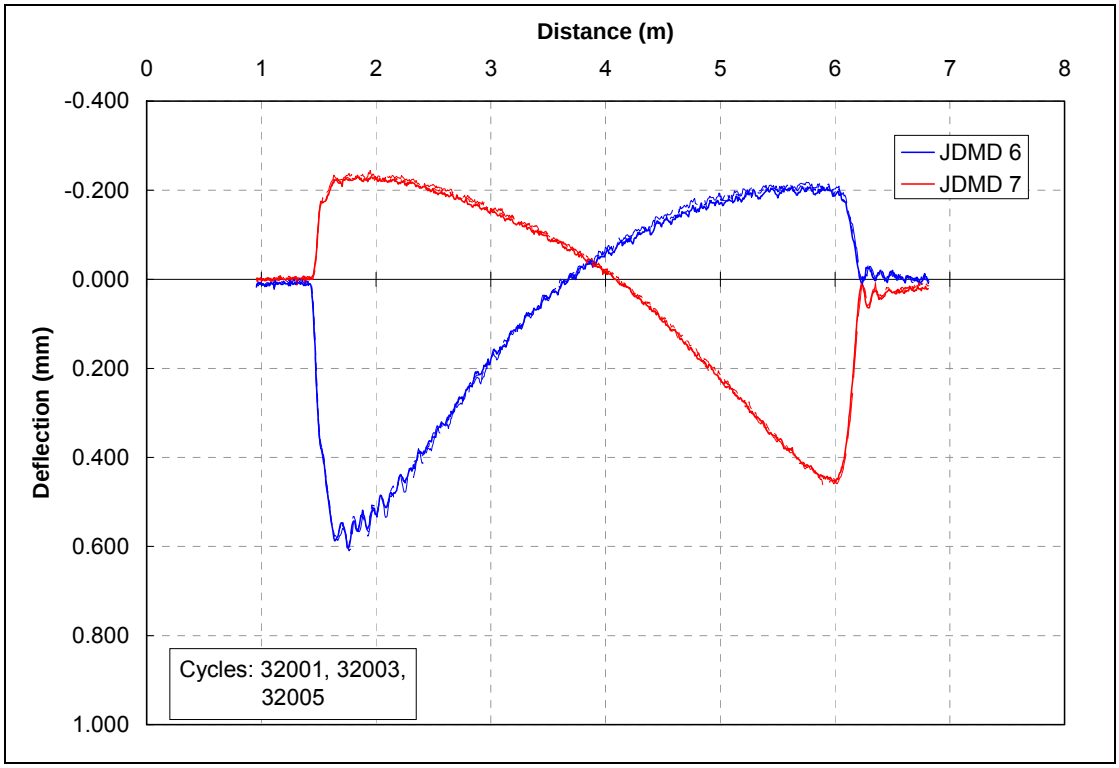

Figure 62. Resilient vertical corner deflection influence lines for the untrafficked side on the ungrouted load test, 597FDUG.

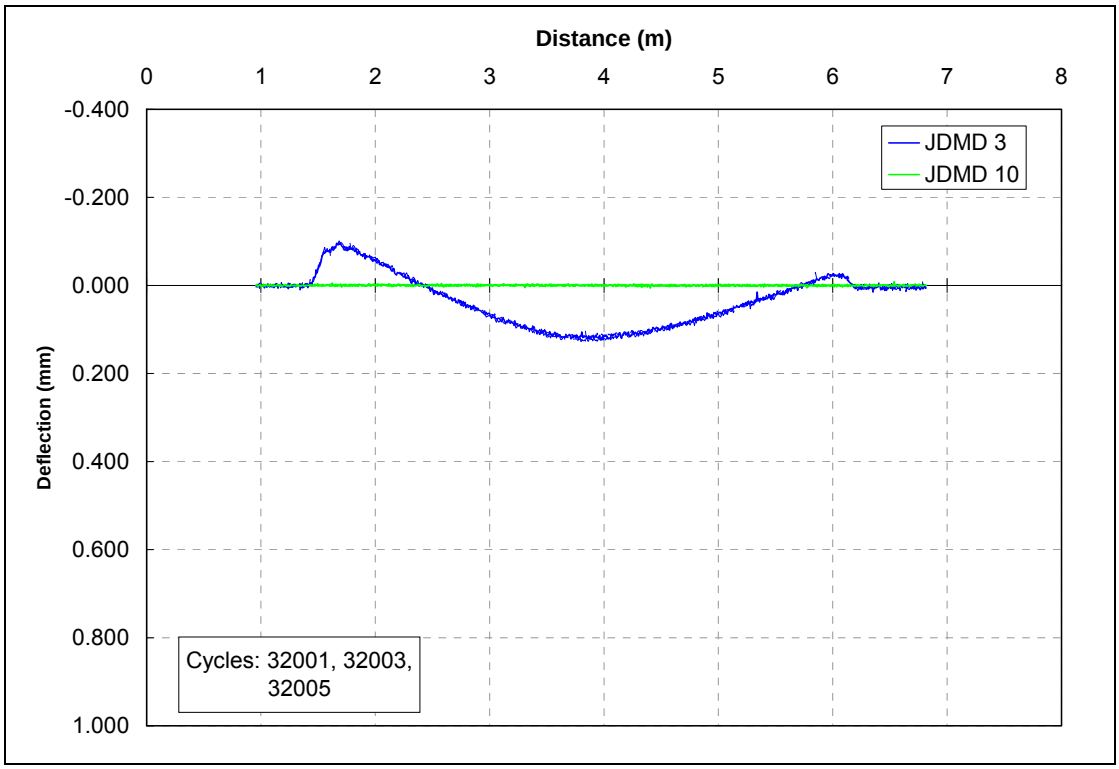

Figure 63. Resilient vertical mid-slab deflection influence lines for the ungrouted load test, 597FDUG.

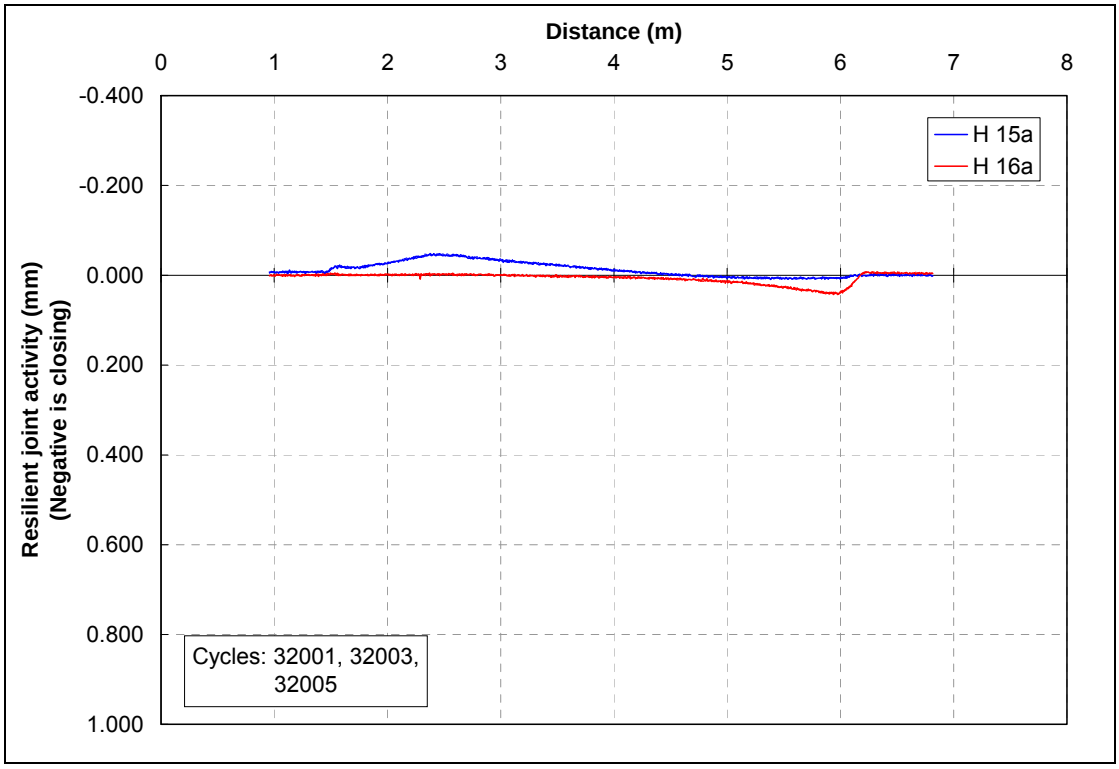

Figure 64. Resilient shoulder joint activity influence lines for the ungrouted load test, 597FDUG.

The resilient activity was minimal at the shoulder joint (Figure 64) and longitudinal joint (Figure 65).

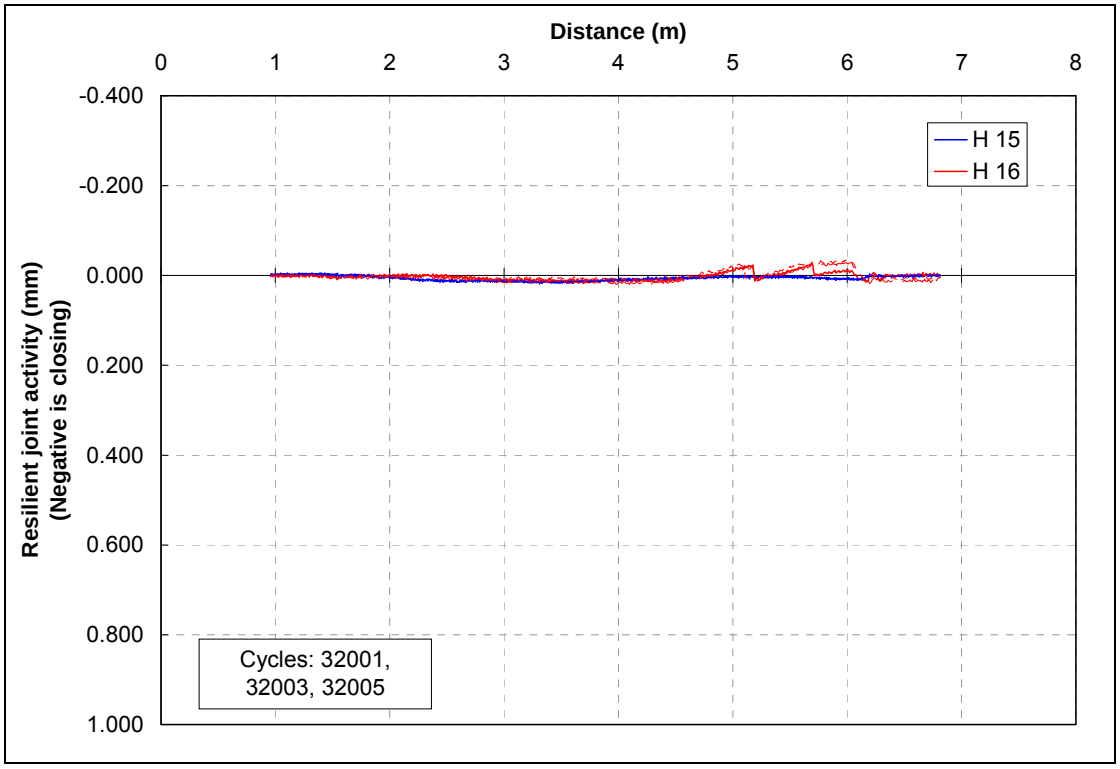

Figure 65. Resilient longitudinal joint activity influence lines for the ungrouted load test, 597FDUG.

Figure 66 shows the resilient transverse joint activity calculated from the horizontal JDMDs H13 and H14. Due to downward rotation of the slab edge under the load, the upper portion (sensors were located at the surface) of the transverse joints closed when the wheel was in the vicinity of the joint and opened when the wheel was on the far end of the slab.

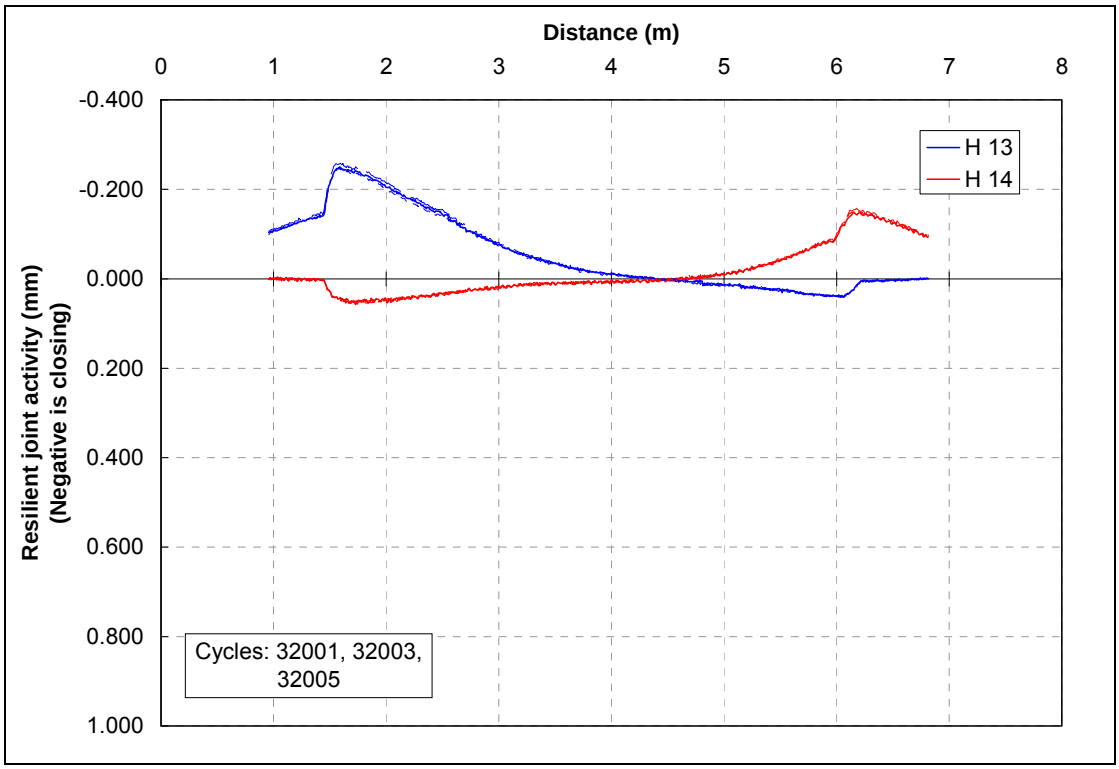

Figure 66. Resilient transverse joint activity horizontal deformation influence lines for the ungrouted load test, 597FDUG.

The resilient vertical corner deflections, of which examples are shown in Figure 60 and Figure 61, were used to calculate the load transfer efficiency at the ungrouted joints. The formulation of the Load Transfer Efficiency (LTE) is shown in Figure 67. This formulation is based on the assumption that the amount of deflection transferred from the approach slab to the leave slab when the approach slab is loaded, is proportional to the load transferred from the approach slab to the leave slab. This is the same definition used for FWD tests. An alternative definition has also been used on other HVS tests that correspond to Westergaard's definition of load transfer efficiency (6, 7).

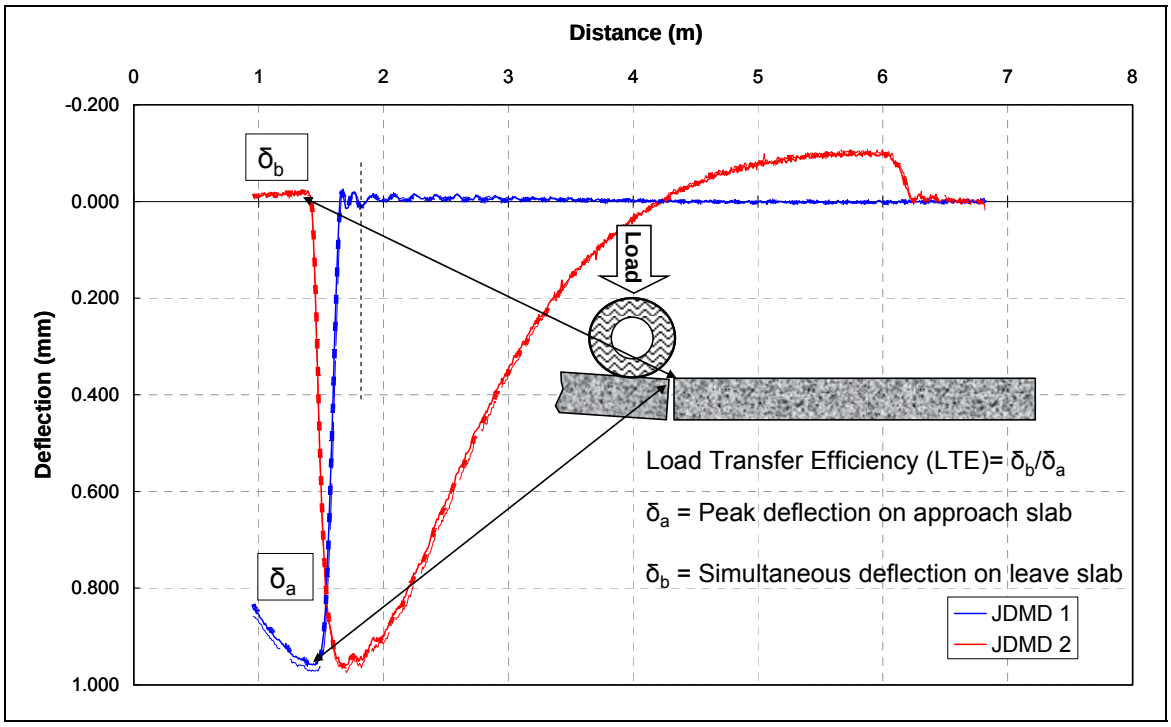

Figure 67. Formulation of the Load Transfer Efficiency.

Figure 68 shows the peak approach slab and simultaneous leave slab deflection at the two trafficked joints of the ungrouted test, 597FDUG. The resilient vertical deflection at JDMD 4 was consistently low throughout the duration of the test. Figure 69 shows the LTE for the duration of the ungrouted test, 597FDUG (approximately 16,000 wheel-load repetitions over a 32-hr period)[4]. In general the LTE was below 20 percent for the duration of the test and only exceeded this level when the deflection at JDMD 4 was approached by the deflection at JDMD 5, not because of load transfer but because of the very low deflection recorded at JDMD 4.

[4] Plots in Figure 68 to Figure 71 show 32,000 load repetitions in the horizontal axis, but since unidirectional traffic was used, the actual number of load passes is 16,000.

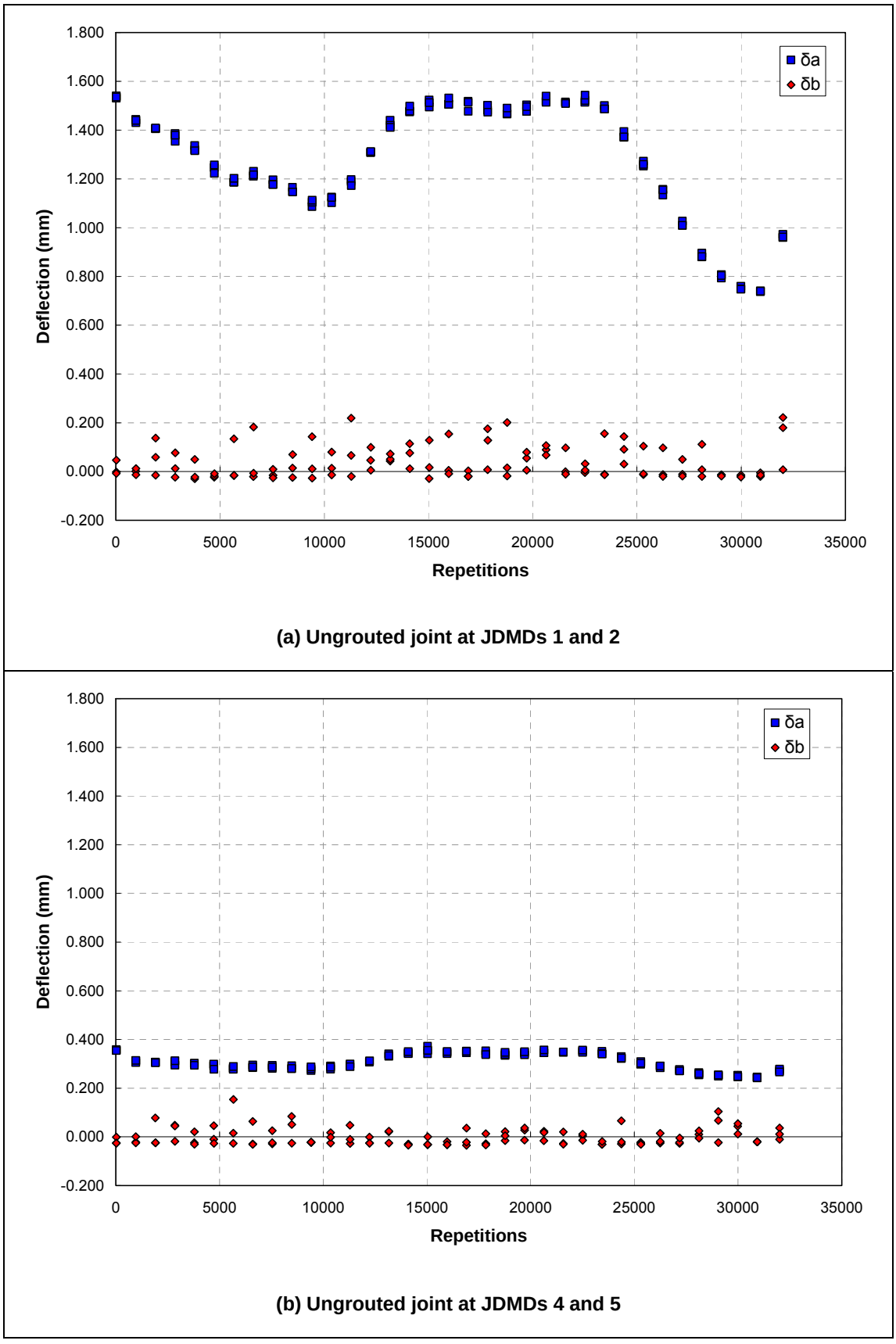

(a) Ungrouted joint at JDMDs 1 and 2

(b) Ungrouted joint at JDMDs 4 and 5

Figure 68. Peak approach slab and simultaneous leave slab deflection for the ungrouted

load test, 597FDUG.

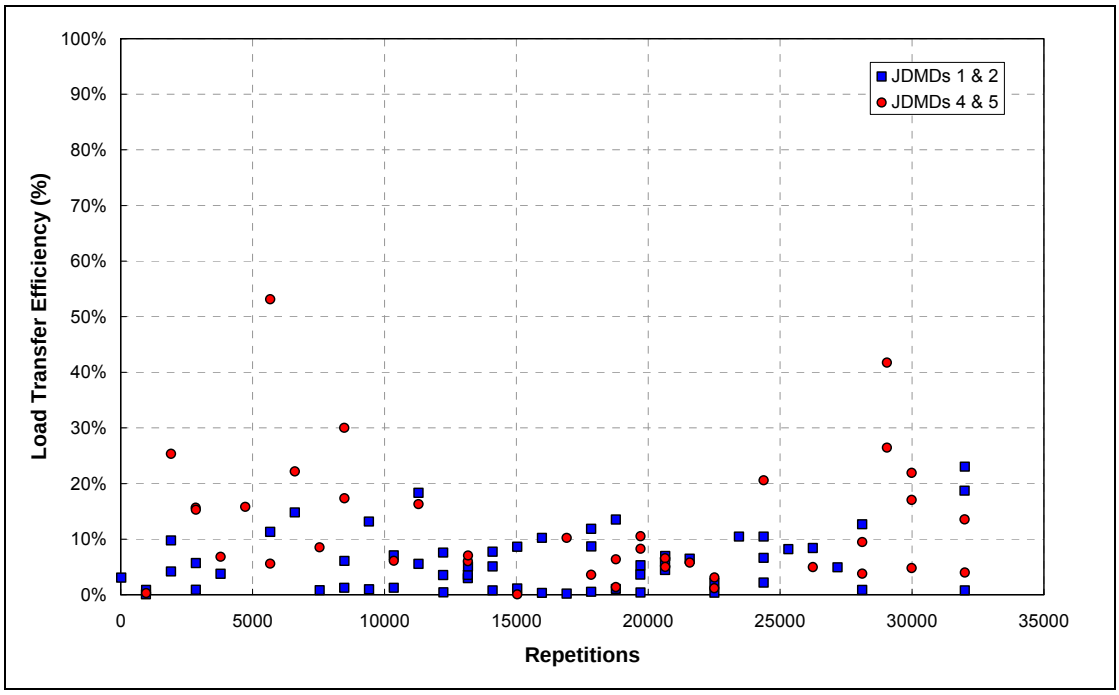

Figure 69. Load Transfer Efficiency for the ungrouted test, 597FDUG.

The resilient transverse joint horizontal deformation activity is shown in Figure 70 for the two trafficked transverse joints on the ungrouted test, 597FDUG. In general the total resilient joint activity was between 0.3 and 0.4 mm at H13 and between 0.2 and 0.3 mm at H14.

Figure 71 shows the mid-slab deflection for the duration of the ungrouted test, 597FDUG. Substantial lifting of about 0.1 mm occurred at the mid-slab position for the duration of the test while the downward deflection under the load was about 0.15 mm, resulting in a total mid-slab resilient movement of about 0.25 mm for the duration of the test.

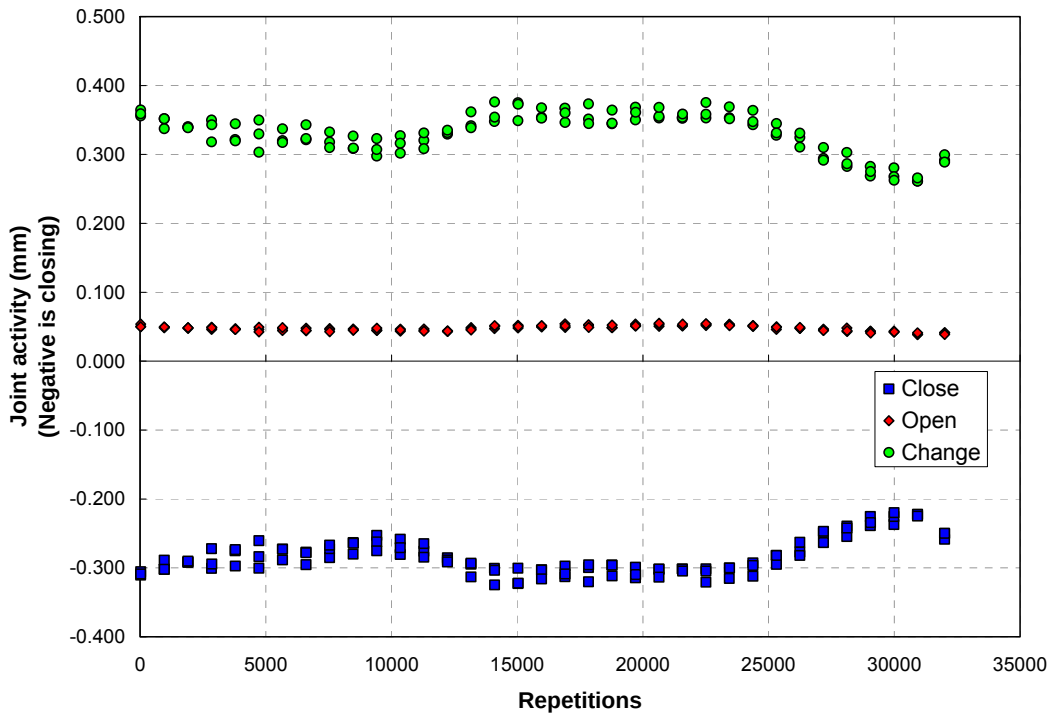

(a) Ungrouted joint at horizontal JDMD H13

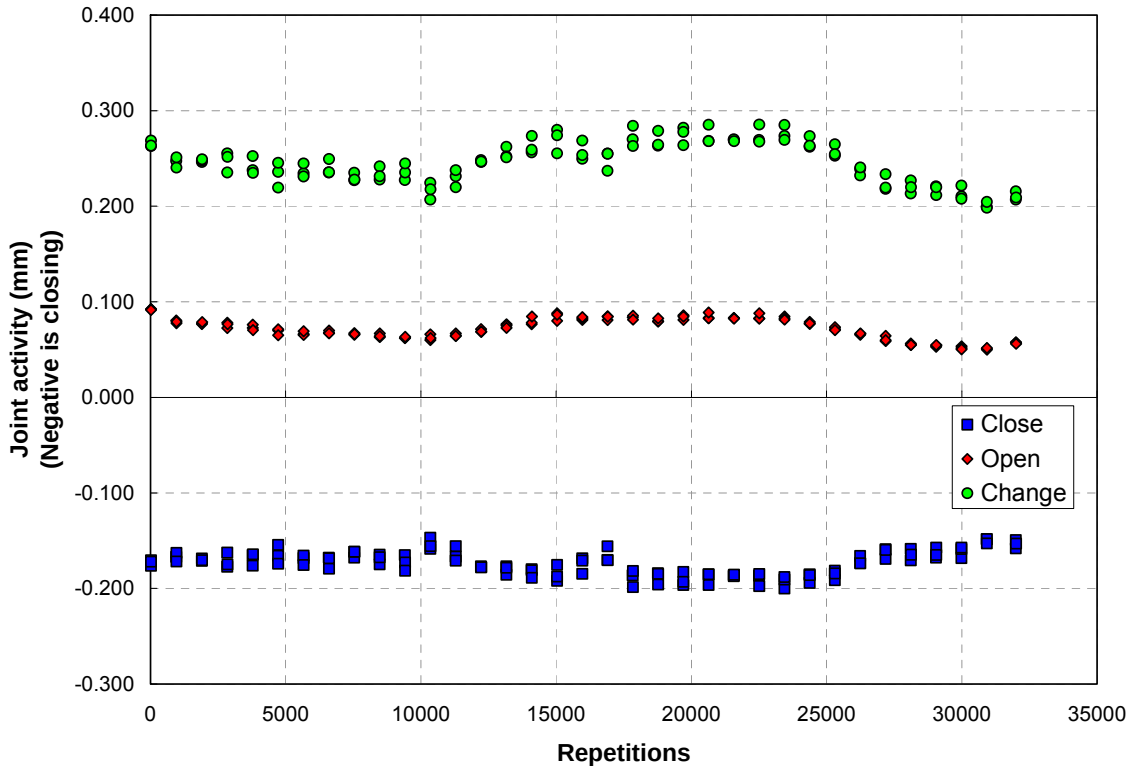

(b) Ungrouted joint at horizontal JDMD H14

Figure 70. Transverse joint activity for the ungrouted load test, 597FDUG.

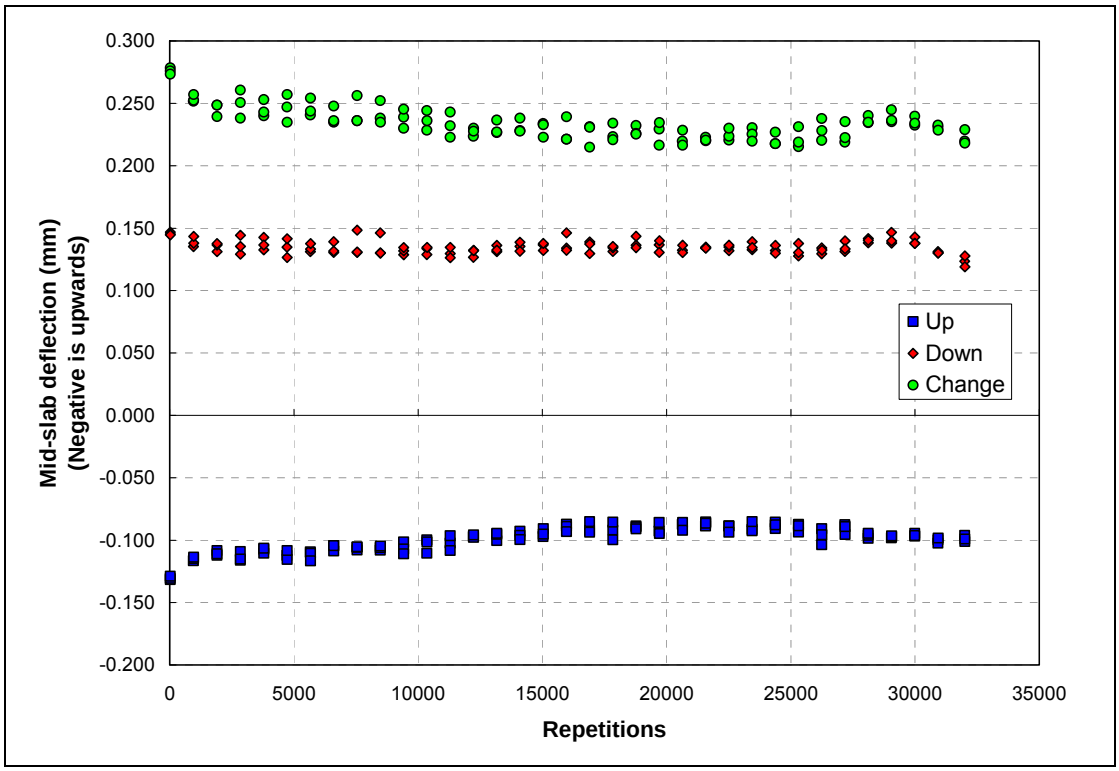

Figure 71. Mid-slab deflection for the ungrouted test, 597FDUG.

The peak resilient deflections plotted in Figure 68, Figure 70, and Figure 71 presented daily variations. The effects of the temperature and sunlight exposure conditions (shade projected on the pavement by the HVS versus exposed pavement) on the resilient deflections was therefore investigated. Figure 72 shows the resilient vertical deflection of the shaded corners plotted against the temperature gradient of the slab. The slab corner at JDMD 4 clearly had the lowest deflection but there is a correlation between the resilient vertical deflection and the temperature gradient of the slab for the other slab corners. Figure 73 shows the resilient vertical deflection of the exposed corners plotted against the temperature gradient of the slab. These slab corners were not directly trafficked but the rocking motion of the unrestrained slabs caused substantial deflection at these slab corners with the corner at JDMD 6 having deflections as high as 0.8 mm.

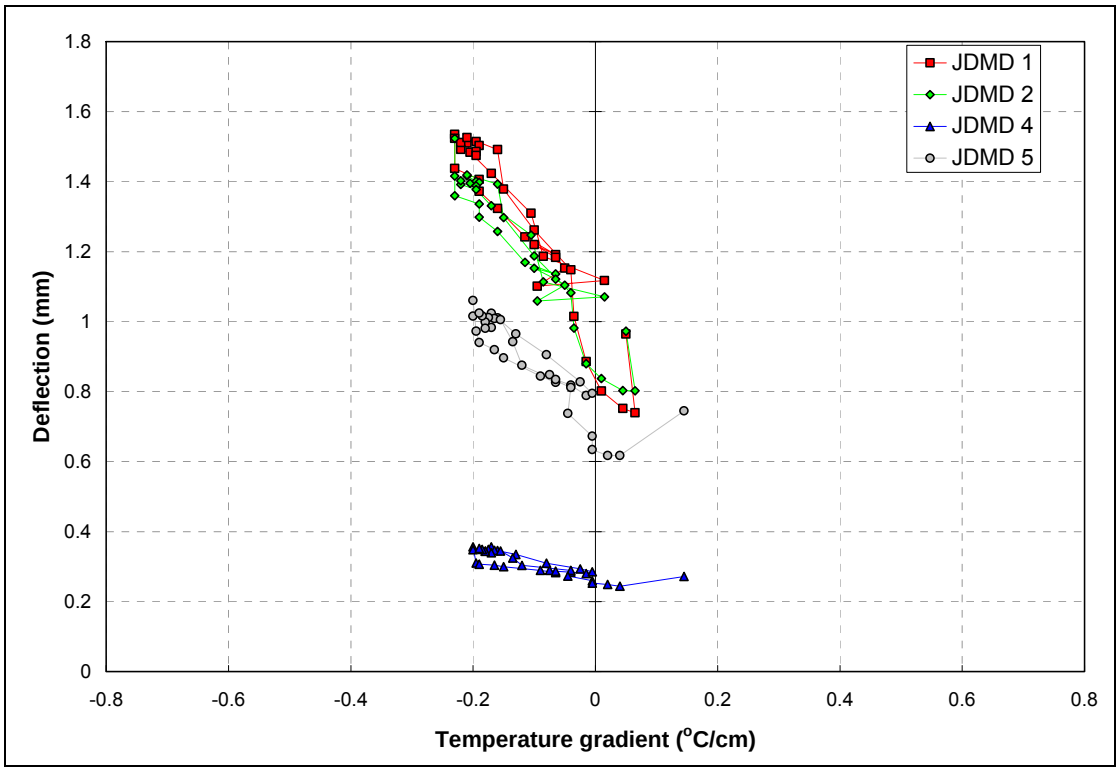

Figure 72. Resilient vertical deflection of the shaded slab corners for the ungrouted test, 597FDUG.

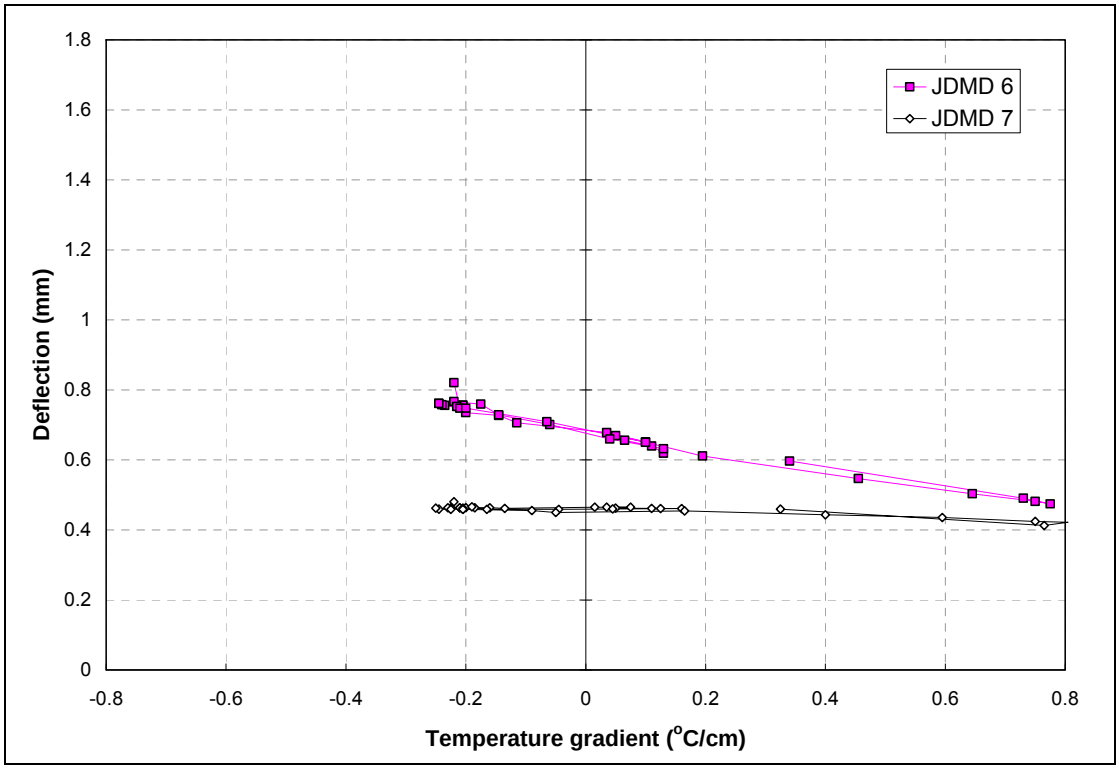

Figure 73. Resilient vertical deflection of the exposed slab corners for the ungrouted test, 597FDUG.

Figure 74 shows the resilient vertical mid-slab edge deflection plotted against the temperature gradient of the slab. The trafficked mid-slab edge at JDMD 3 had a significantly higher resilient deflection than the untrafficked edge at JDMD 10 with no load transfer to the far edge of the untrafficked slab (JDMD 10). The mid-slab edge deflection does not seem to be correlated to the temperature gradient of the slab but the temperature gradient range was small because the trafficked edge of the slab was shielded by the HVS.

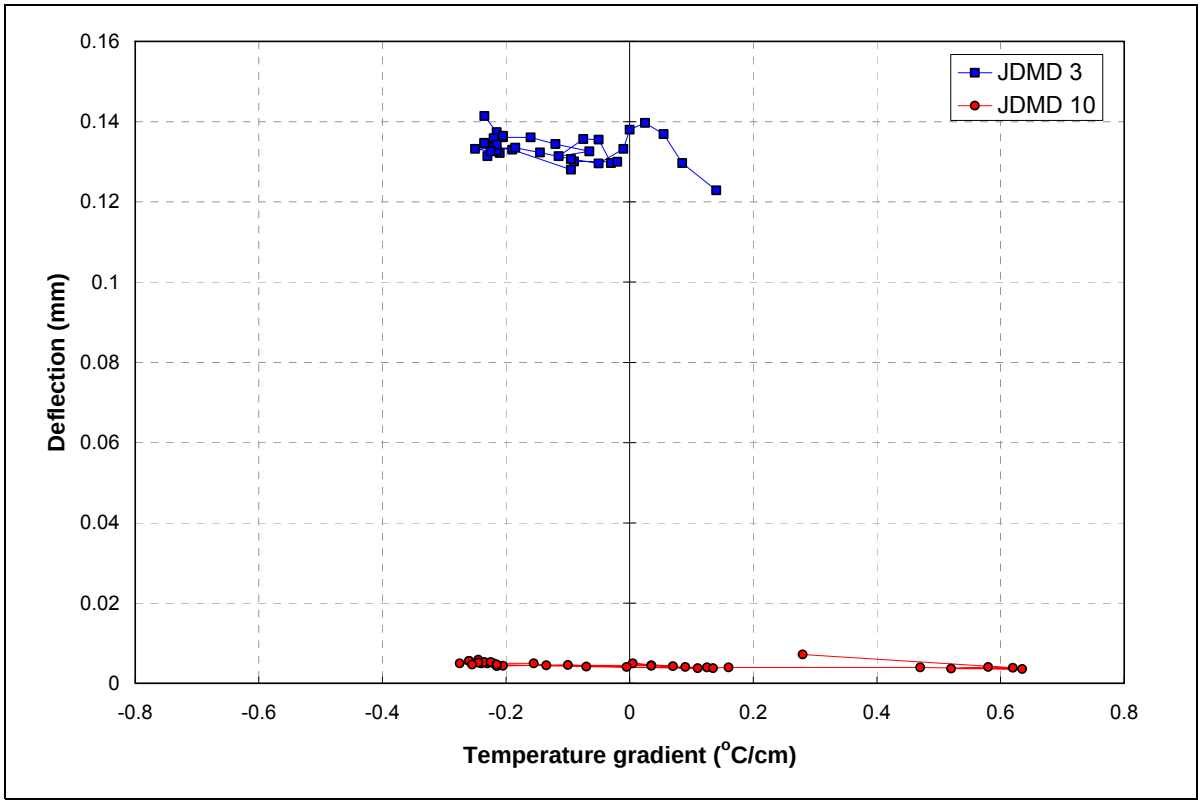

Figure 74. Resilient vertical deflection of the slab mid-slab edge for the ungrouted test. 597FDUG.

Figure 75 shows the resilient transverse joint horizontal deformation activity plotted against the surface temperature, and Figure 76 shows the resilient longitudinal joint horizontal joint activity plotted against the surface temperature for the joint between the two rows of slabs (H15 and H16) and the joint between the trafficked slabs and the AC shoulder [H15(a) and H16(a)].

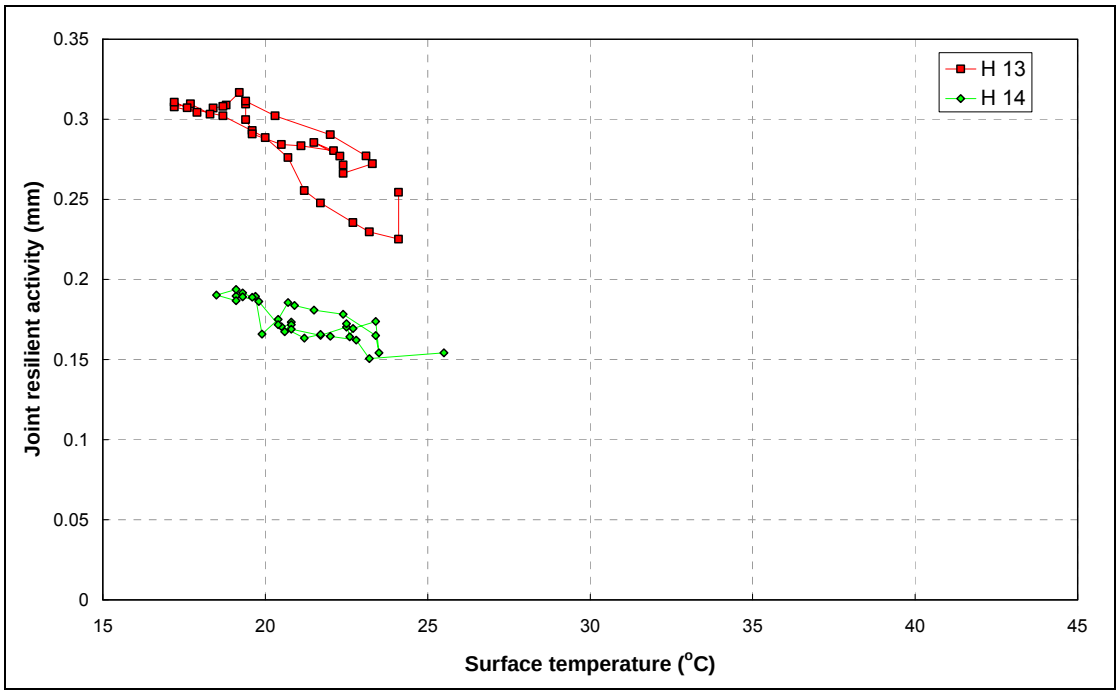

Figure 75. Resilient transverse joint activity for the ungrouted test, 597FDUG.

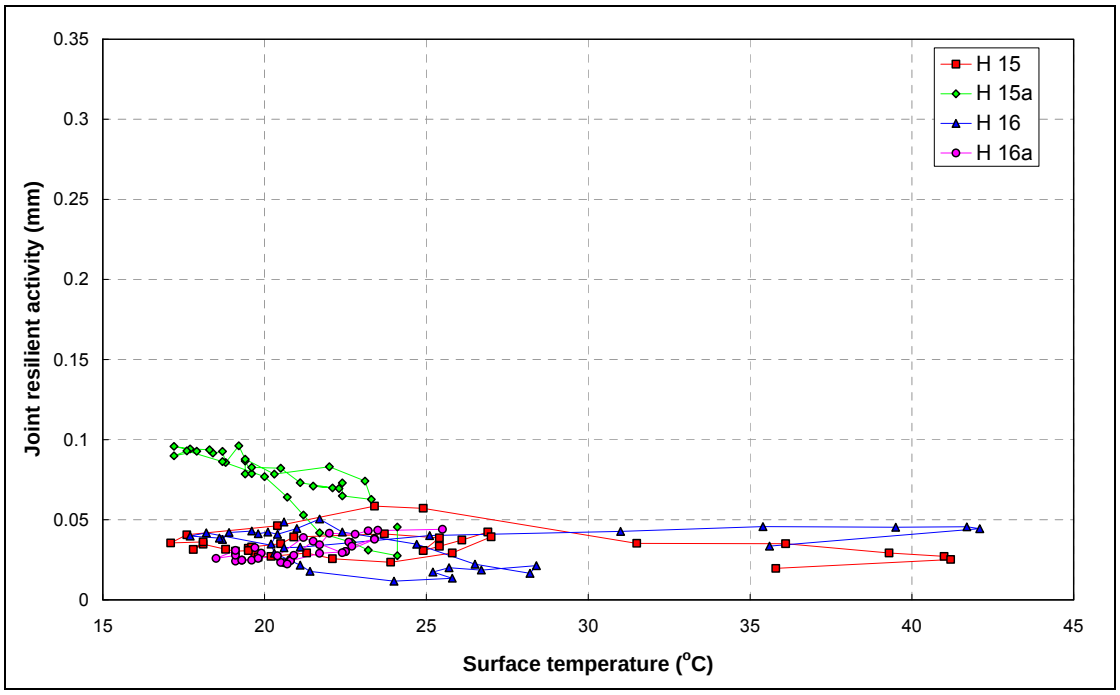

Figure 76. Resilient longitudinal joint activity for the ungrouted test, 597FDUG.

In summary the following observations are made regarding the ungrouted load test, 597FDUG:

- Thermal curl response:

- The slab corner at JDMD 4 was shaded by the HVS and had a total thermal curl movement of only 0.5 mm for a temperature gradient range from -0.2 to +0.2°C/cm (temperature differential top to bottom of -4 to +4°C). The slab corner at JDMD 4 seems to be very stiff in terms of thermal curl response.
- The slab corner at JDMD 6 was exposed and had a total thermal curl movement of 1.6 mm for a temperature gradient range from - 0.2 to +0.8°C/cm (temperature differential of -4 to +18°C).
- The transverse joints at H13 and H14 had total thermal curl joint activity of 0.3 mm over a temperature range of 17 to 24°C.
- The longitudinal joint between the slab and the AC shoulder had a total thermal curl joint activity of 0.2 mm over a temperature range of 17 to 24°C.
- The longitudinal joint at H15 had a total thermal curl joint activity of 0.9 mm over a temperature range of 17 to 42°C.

- Resilient deflection response:
  - The temperature gradient range on the trafficked portion of the test section was limited to a range between -0.2 and +0.2°C/cm because of the shading effect of the HVS. Within this temperature gradient range, the slab corner at JDMD 4 had the lowest resilient deflection of between 0.2 and 0.4 mm. Again, the slab corner at JDMD 4 seems to be stiff compared to the other slab corners. The slab corner at JDMD 5 adjacent to JDMD 4 had a resilient deflection between 0.6 and 1.0 mm. The slab corners at the other end of the test section (JDMDs 1 and 2) had the highest deflections, between 0.8 and 1.6 mm.
  - The exposed slab corners at JDMDs 6 and 7 had a wider temperature gradient range from about -0.2 to +0.8 °C/cm (temperature differential of -4 to +18°C). The resilient deflections ranged between 0.4 and 0.8 mm for this temperature gradient range but these corners were not trafficked and the deflection is the result of the rocking of the unrestrained slabs.
  - The resilient mid-slab edge deflection at JDMD 3 ranged between 0.12 and 0.14 mm over a temperature gradient range of -0.2 to +0.2°C/cm (temperature differential of -4 to +4°C). No resilient deflection was transferred to the JDMD 10 on the far side of the opposing lane of slabs.

- The resilient transverse joint horizontal deformation activity at the first joint of the test section varied between 0.2 and 0.31 mm for a temperature range of 17 to 24°C. The corresponding horizontal joint activity at the second joint of the test section varied between 0.15 and 0.2 mm for the same temperature range.
- The resilient longitudinal joint horizontal deformation activity was generally below 0.05 mm with only the longitudinal joint between the slab and the AC shoulder ranging between 0.05 and 0.1 mm at the horizontal JDMD H15(a).

4.4 Load Test 598FDUG

Figure 77 shows the instrumentation layout for the second ungrouted test, 598FDUG, which started at 22h00 on May 30, 2005, and ended at 07h00 on June 1, 2005, at 32,088 repetitions of a 60-kN load applied in unidirectional mode from the cabin to the tow-end of the HVS (from left to right in terms of the layout shown in Figure 77).

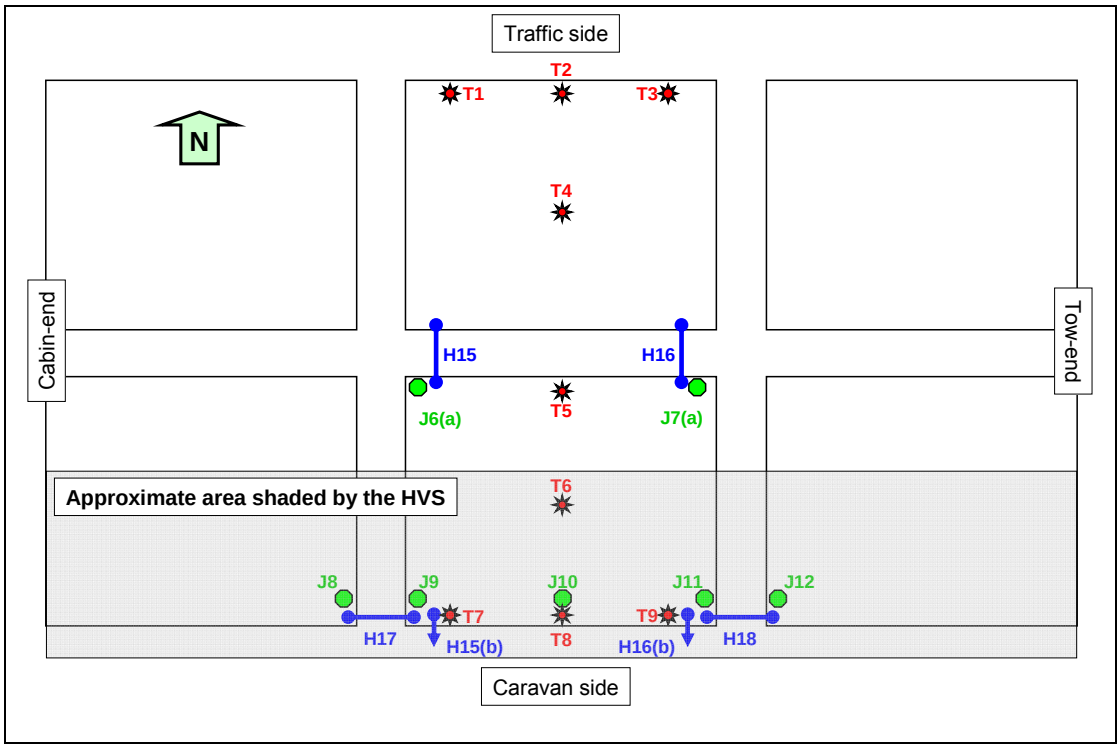

Figure 77. Thermocouples and JDMDs monitored during the second ungrouted test, 598FDUG.

The average slab temperature and temperature gradient were calculated from the temperature data recorded at the five depths for each of the thermocouples shown in Figure 77. The average slab temperature is shown in Figure 78 and the temperature gradient in Figure 79. The temperature on the shaded portion of the slabs stayed between 20°C and 30°C, while the

temperature at the exposed locations ranged from 15°C to 35°C, reaching the maximum between 16h00 and 17h00 on May 31, 2005. The exposed and shaded thermocouples all reached a zero temperature gradient at 19h00 on May 31, 2005. The JDMD readings at 19h00 on May 31, 2005 were therefore assumed to represent the neutral position for all the JDMD locations.

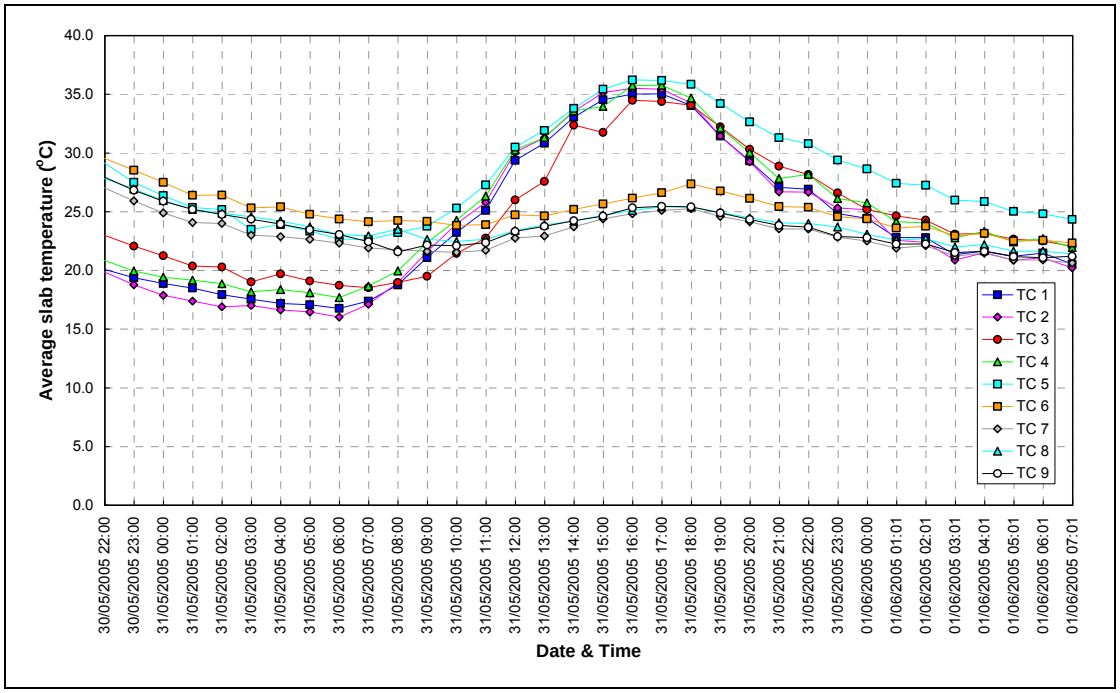

Figure 78. Average slab temperature during the ungrouted test, 598FDUG.

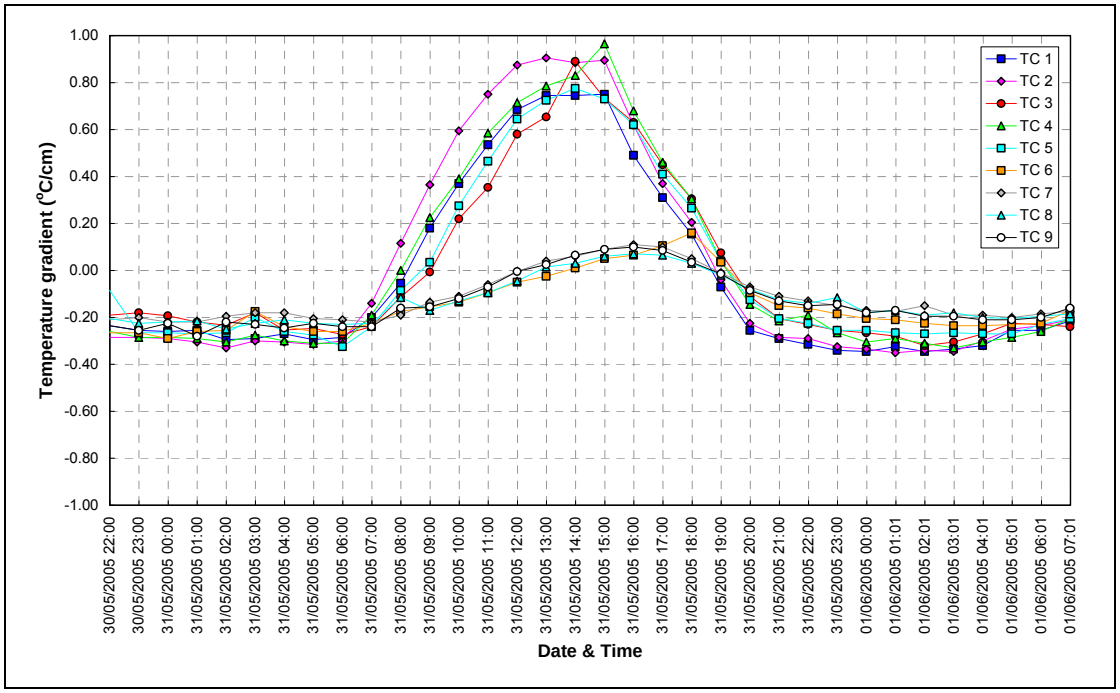

Figure 79. Temperature gradient during the ungrouted test, 598FDUG.

4.4.1 Thermal Curl Response

Figure 80 and Figure 81 show the transient thermal curl behavior of the slabs during the ungrouted load test 598FDUG in terms of the vertical corner positions and joint activity. Figure 82 and Figure 83 show the difference between the temperature gradient and thermal curl of a slab corner shaded by the HVS and an exposed corner. Regardless of these differences, the thermal curl of the shaded and exposed slab corners are determined by the temperature gradient as illustrated by Figure 84 for the shaded corners and by Figure 85 for the exposed corners. The relationship between transverse and longitudinal joint thermal curl activity and surface temperature is shown in Figure 86 for the transverse joints and in Figure 87 for the longitudinal joints.

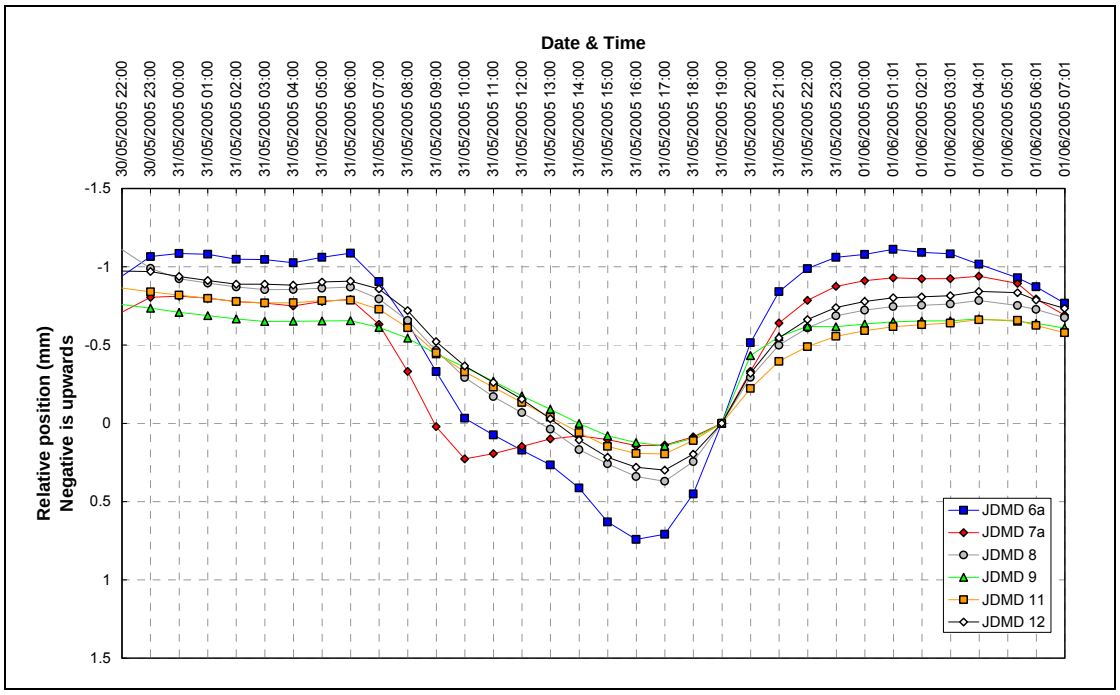

Figure 80. Adjusted thermal curl vertical position of the slab corners during the ungrouted load test, 598FDUG.

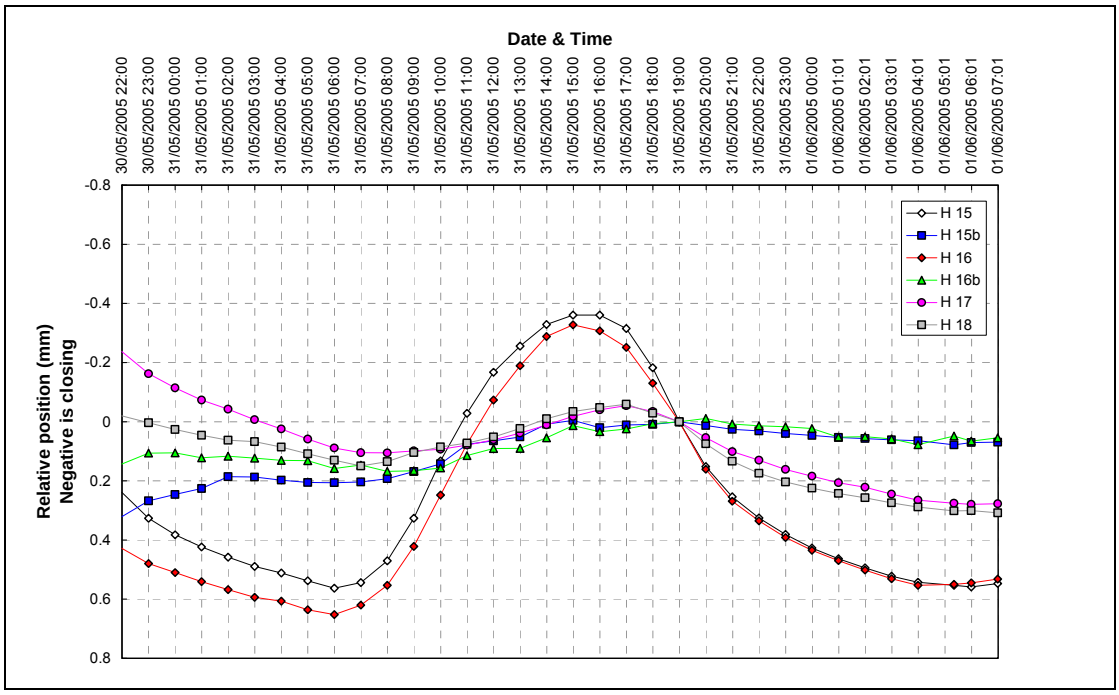

Figure 81. Adjusted thermal curl horizontal joint activity during the ungrouted load test, 598FDUG.

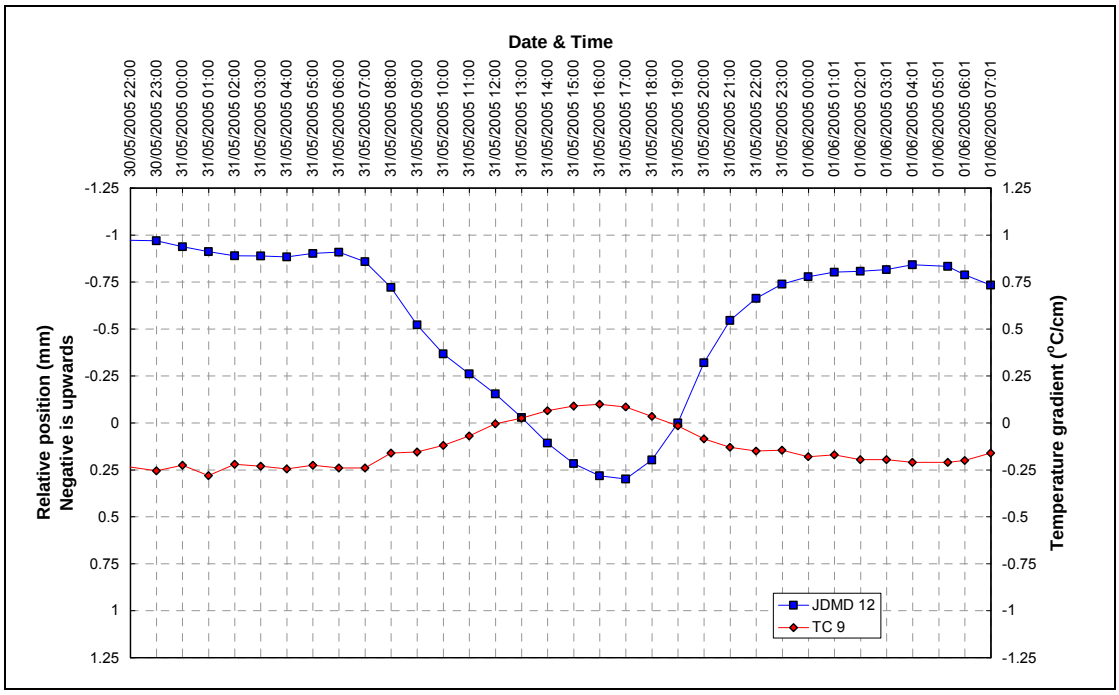

Figure 82. Adjusted thermal curl vertical position and temperature gradient for a shaded slab corner during the ungrouted load test, 598FDUG.

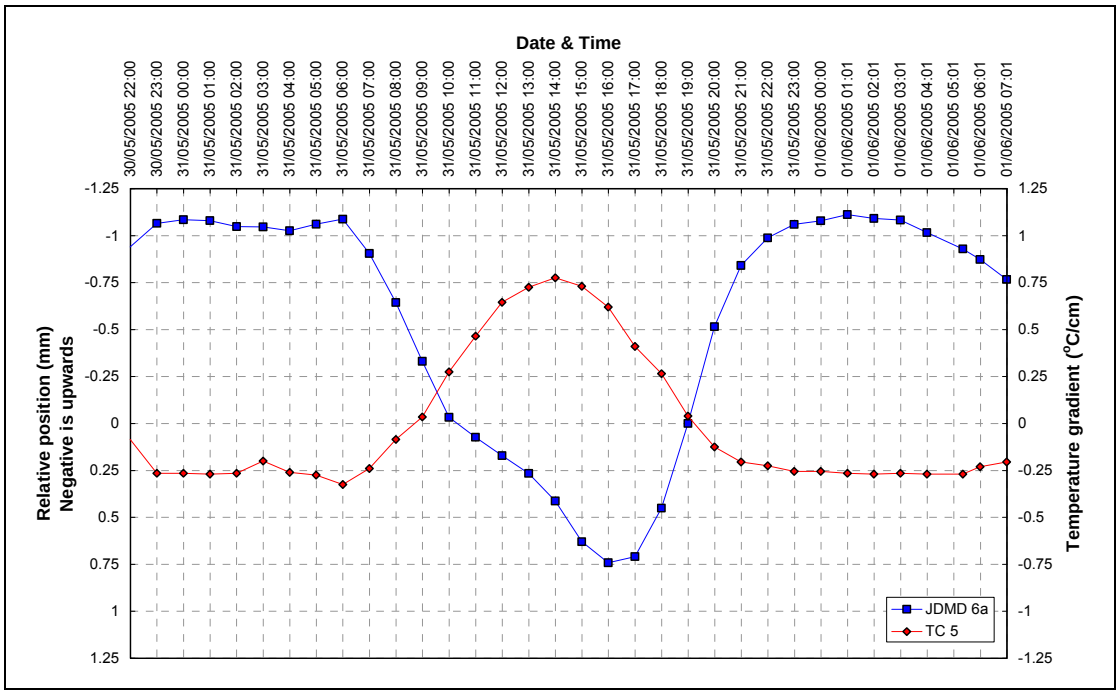

Figure 83. Adjusted thermal curl vertical position and temperature gradient for an exposed slab corner during the ungrouted load test, 598FDUG.

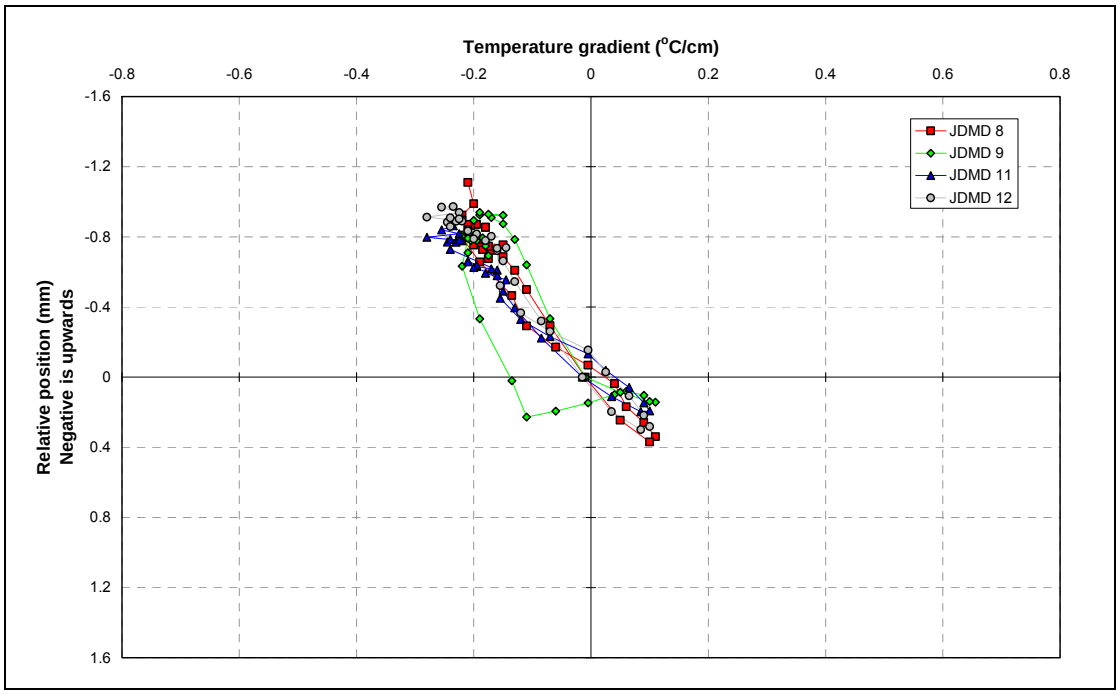

Figure 84. Relationship between thermal curl and temperature gradient for the shaded slab corners during the ungrouted load test, 598FDUG.

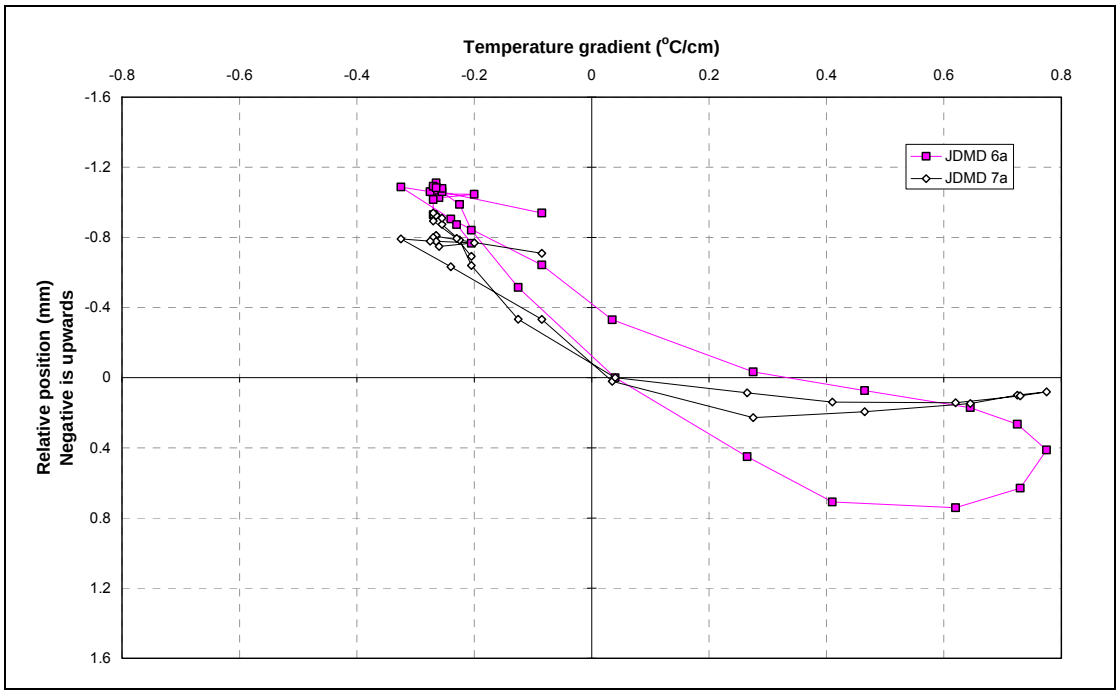

Figure 85. Relationship between thermal curl and temperature gradient for the exposed slab corners during the ungrouted load test, 598FDUG.

The shapes of the curves in Figure 85 at the upper end of the positive gradient indicate better support to the slab from the underlying layers under Test 598FDUG compared to Test 597FDUG. In Figure 57 it was shown that when the gradient varies from 0.6 to 0.8°C/cm the corners of the slab on the northern section move further down by about 0.2 or 0.4 mm, depending on which joint is analyzed. Such gradients occur when the top of the slab is 13°C to 18°C warmer than the bottom. When this temperature differential was observed on the southern section, the corners were not moving downward because they were in full contact with the under layer. These results are from the inside corners (at the longitudinal joint), where there was direct exposure to sunlight. The outside corner did not experience high thermal gradient due to the shading of the slabs by the HVS (see Figure 84 and Figure 56).

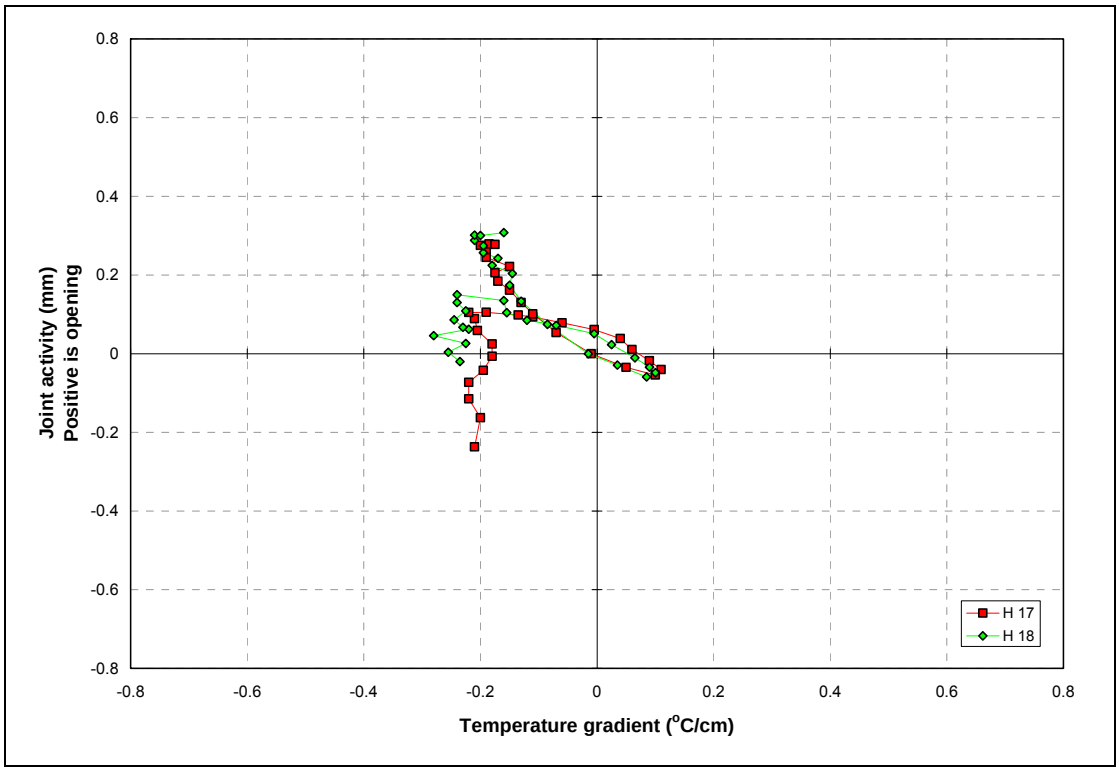

Figure 86. Relationship between transverse joint thermal curl activity and surface temperature during the ungrouted load test, 598FDUG.

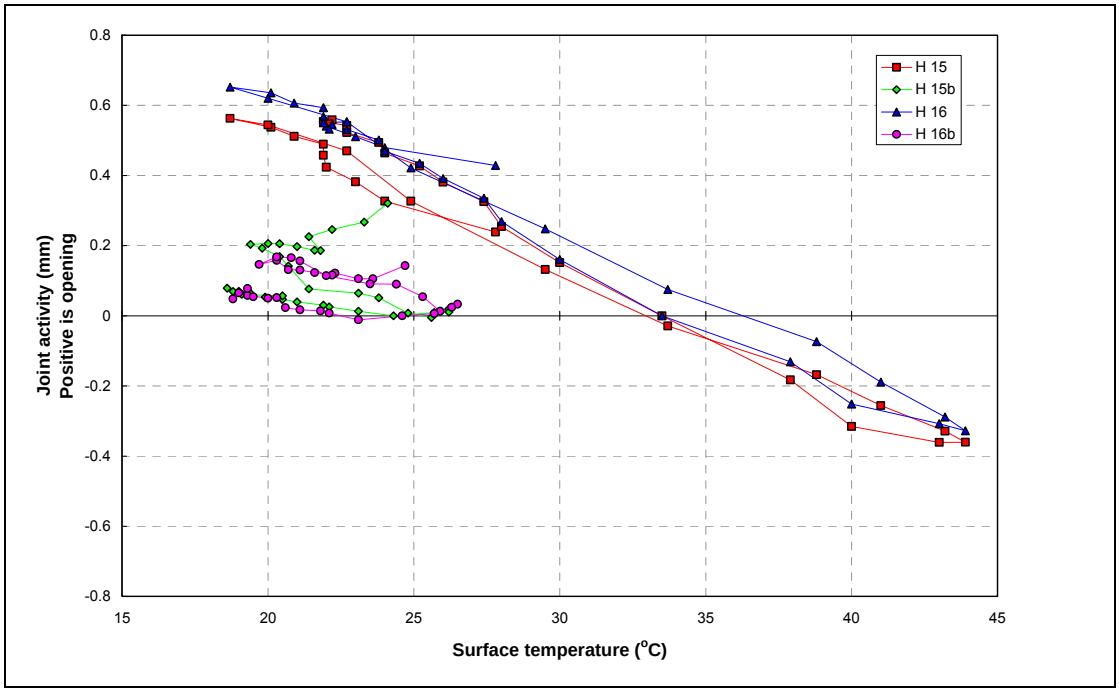

Figure 87. Relationship between longitudinal joint thermal curl activity and surface temperature during the ungrouted load test, 598FDUG.

4.4.2 Resilient Deflection Response

Figure 88 and Figure 89 show the vertical deflection influence lines for the first and second joints respectively on Test 598FDUG at the end of the test. The deflection response at the first joint is asymmetrical with a peak resilient vertical deflection of almost 2 mm at JDMD 8 while the peak deflection at the adjacent JDMD 9 is only 0.8 mm. This is similar to the behavior observed at the second joint on 597FDUG. There is very little load transfer at the joint, with the deflection recorded by JDMD 8 immediately rebounding to zero as the wheel leaves the approach slab. The influence lines for JDMD 9 show that the slab rocked around its transverse axis and the corner at JDMD 9 lifted by about 0.25 mm when the wheel was at the opposite end of the slab. The deflection response at the second joint is symmetrical with a peak resilient vertical deflection of 1.8 mm at both JDMDs 11 and 12.

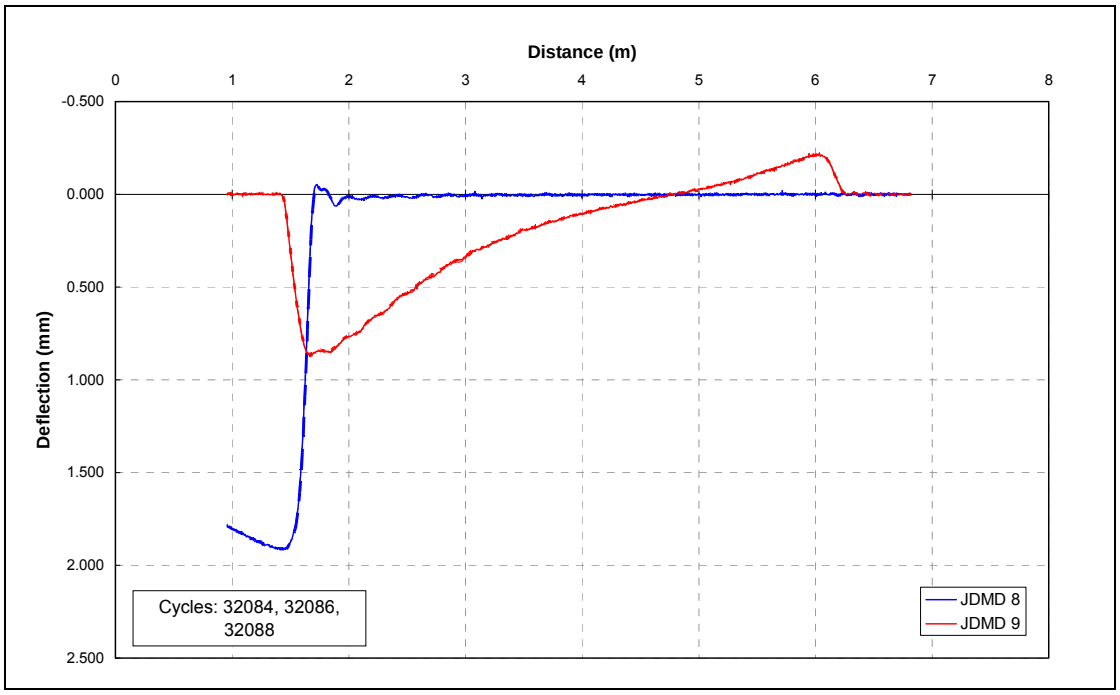

Figure 88. Resilient vertical corner deflection influence lines for the first joint on the ungrouted load test, 598FDUG.

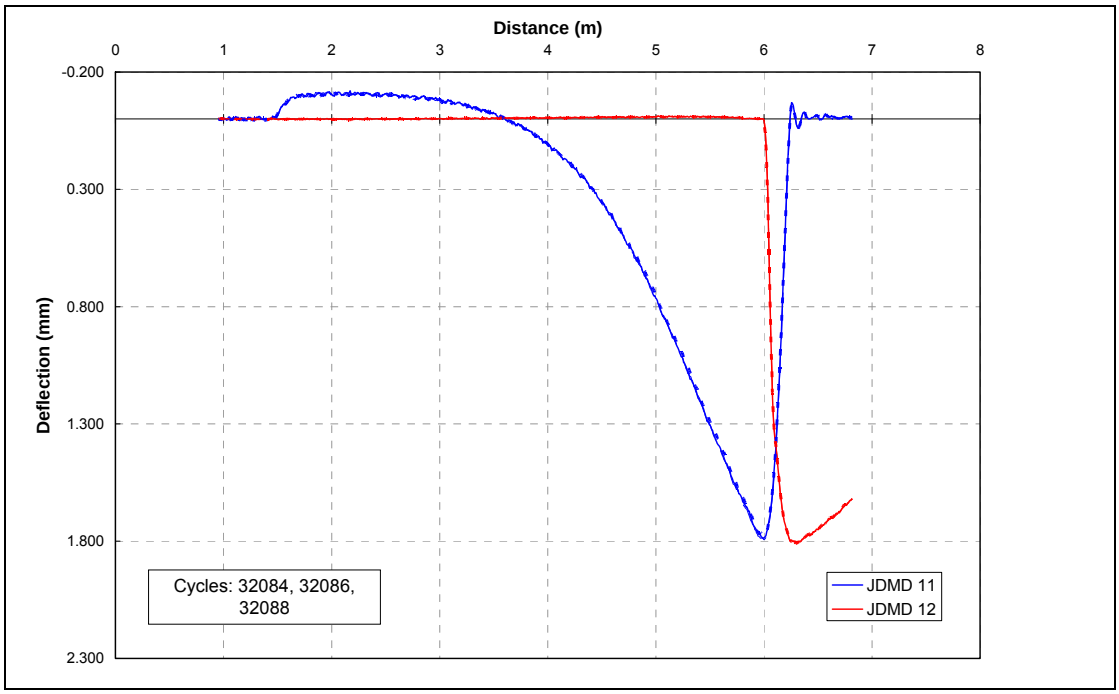

Figure 89. Resilient vertical corner deflection influence lines for the second joint on the ungrouted load test, 598FDUG.

The vertical deflection influence lines from JDMDs 6a and 7a installed at the untrafficked corners of the test slab also showed that the slab rocked around its transverse axis with the response at JDMD 6a being synchronized with the response of JDMD 8 and JDMD 7a with JDMD 11 as is shown in Figure 90. The vertical mid-slab deflection influence lines plotted in Figure 91 show that even the mid-slab position on the trafficked slab (JDMD 10) lifted slightly when the wheel load was at the eastern end of the slab.

The resilient horizontal deformation activity, that is opening and closing, was minimal at the shoulder joint (Figure 92) and the longitudinal joint (Figure 93).

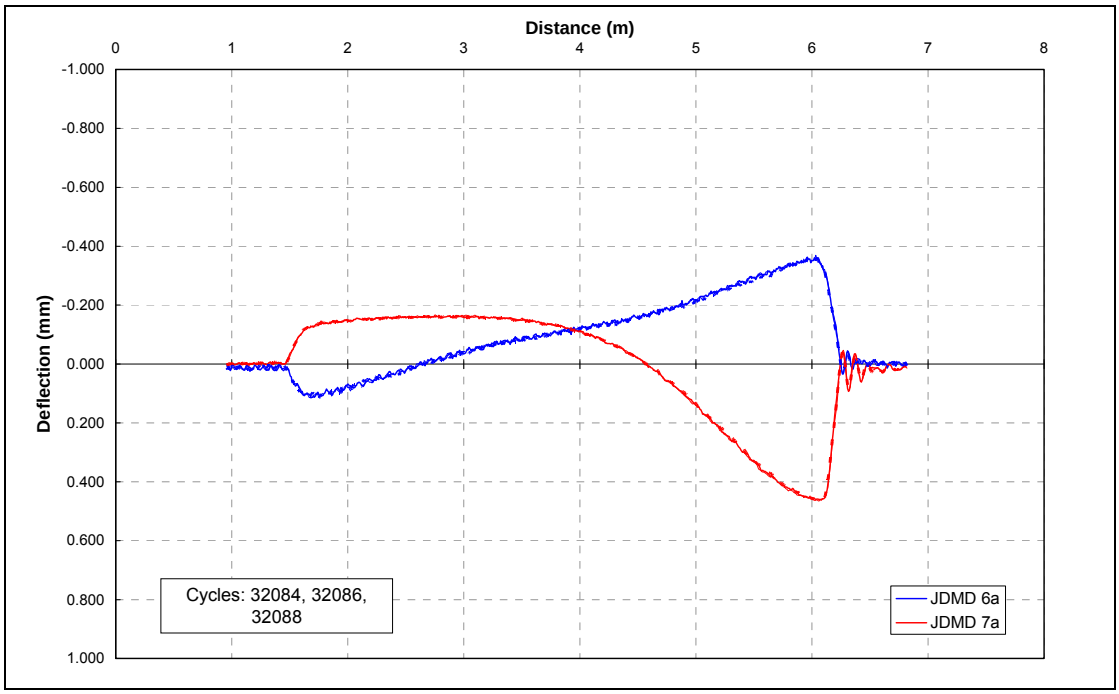

Figure 90. Resilient vertical corner deflection influence lines for the untrafficked joints on the ungrouted load test, 598FDUG.

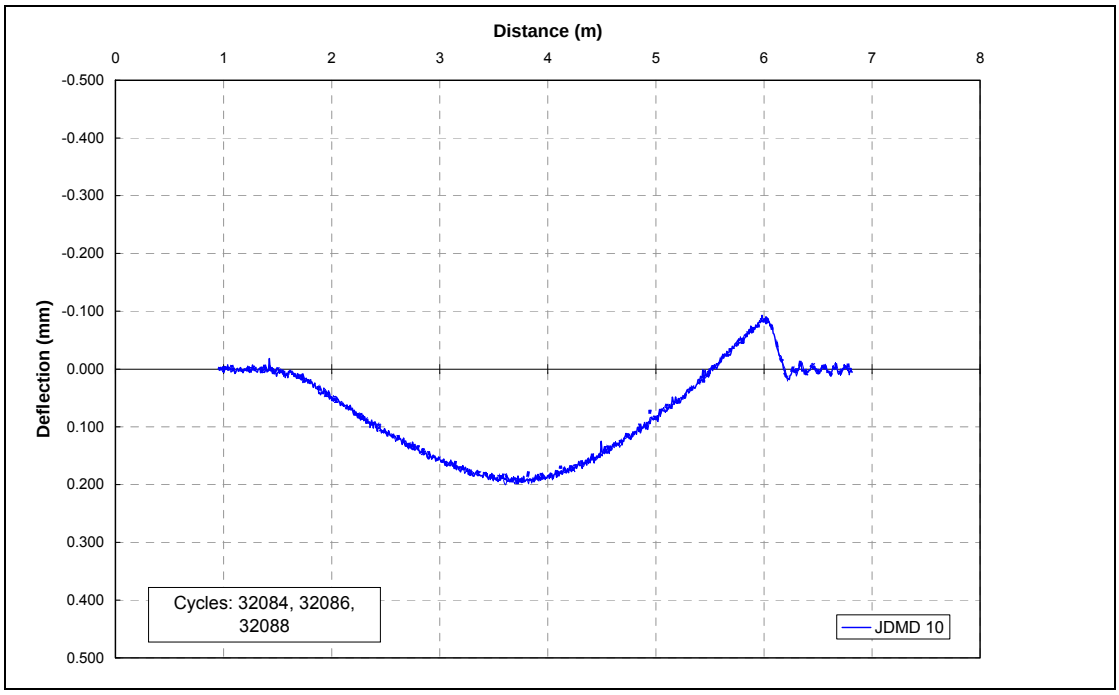

Figure 91. Resilient vertical mid-slab deflection influence lines for the ungrouted load test, 598FDUG.

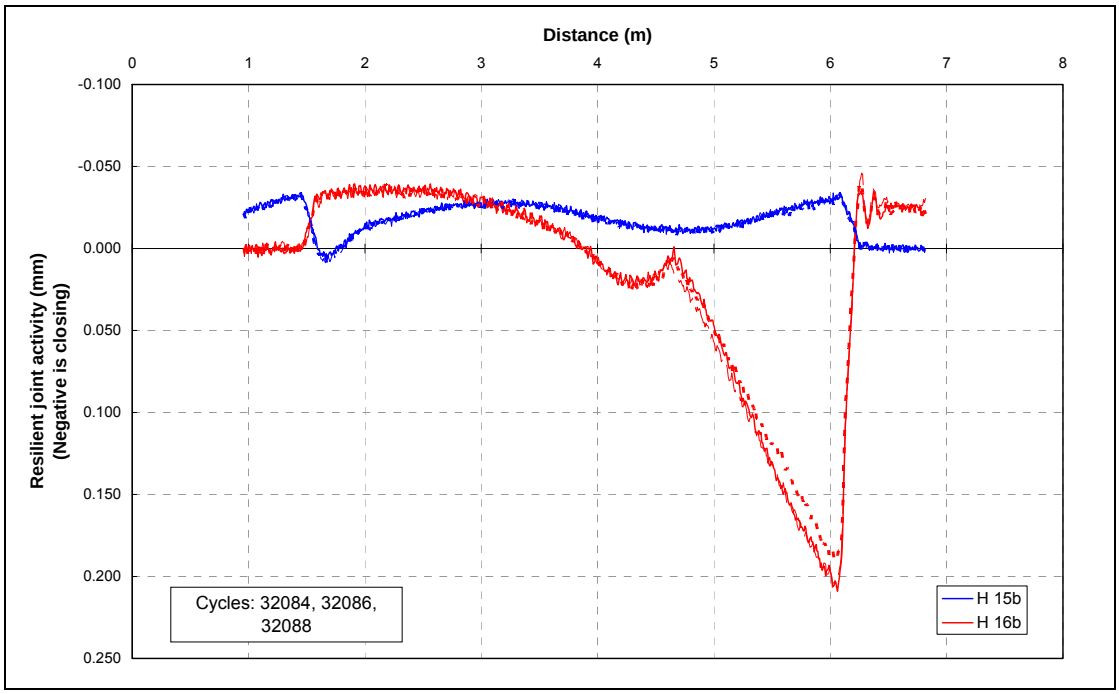

Figure 92. Resilient shoulder joint activity influence lines for the ungrouted load test, 598FDUG.

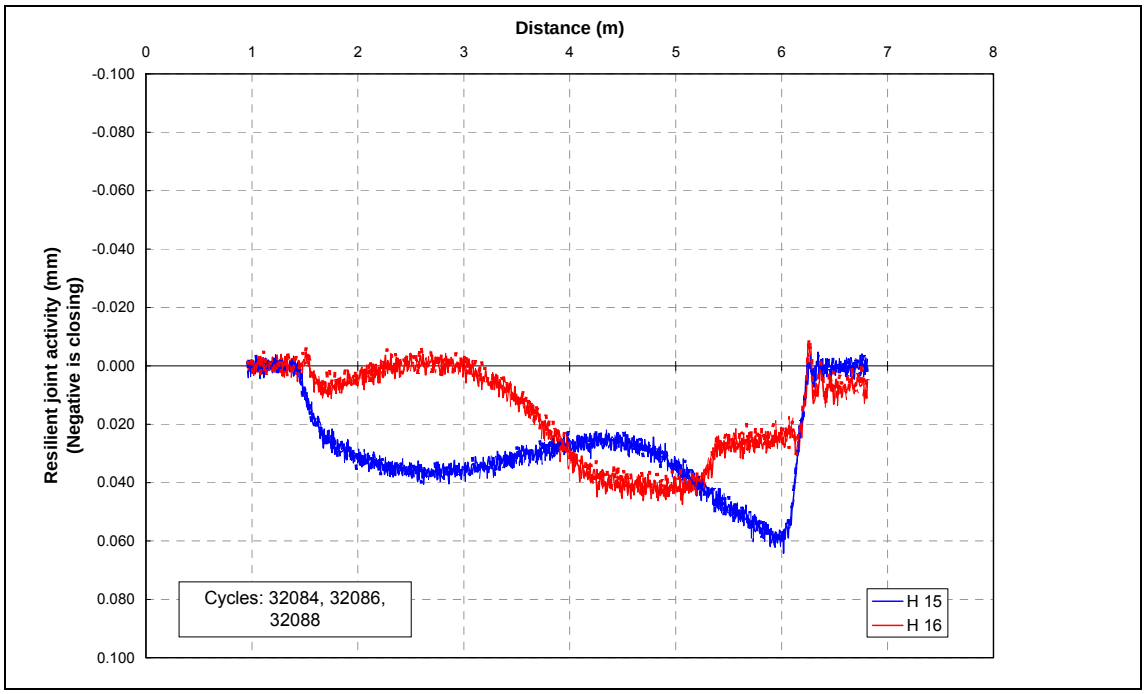

Figure 93. Resilient longitudinal joint activity influence lines for the ungrouted load test, 598FDUG.

Figure 94 shows the resilient transverse joint horizontal deformation activity calculated from the horizontal JDMDs H17 and H18. The surface of the transverse joints closed when the wheel was in the vicinity of the joint and opened when the wheel was on the far end of the slab,

with much of this measured deformation caused by rotation of the slab surfaces under the wheel loading.

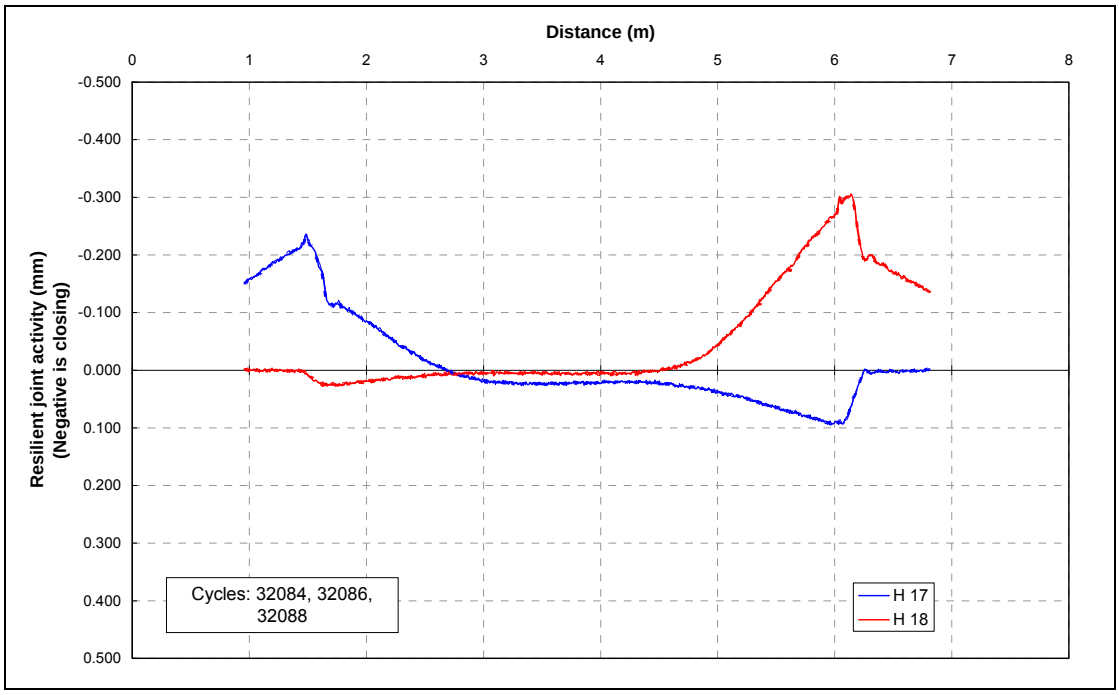

Figure 94. Resilient transverse joint activity influence lines for the ungrouted load test, 598FDUG.

The resilient vertical corner deflections, examples of which are shown in Figure 88 and Figure 89, were used to calculate the Load Transfer Efficiency (LTE) at the ungrouted joints according to the equation for LTE shown in Figure 67.Figure 95 shows the peak approach slab and simultaneous leave slab deflection at the two trafficked joints of the ungrouted test, 598FDUG. Figure 96 shows the LTE for the duration of the ungrouted test, 598FDUG. In general the LTE was below 10 percent for the duration of the test.

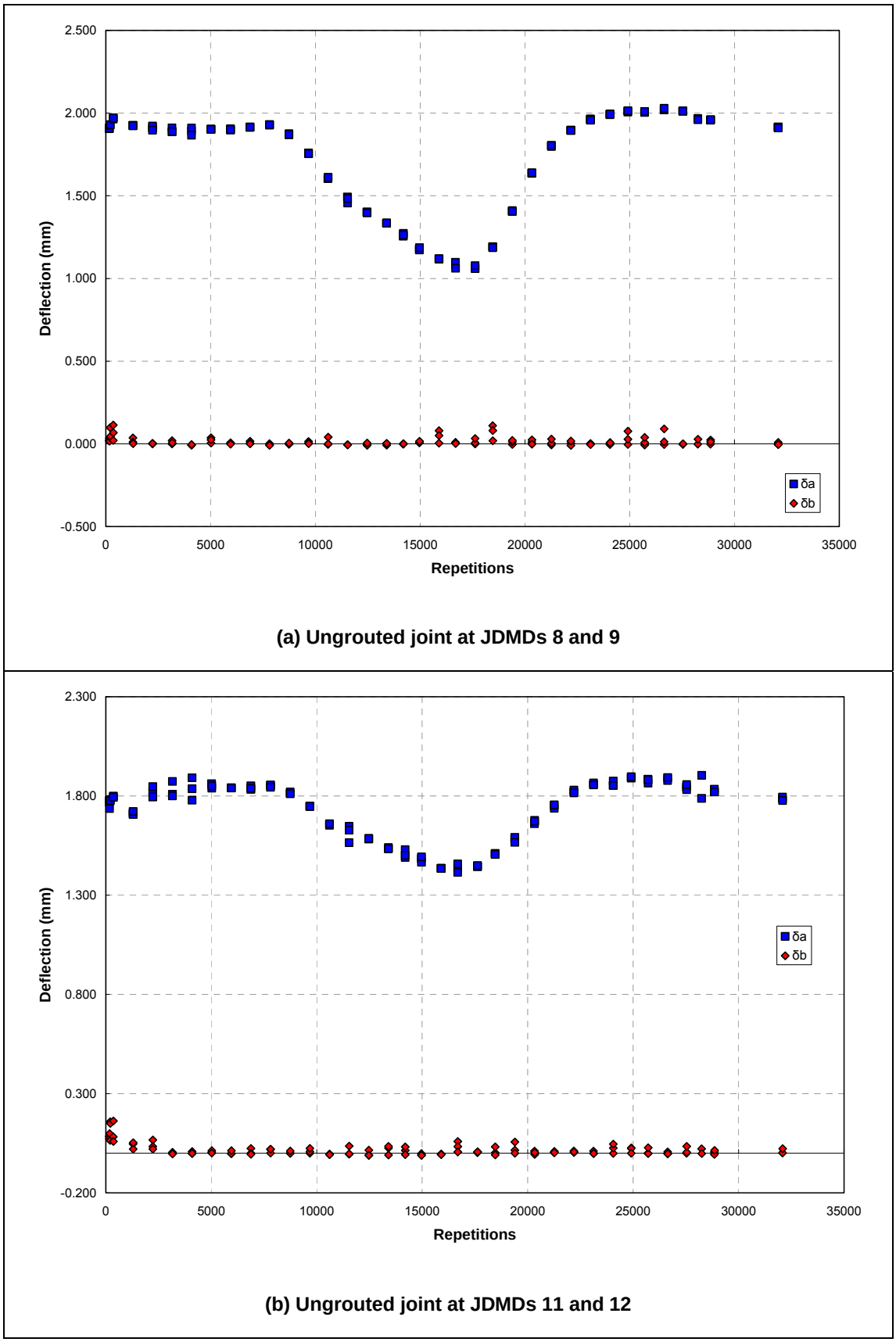

(a) Ungrouted joint at JDMDs 8 and 9

(b) Ungrouted joint at JDMDs 11 and 12

Figure 95. Peak approach slab and simultaneous leave slab deflection for the

ungrouted load test, 598FDUG.

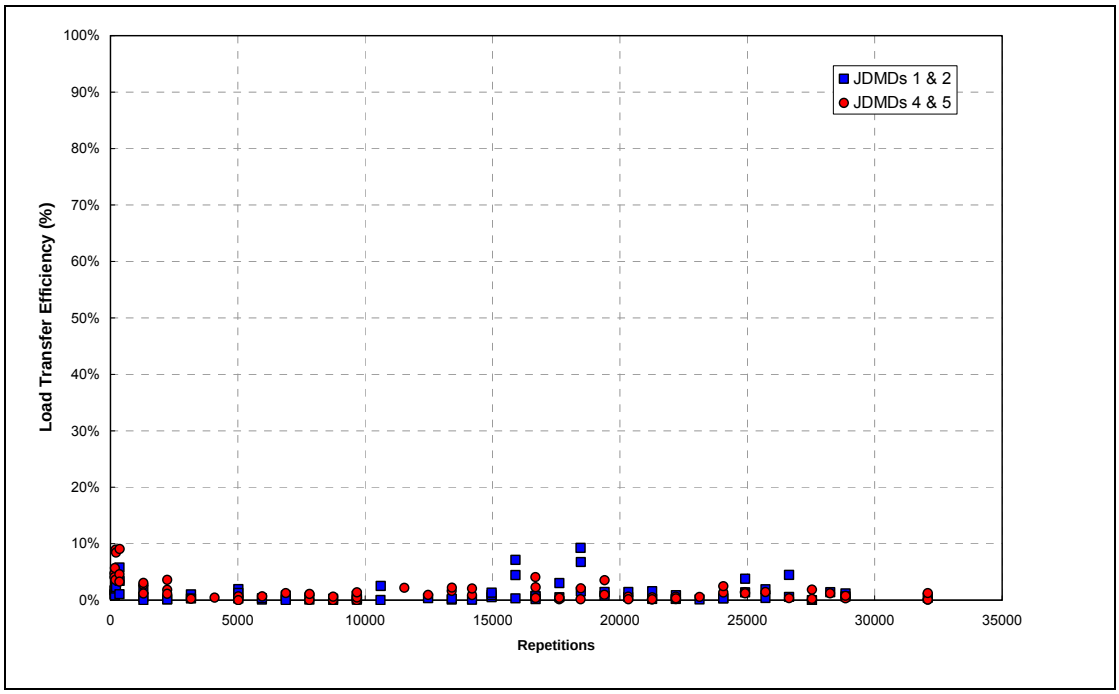

Figure 96. Load Transfer Efficiency for the ungrouted test, 598FDUG.

The resilient transverse joint horizontal deformation activity is shown in Figure 97 for the two trafficked transverse joints on the ungrouted test, 598FDUG. In general the total resilient transverse joint horizontal deformation activity was between 0.2 and 0.4 mm at H17 and between 0.25 and 0.5 mm at H18.

Figure 98 shows the mid-slab deflection for the duration of the ungrouted test, 598FDUG. Lifting of slightly more than 0.1 mm occurred at the mid-slab position for the duration of the test while the downward deflection under the load was about 0.2 mm resulting in a total mid-slab resilient movement of around 0.3 mm for the duration of the test.

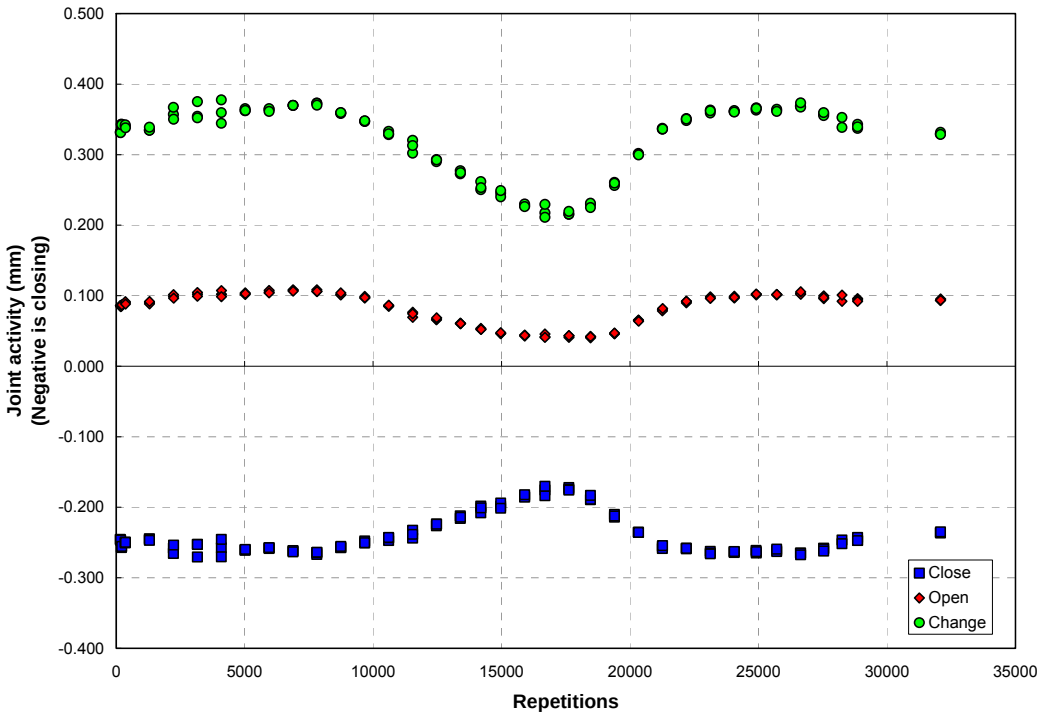

(a) Ungrouted joint at horizontal JDMD H17

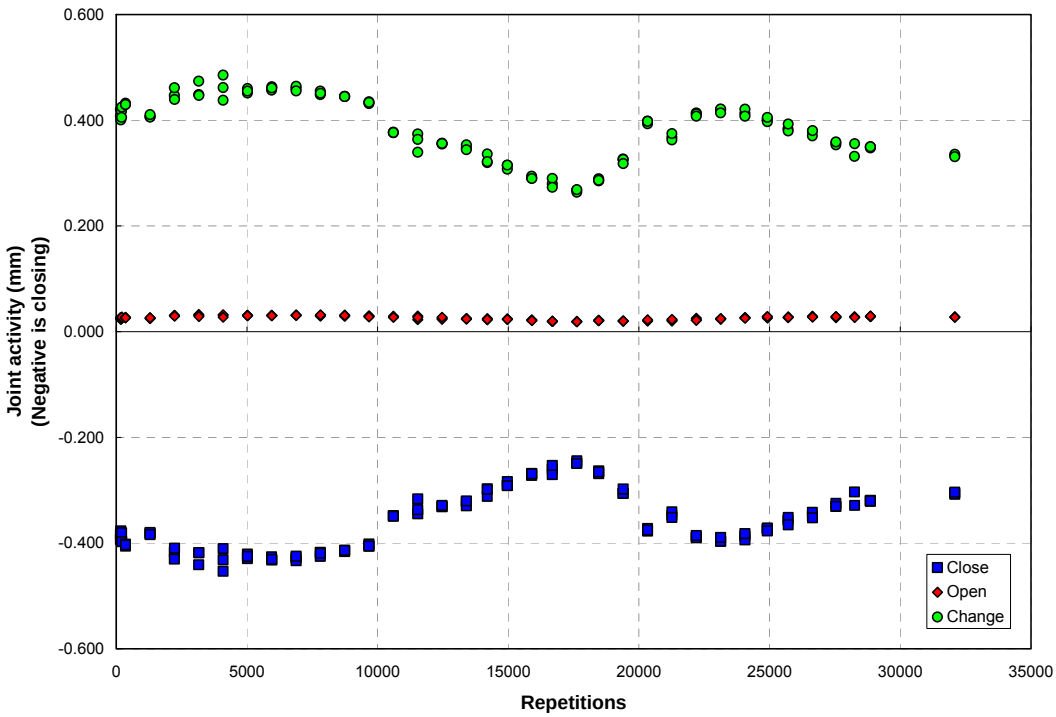

(b) Ungrouted joint at horizontal JDMD H18

Figure 97. Transverse joint activity for the ungrouted load test, 598FDUG.

Figure 98. Mid-slab deflection for the ungrouted test, 598FDUG.

The peak resilient deflections plotted in Figure 95, Figure 97, and Figure 98 vary with time, and therefore the effect of the temperature conditions on the resilient deflections was investigated. Figure 99 shows the resilient vertical deflection of the shaded corners plotted against the temperature gradient of the slab. The slab corner at JDMD 9 clearly had the lowest deflection but there is a correlation between the resilient vertical deflection and the temperature gradient of the slab for all the slab corners. Figure 100 shows the resilient vertical deflection of the exposed corners plotted against the temperature gradient of the slab. These slab corners were not directly trafficked but the rocking motion of the unrestrained slabs caused substantial deflection at them, with the corner at JDMD 7a having deflections almost as high as 0.6 mm.

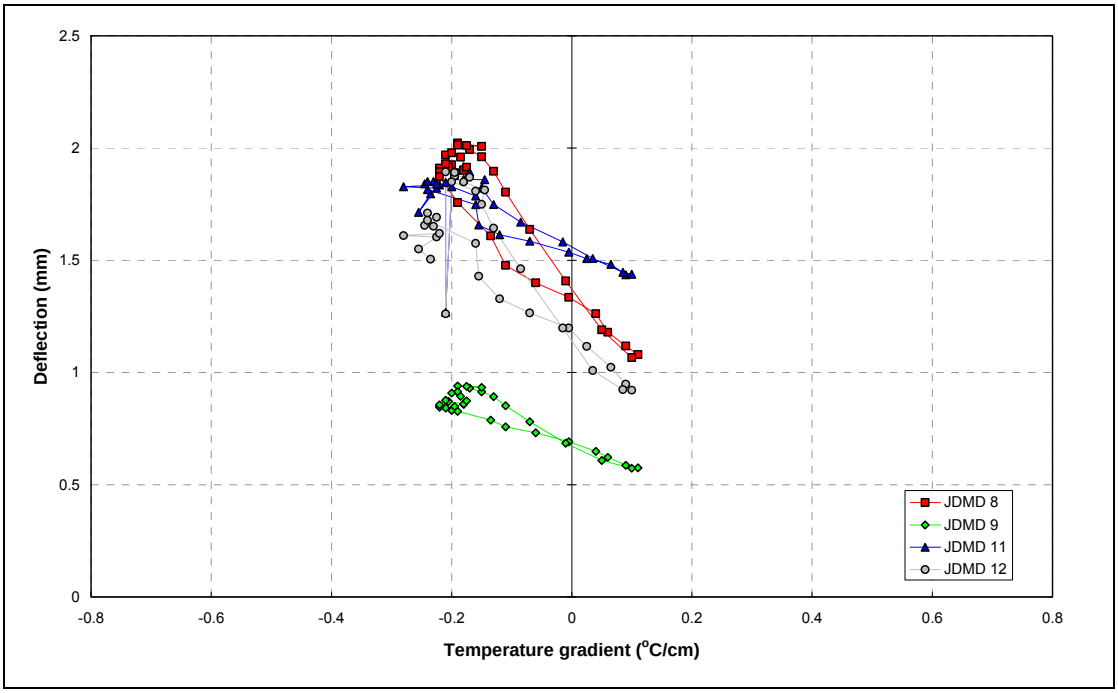

Figure 99. Resilient vertical deflection of the shaded slab corners for the ungrouted test, 598FDUG.

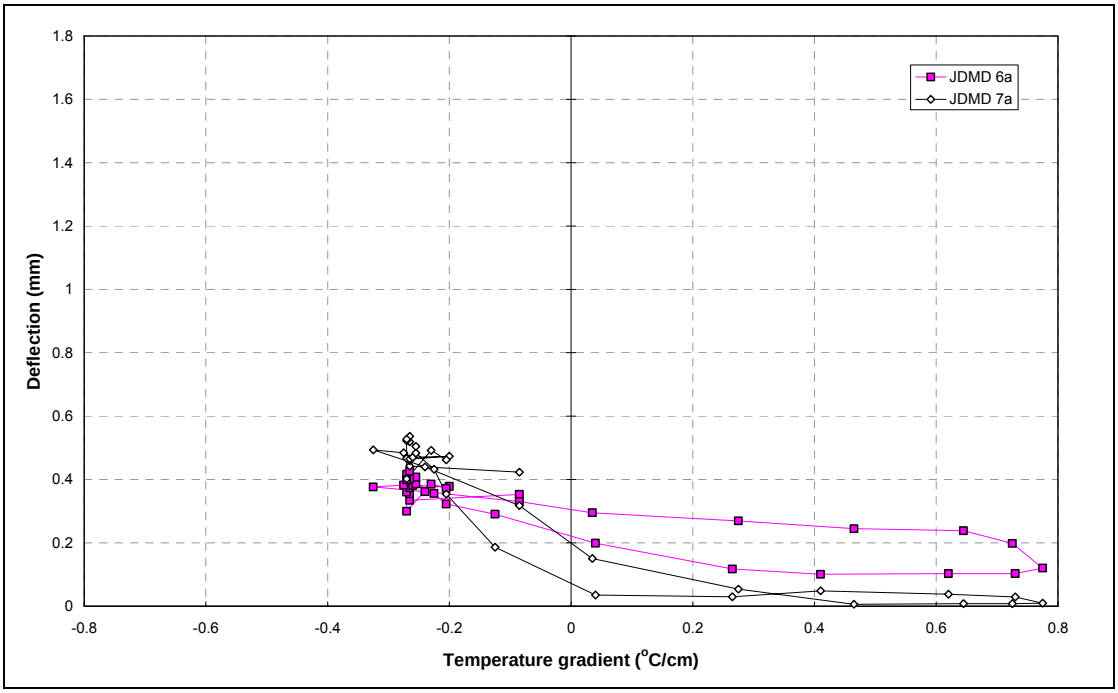

Figure 100. Resilient vertical deflection of the exposed slab corners for the ungrouted test, 598FDUG.

Figure 101 shows the resilient vertical mid-slab edge deflection plotted against the temperature gradient of the slab. The trafficked mid-slab edge at JDMD 10 had a resilient

deflection around 0.2 mm for the duration of the test and does not seem to be correlated with the temperature gradient of the slab. However, the temperature gradient range was small because the trafficked edge of the slab was shaded by the HVS.

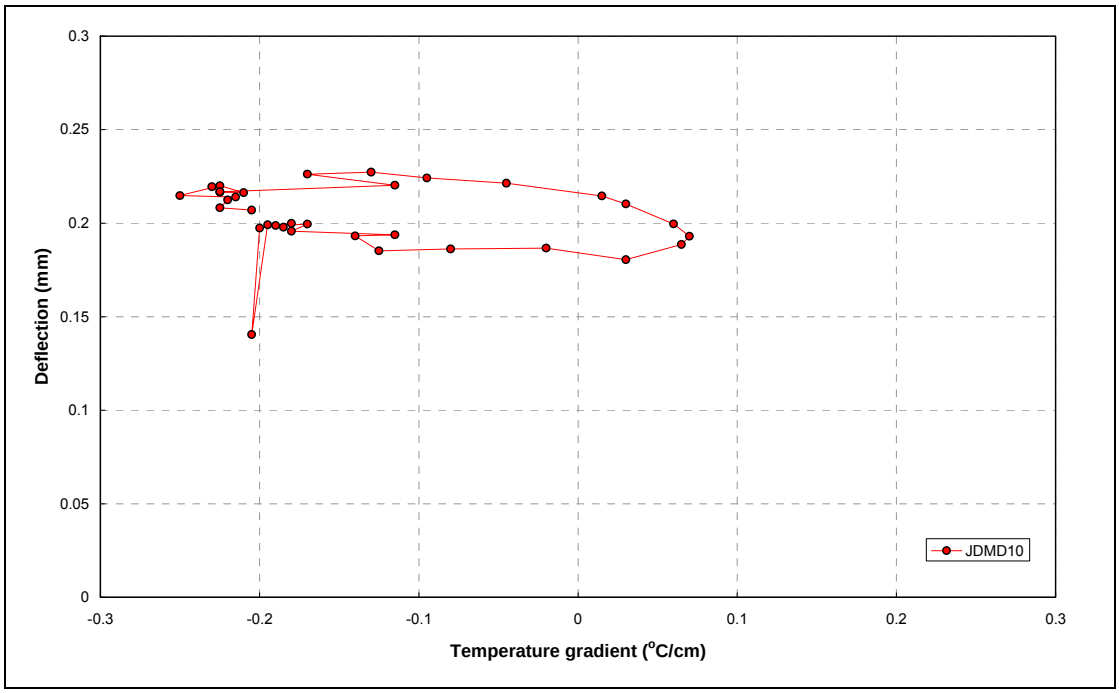

Figure 101. Resilient vertical deflection of the slab mid-slab edge for the ungrouted test, 598FDUG.

Figure 102 shows the resilient transverse joint horizontal deformation activity plotted against the surface temperature, and Figure 103 shows the resilient longitudinal joint horizontal deformation activity plotted against the surface temperature for the joint between the two rows of slabs (H15 and H16) and the joint between the trafficked slabs and the AC shoulder [H15(b) and H16(b)].

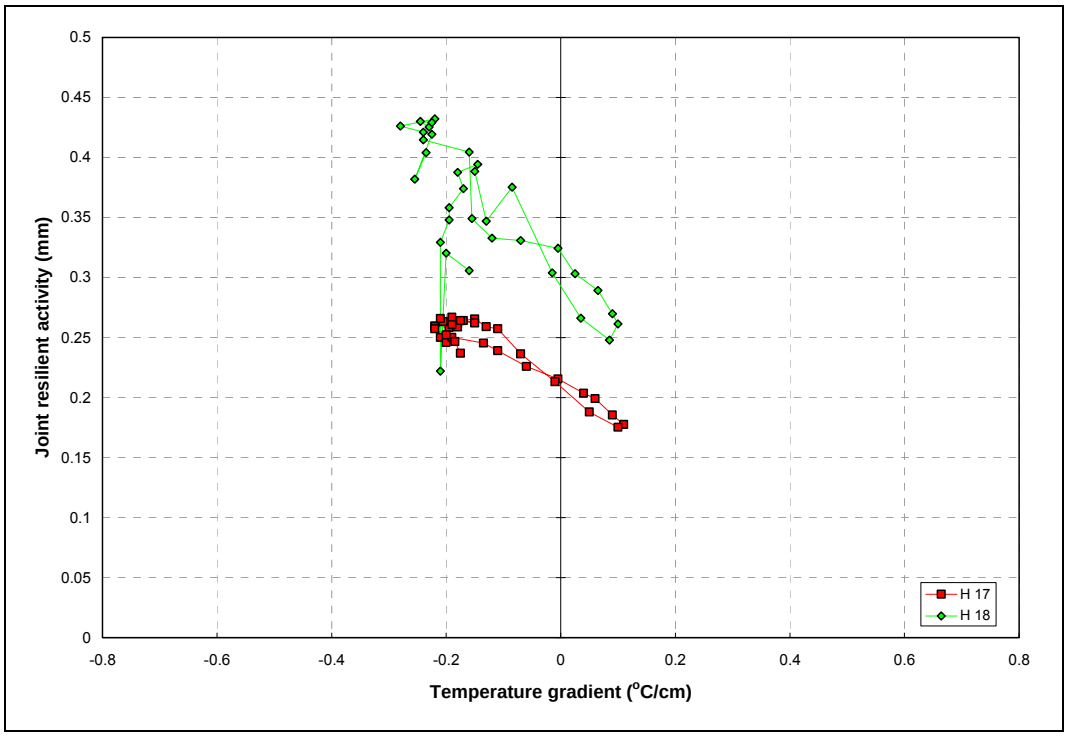

Figure 102. Resilient transverse joint horizontal deformation activity for the ungrouted test, 598FDUG.

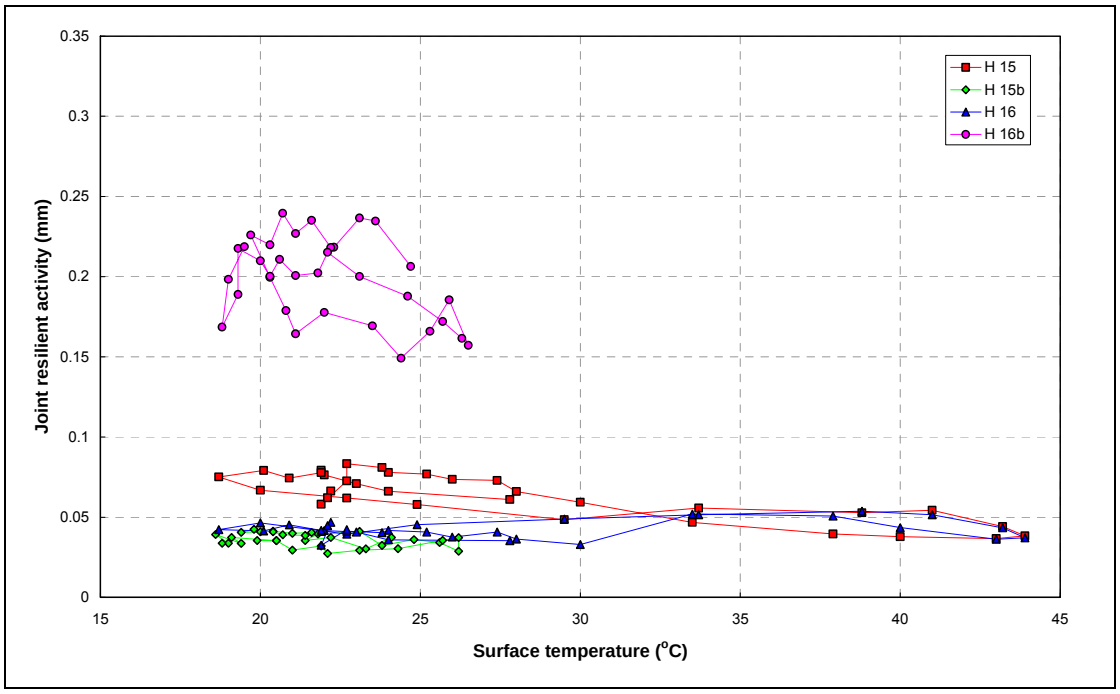

Figure 103. Resilient longitudinal joint horizontal deformation activity for the ungrouted test, 598FDUG.

In summary the following observations are made regarding the ungrouted load test, 598FDUG:

- Thermal curl response:
    - All the shaded slab corners had a total thermal curl movement of 1.6 mm over a temperature gradient range from -0.2 to +0.2°C/cm (equivalent to a temperature differential of -4 to +4°C).
    - The exposed slab corners had a similar total thermal curl movement of 1.6 mm but in this case over a temperature gradient range from -0.4 to +0.8°C/cm (equivalent to a temperature differential of -8 to +18°C).
    - The transverse joints at H17 and H18 had total thermal curl joint horizontal deformation activities of 0.5 mm and 0.4 mm respectively over a temperature range from 17°C to 26°C.
    - The longitudinal joint between the slab and the AC shoulder had a total thermal curl joint horizontal deformation activity of 0.2 mm over a temperature range from 17°C to 26°C.
    - The longitudinal joint at H15 and H16 had a total thermal curl joint activity of 1.0 mm over a temperature range from 17°C to 44°C.
- Resilient deflection response:
    - The temperature gradient range on the trafficked portion of the test section was limited to a range between -0.2 and +0.1°C/cm because of the shading effect of the HVS. Within this temperature gradient range, the slab corner at JDMD 9 had the lowest resilient deflection of between 0.5 and 1.0 mm. The other slab corners had resilient deflections between 1.0 and 2.0 mm. The slab corner at JDMD 9 seems to be stiff in comparison with the other slab corners in terms of resilient deflection response.
    - The exposed slab corners at JDMDs 6a and 7a had a wider temperature gradient range from about -0.4 to +0.8 °C/cm (temperature differential of -8 to +17°C). The resilient deflections ranged between 0.0 and 0.6 mm for this temperature gradient range but these corners were not trafficked and the deflection is the result of the rocking of the unrestrained slabs.
    - The resilient mid-slab edge deflection at JDMD 10 varied around 0.2 mm over a temperature gradient range of -0.25 to +0.1 °C/cm (temperature differential of -6 to +2°C).

- The resilient transverse joint activity at the first joint of the test section varied between 0.25 and 0.45 mm for a temperature range of 17°C to 26°C. The corresponding joint activity at the second joint of the test section varied between 0.17 and 0.27 mm for the same temperature range.
- The resilient longitudinal joint horizontal deformation activity was generally below 0.1 mm with only the longitudinal joint between the slab and the AC shoulder ranging between 0.15 and 0.25 mm toward the eastern end of the test section at the horizontal JDMD H16b.

A transverse crack (Figure 104) was noticed on both test sections after completion of the ungrouted tests. This crack is believed to be the result of the load imposed on the slabs by the outriggers of the HVS and is not traffic related.

Figure 104. Part of a nontraffic-related tranvserse crack noticed on both sections after completion of the ungrouted tests.

5 TESTS PERFORMED AFTER GROUTING

5.1 Thermal Curl Test 598FDTC

Testing continued after grouting of the slabs. The first set of tests after grouting consisted of tracking the thermal curl of the grouted slabs over a 24-hour period from 07h02 on June 7, 2005, to 07h02 on June 8, 2005, without any load being applied to the slabs. The instruments monitored on an hourly basis during this time period are shown in Figure 105.

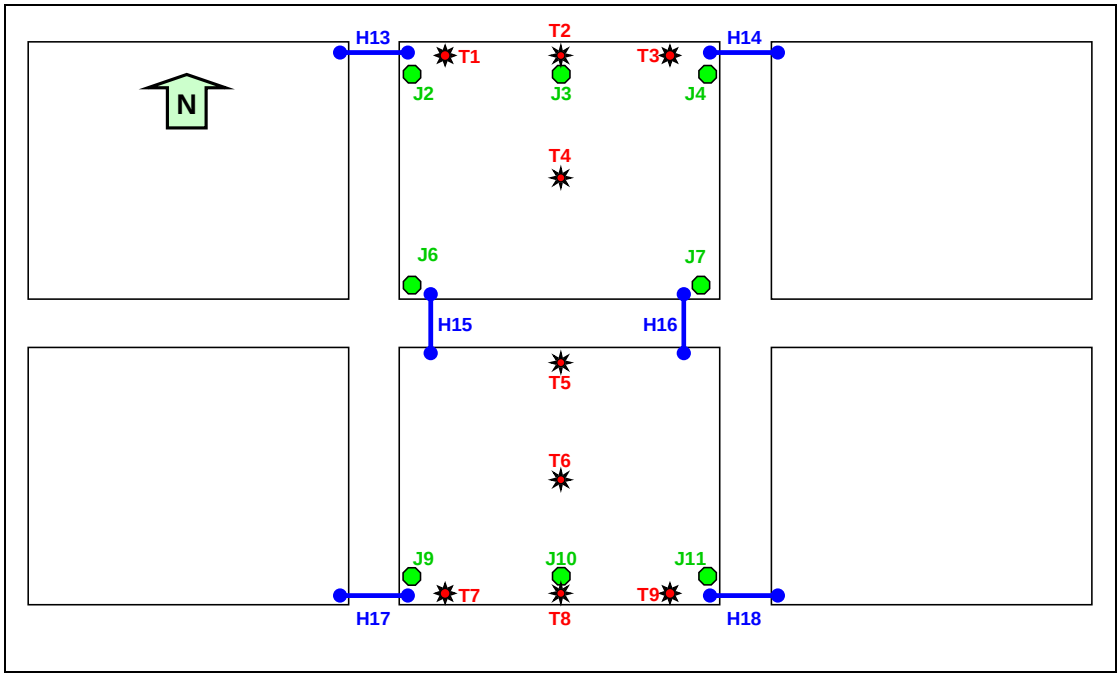

Figure 105. Thermocouples and JDMDs monitored during the thermal curl test on the grouted slabs.

The average slab temperature and temperature gradient were calculated from the temperature data recorded at the five depths for each of the thermocouples shown in Figure 105. The average slab temperature is shown in Figure 106, and the temperature gradient in Figure 107. The temperature data was collected electronically using the Data Acquisition System (DAS). This system failed for thermocouples 1, 2, and 4 after noon on June 7, and the temperature data for these thermocouples are incorrect from this time to the end of the test.

The JDMDs can only measure the relative movement of the slab from the start of the test, with no indication of the neutral position of the slab. An assumption therefore had to be made that the slabs were in a neutral position at the time the temperature gradient was zero, which occurred at 09h00 on June 7. The JDMD readings at 09h00 on June 7, 2005, were therefore assumed to represent the neutral position of the slab and all other measurements were adjusted relative to the measurement taken at this time.

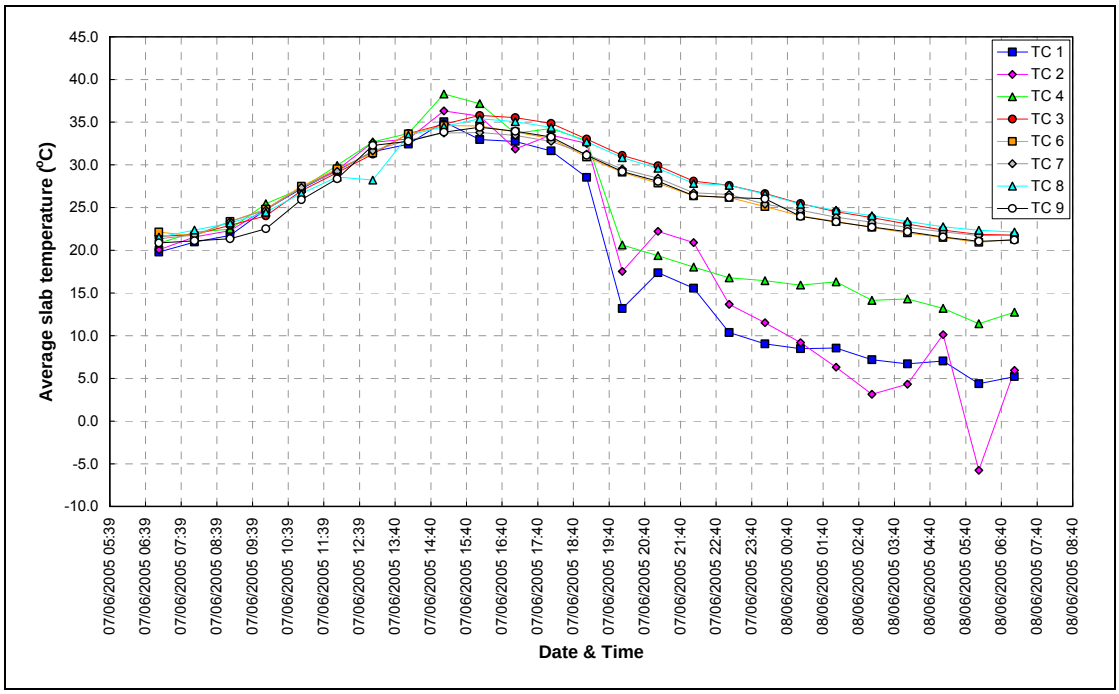

Figure 106. Average slab temperature during the grouted thermal curl test.

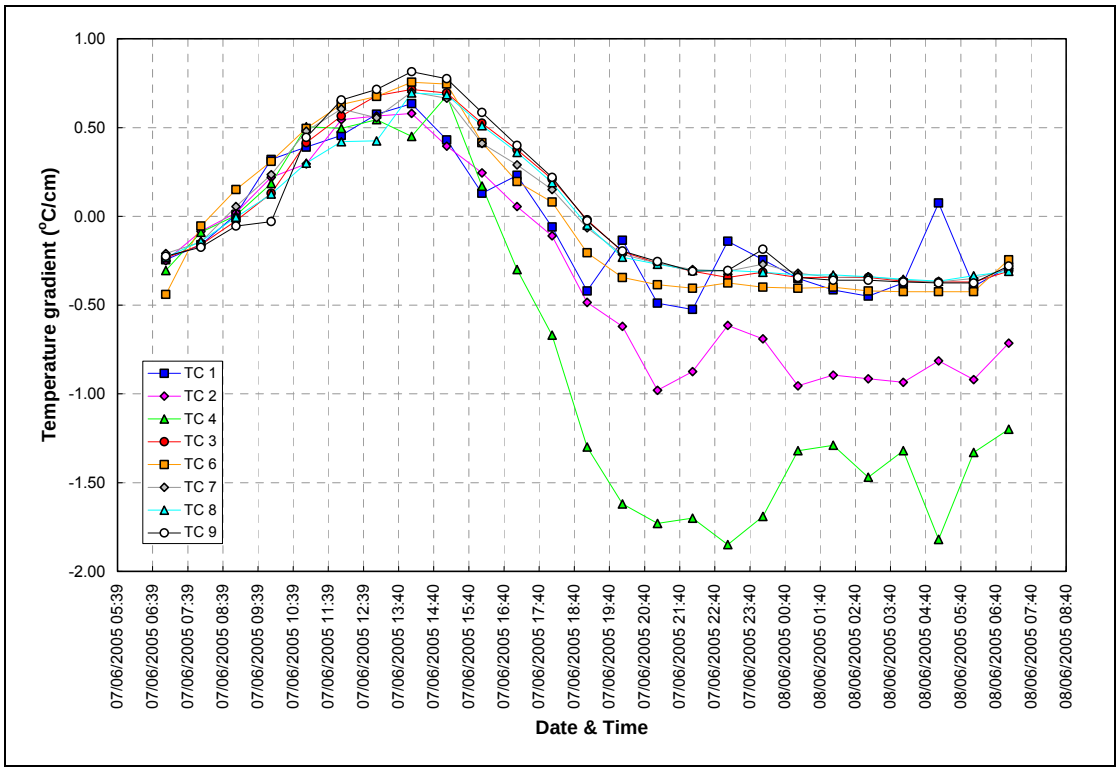

Figure 107. Temperature gradient during the grouted thermal curl test.

Figure 108 shows the relative movement (in terms of the previously determined neutral position) of all the vertical JDMDs shown in Figure 105 at the corners of the slabs. As expected, the corners curled upward during nighttime when the slabs had a negative temperature gradient

(warmer at the bottom than at the top of the slab). The highest vertical movement occurred at JDMD 2 with a range from 0.6 mm downward to 0.8 mm upward (1.4 mm total). Figure 109 shows the adjusted joint activity recorded by the horizontal JDMDs. Again, as expected the joints closed up during higher daytime temperatures. The range of grouted transverse joint opening and closing, with the dowels mobilized by the grouting, was from 0.2 mm to -0.3 mm, giving a total joint activity of 0.5 mm, while the tied longitudinal joint only had a total joint activity of 0.3 mm.

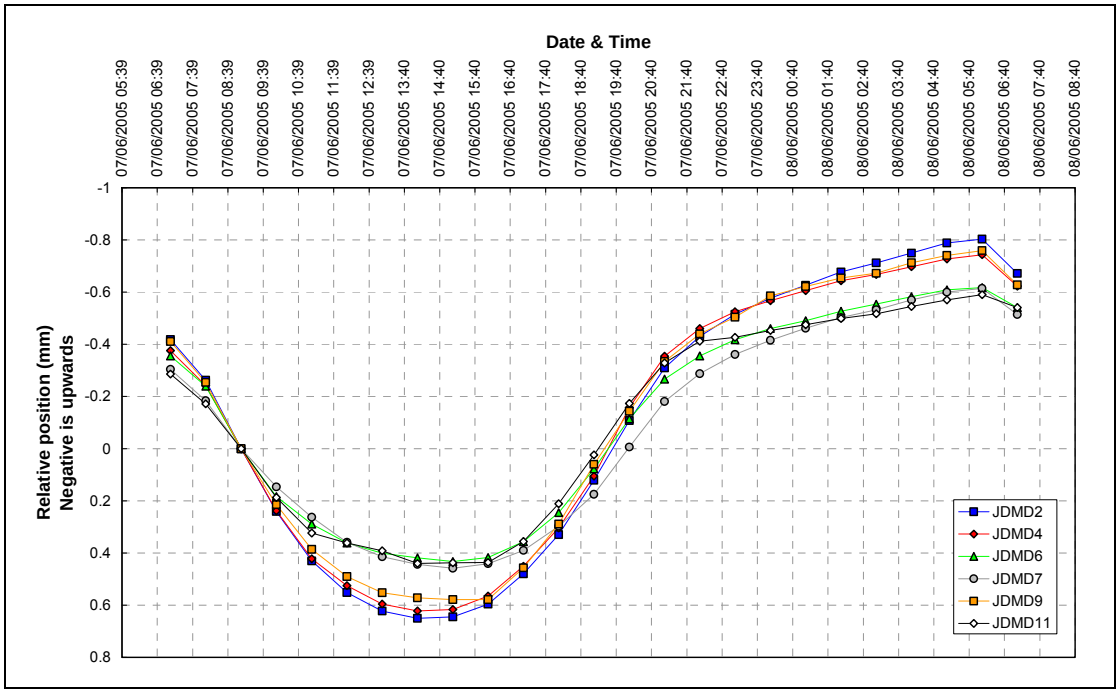

Figure 108. Adjusted vertical movement of the slab corners during the grouted thermal curl test.

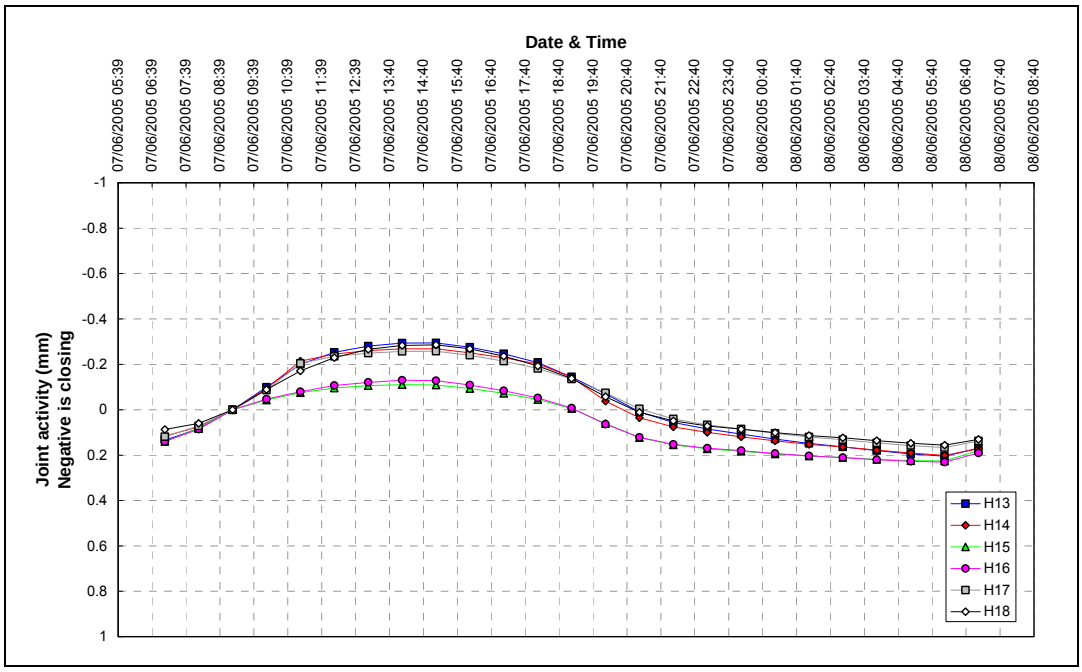

Figure 109. Adjusted horizontal joint activity during the grouted thermal curl test.

In an effort to determine the relationship between temperature gradient and vertical curl, the adjusted JDMD readings were plotted with the temperature gradient data. Figure 110 shows a typical example of the adjusted vertical movement at JDMD 4 plotted with the temperature gradient calculated from the temperature data for the closest thermocouple, TC 3. It is apparent that the vertical curl is correlated with the temperature gradient.

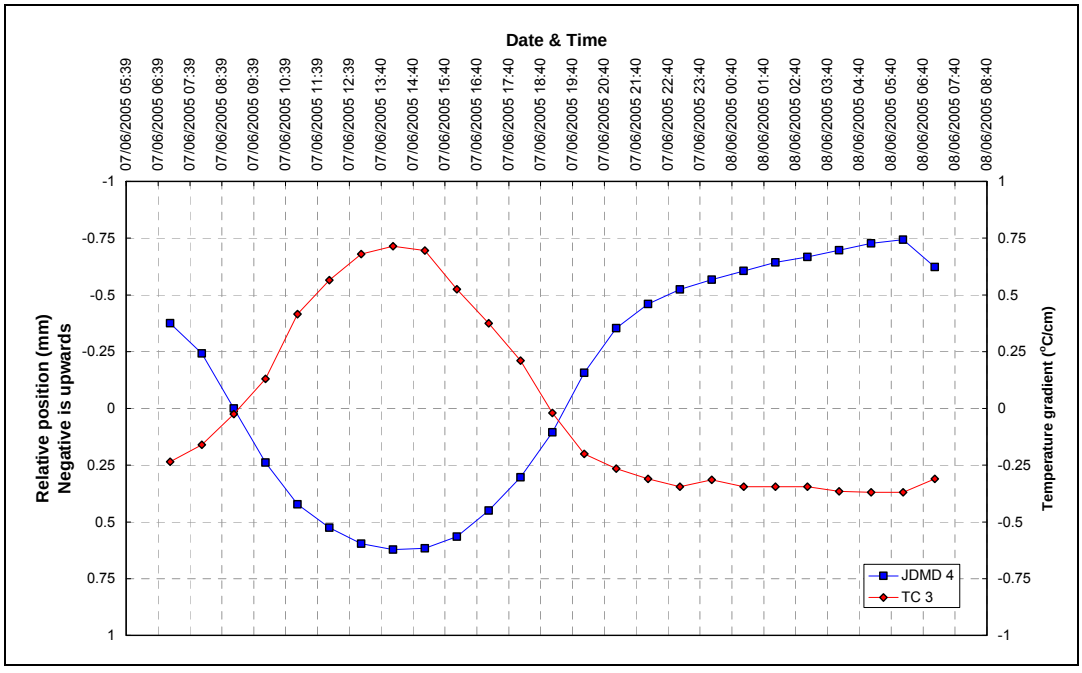

Figure 110. Example of the relationship between the temperature gradient and vertical movement of the slab corners for the grouted slabs.

This correlation was explored further by plotting the adjusted vertical corner movement against the temperature gradient for the JDMDs with thermocouples in close proximity. The results from this process are shown in Figure 111, and there is a strong correlation between the thermal curl of the slab corners and the temperature gradient.

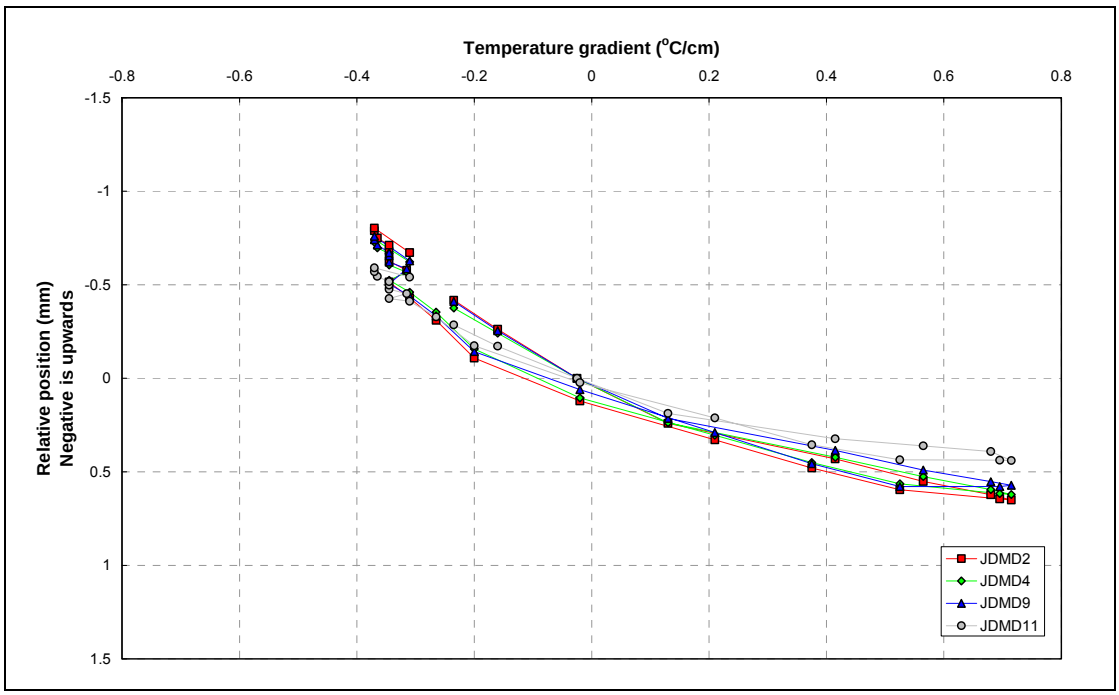

Figure 111. The correlation between the temperature gradient and vertical movement of the slab corners for the grouted slabs.

The thermal curl response of the slab corners after grouting is greatly reduced, compared to the thermal curl before grouting where the slab corner at JDMD 4 moved significantly less than the other corners.

A similar analysis was done for the horizontal deformation joint activity by plotting the joint activity against temperature gradient as shown in Figure 112. As was previously noted, horizontal deformation at the joint is primarily controlled by the expansion and contraction of the slabs, and the deformation is less well correlated with temperature gradient, which rotates the faces of the joints rather than making them expand and contract. The result from this process is shown in Figure 113 and yields a linear correlation between the slab's temperature and the joint's opening and closing.

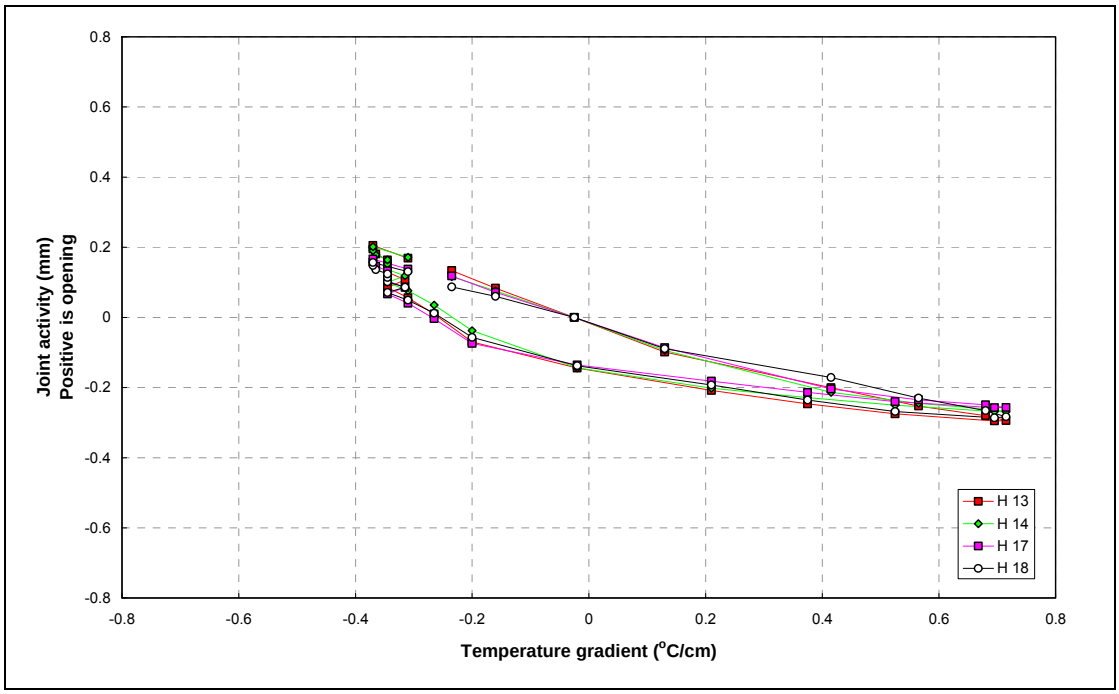

Figure 112. The correlation between the temperature gradient and horizontal joint activity for the grouted slabs.

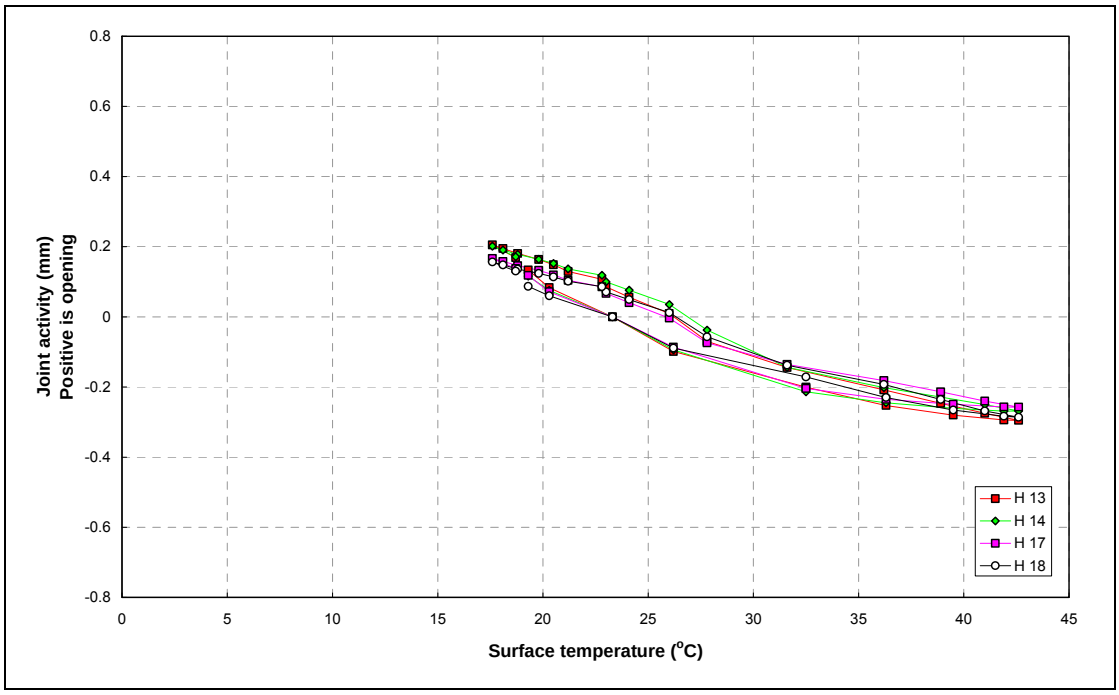

Figure 113. The correlation between the surface temperature and horizontal joint activity for the grouted slabs.

In summary, the following observations are made regarding the grouted thermal curl test on HVS Test Section 598FDTC:

- The vertical curl at the corners of the restrained slabs was 1.4 mm for all the JDMDs over a temperature gradient range from -0.4°C/cm to +0.7°C/cm.
- The horizontal joint activity had a total movement of 0.5 mm for a surface temperature range from about 20°C to 40°C. Although this is less than the joint activity for the ungrouted tests, the bond-breaker applied to the dowel bars and joint seem to allow some horizontal movement caused by thermal expansion as is desired.
- There is a strong correlation between the temperature gradient and the vertical movement at the slab corners caused by thermal curl.
- There is a strong correlation between the surface temperature and horizontal joint activity.

5.2 Load Tests 597FD

The thermal curl test on Section 598FDUG concluded the set of preliminary tests in this experiment and signified the beginning of the longer-term tests. In June 2005, HVS2 was moved to Section 597FD where it was used to apply more than one million wheel load repetitions until September 2005 (see Table 2). The test was conducted under dry conditions (no water added to the pavement), with an aircraft tire using very high load levels. Test 597FD continued later under wet conditions. Only data relevant to the comparison to the ungrouted condition is presented in this report. The rest of the long-term loading data on Section 597FD are presented in references (2) and (3).

An example of typical JDMD deflection bowls from the corners of the slabs at the west joint of Section 597FD under 60 kN loading is shown in Figure 114 for the 74th, 76th, and 78th load repetitions after grouting. Similar results were also obtained for the other two JDMDs at the east joint. The peak deflections on the approach slabs and the simultaneous deflection on the leave slabs were extracted from the JDMD deflection bowls to calculate the Load Transfer Efficiency (LTE).

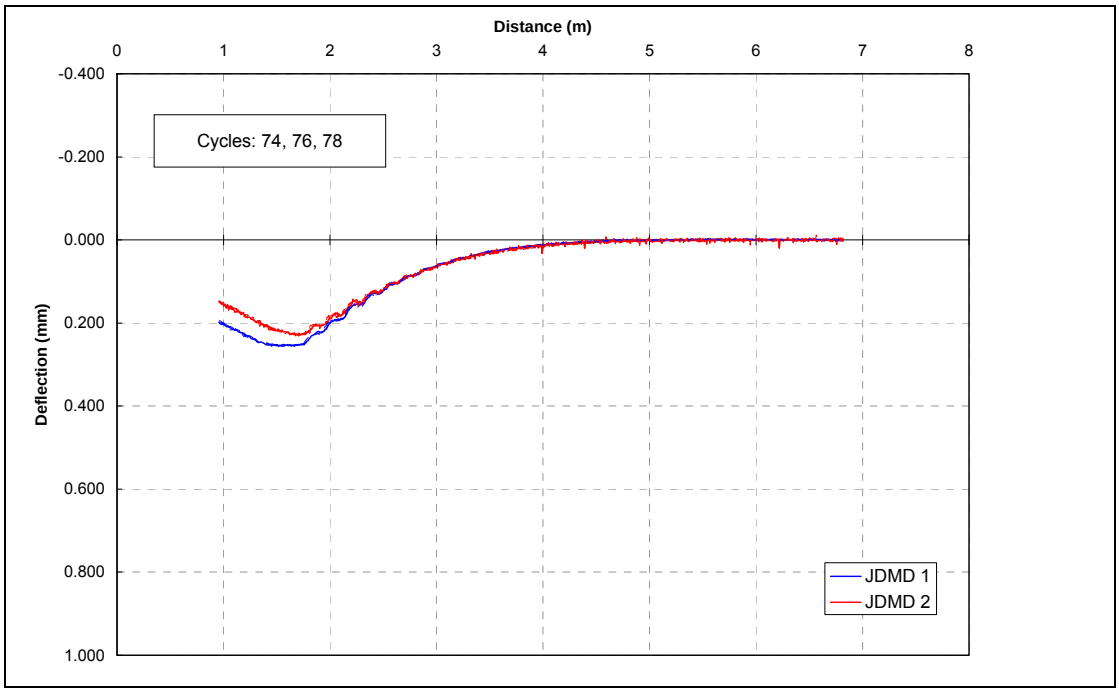

Figure 114. Resilient vertical corner deflection influence lines for the west joint in Test 597FD (after grouting).

The vertical mid-slab deflection was also recorded and a typical example of the mid-slab deflection bowl is shown in Figure 115.

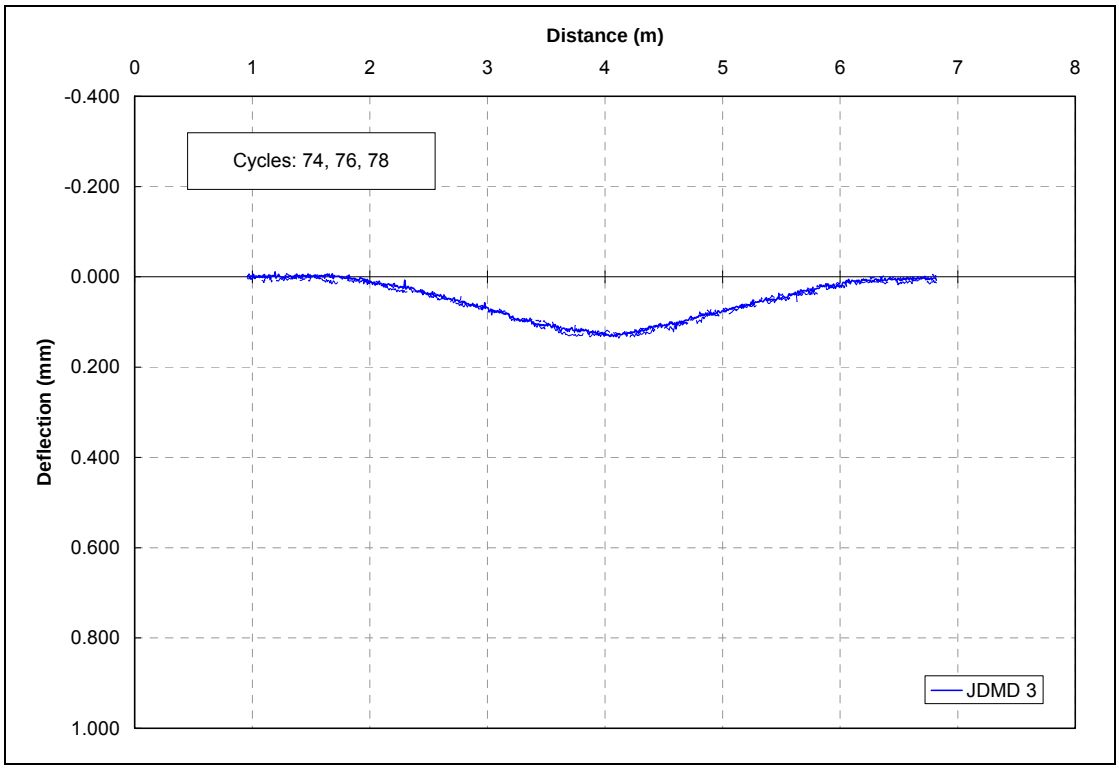

Figure 115. Resilient vertical mid-slab deflection influence lines in Test 597FD (after grouting).

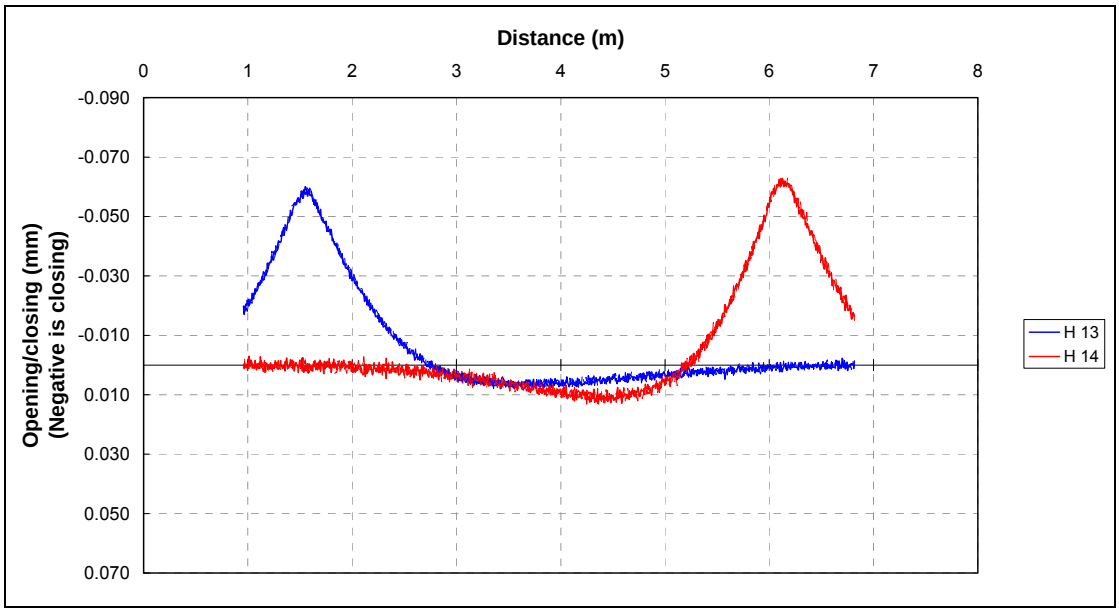

Figure 116. Resilient transverse joint activity influence lines in Test 597FD (after grouting).

The traffic load levels were increased as the test progressed. Periodic data collection at 60kN allowed for tracking the pavement's responses to a fixed load level. Figure 117 shows a summary of the peak approach slab deflection, simultaneous leave slab deflection and LTE from JDMDs 1 and 2 for most of the duration of test 597FD, with the load levels indicated at the top of the chart (the data is at 60kN despite the increasing traffic load levels).

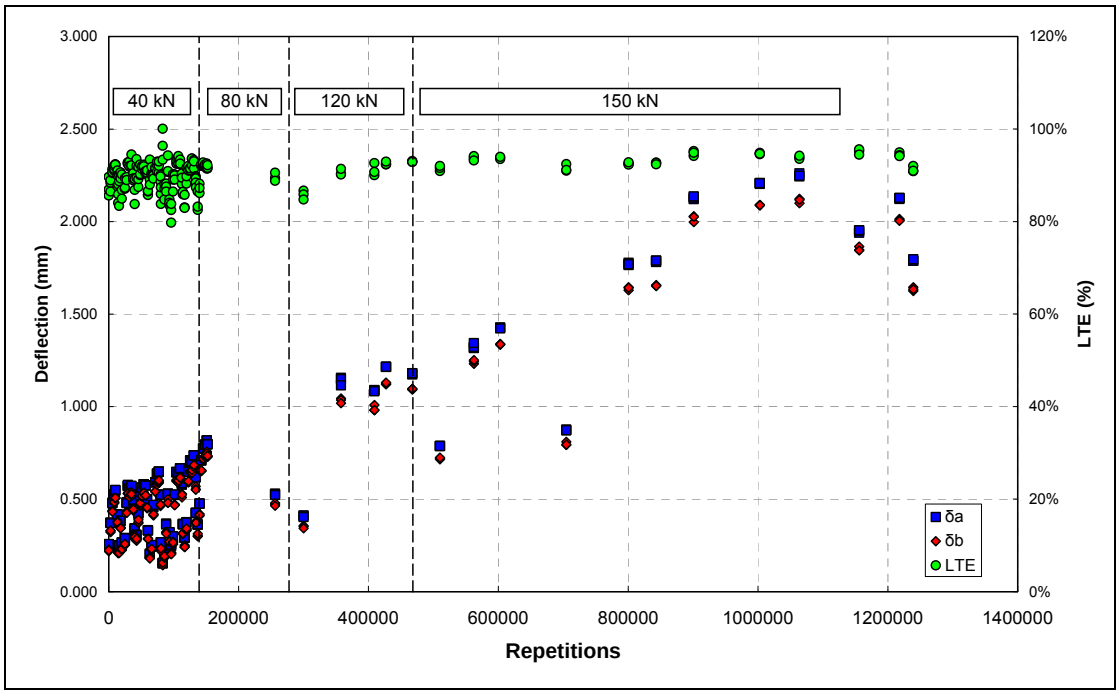

Figure 117. JDMD deflection and LTE summary for the west joint at 60 kN for the duration of test 597FD.

The 60 kN deflection data exhibits an increase in deflection with increasing load repetitions. The 60 kN JDMD deflection and LTE were therefore plotted against the temperature gradient of the slab. The initial deflection and LTE results for approximately the first 100,000 load repetitions are shown in Figure 118.

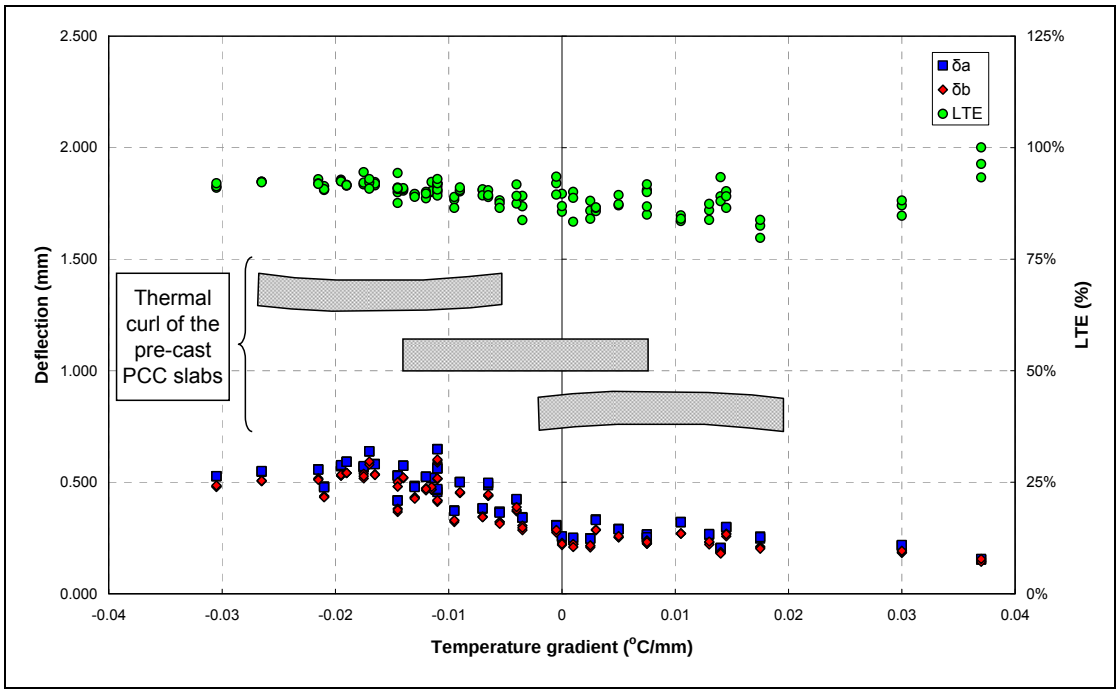

Figure 118. Initial JDMD deflection and LTE data for west joint at 60 kN plotted against the slab temperature gradient.

5.3 Load Tests 598FD

No load test results from Test 598FD are presented in this report, as this was not part of preliminary HVS testing. The HVS machine was moved to Section 598FD in September 2005, and until February 2006 it tested the pavement with a set of dual truck tires, applying a considerable number of load repetitions, also in dry condition. Water was added to the joints in Section 598FD starting in February 2006, and trafficking continued until May 2006 in wet condition. At that point, the HVS machine was returned to Section 597FD to subject the pavement to more traffic in wet condition with the aircraft tire.

6 PAVEMENT RESPONSES BEFORE AND AFTER GROUTING

6.1 Comparison of Thermal Deformations

Figure 119 shows the peak vertical thermal movement of the slabs at different locations. The grouting of the slabs had a significant effect on the vertical curl of the slabs along the longitudinal joint, where the curl was reduced from a range of ±1.5 mm to ±0.5 mm. Figure 119(a) and (c) show that the corners moved upwards at night and downwards during the day, as expected. The absence of more sensors throughout the width of the slab prevents detailed measurement of the actual shape of the deformed slabs in Figure 119(b) and (d). In the ungrouted condition each slab most likely curled separately, while after grouting the presence of tie-bars and grout in the joint (coming from the tie-bar grout slots) forced at least partial transfer of moment and displacements, which actually changed the shape of the two-slab system. The probable shapes of each slab in its most deformed states are outlined in the charts.

Figure 120 shows a comparison of the thermal curl joint activity before and after grouting. Grouting had a significant effect on the magnitude of joint closing during the day but not much effect on the magnitude of joint opening at night. The amount by which both the transverse and longitudinal joints closed was reduced from 0.75 mm before grouting to 0.25 mm and less after grouting. A certain amount of horizontal movement is required at the transverse joint to accommodate thermal expansion and a bond-breaker was applied to the dowels in the joints before grouting. Although the amount of movement is not the same after grouting as before, a certain amount of movement is still allowed and the bond-breaker seems to be effective in permitting expansion and contraction of the slabs.

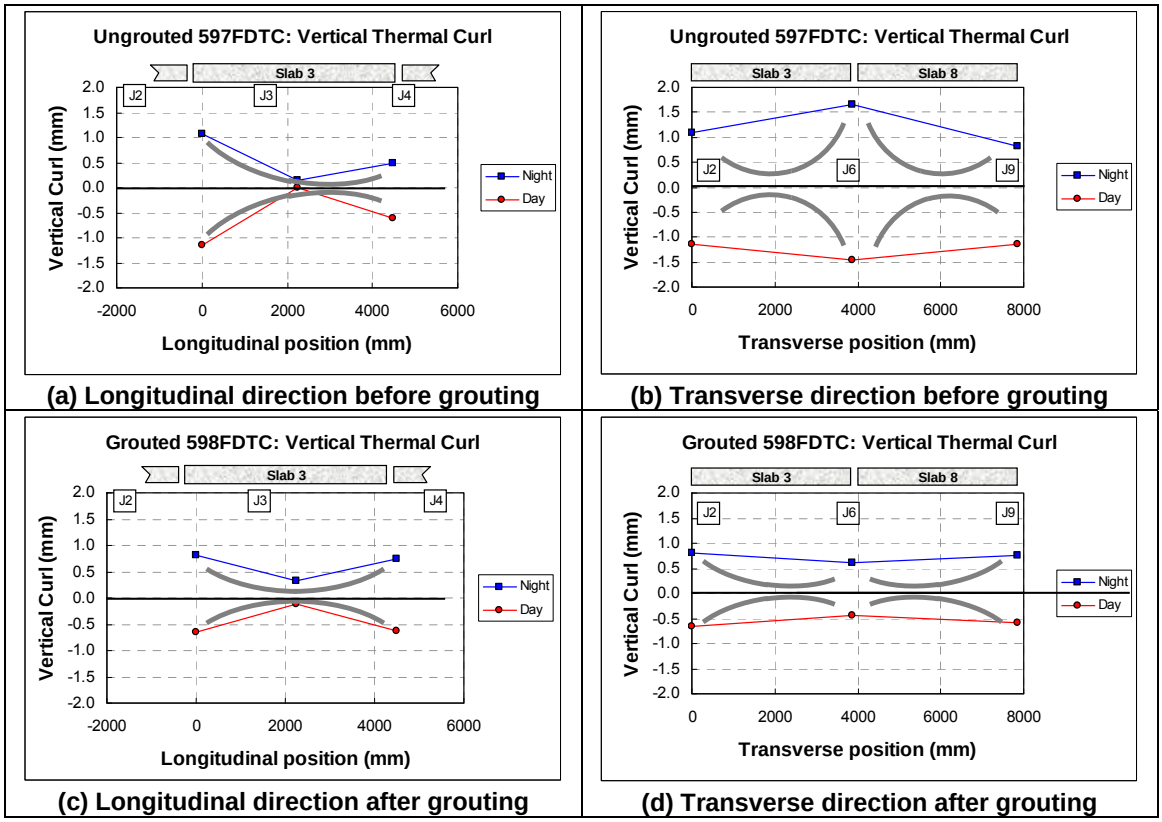

(a) Longitudinal direction before grouting **(b) Transverse direction before grouting**

(c) Longitudinal direction after grouting **(d) Transverse direction after grouting**

Figure 119. Comparison of the vertical deformations caused by thermal curl of the slabs before and after grouting.

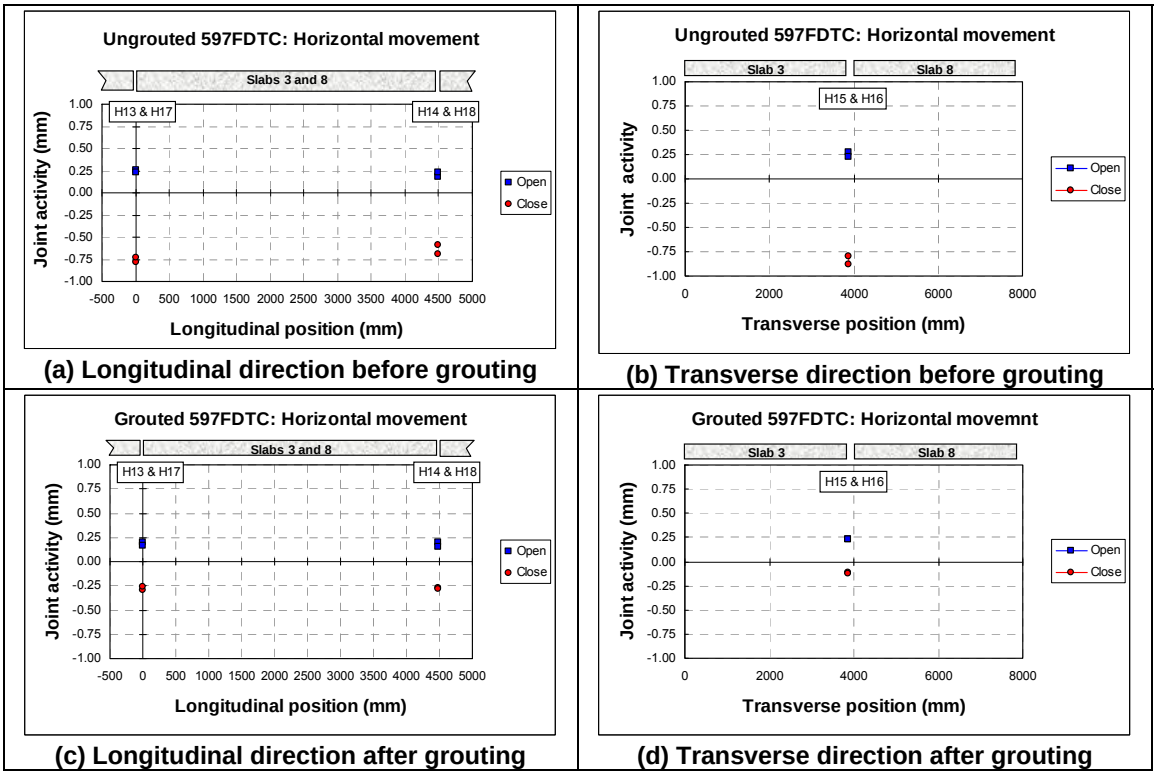

Figure 120. Comparison of the horizontal deformations caused by thermal activity of the slabs before and after grouting.

6.2 Comparison of Load Responses

As expected, pavement responses improved greatly after grouting. Figure 121 shows typical deflection curves at one of the transverse joints before and after grouting in Section 597FD. The following effects of grouting the joints can be observed:

- Both sides of the joint move together after grouting, while they acted independently to the wheel load in the ungrouted condition.
- The vertical deflection at the transverse joint after grouting decreased to one-quarter of the value measured before grouting (from about 1.0 mm to 0.25mm). This reduction in deflection is expected to reduce the flexural stresses responsible for fatigue cracking.
- Rocking of the slab is eliminated, as indicated by the lack of movement when the wheel load is near the opposite joint. Slab rocking in the ungrouted condition resulted in about 0.1 mm of up-lifting.

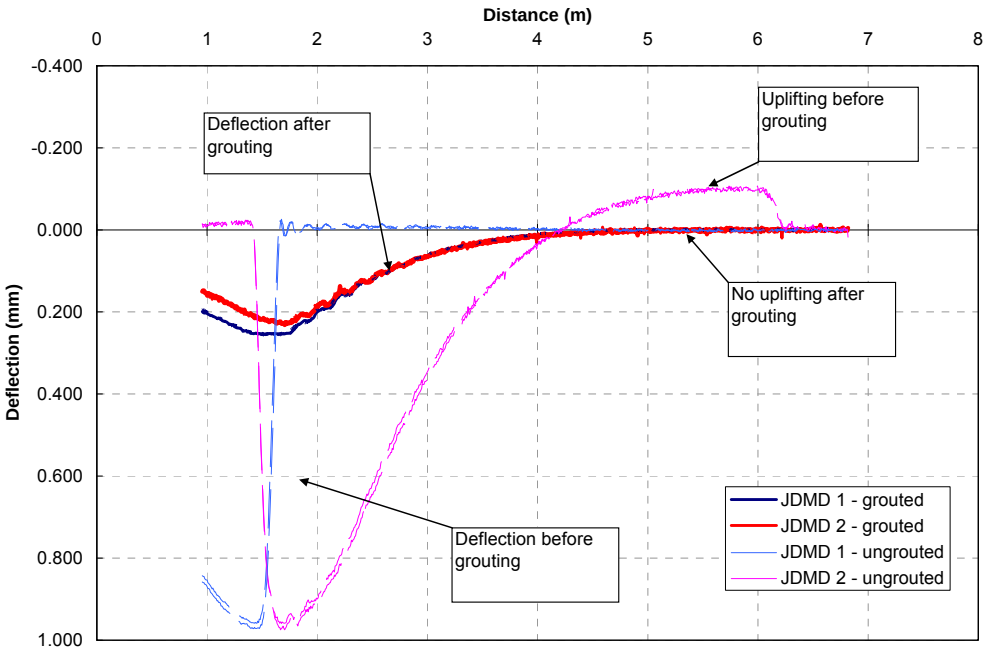

Figure 121. Typical vertical corner deflection influence lines from west joint in Test 597FD before and after grouting.

Maximum vertical deflections at the mid-slab edge caused by the wheel load were not affected by grouting. However, the up-lifting due to corner loading was eliminated, as shown in Figure 122.

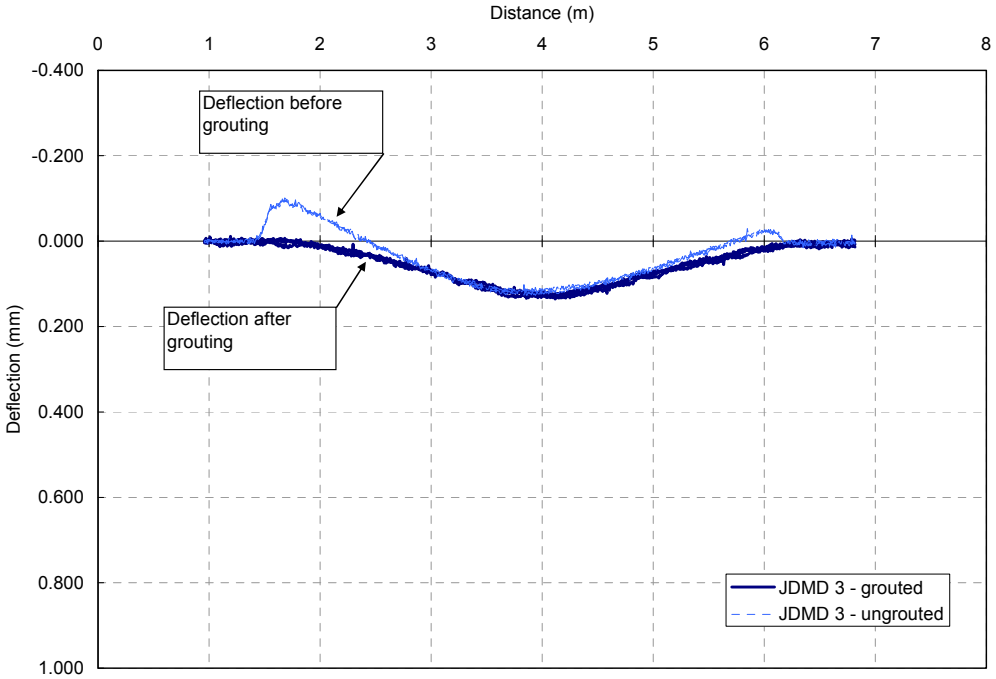

Figure 122. Typical JDMD data obtained at mid-slab in Test 597FD before and after grouting.

Regarding transverse joint activity, the magnitude of the movement was significantly reduced, and activity continuity was observed as the wheel load crosses over the joints, as seen in Figure 123. The joint activity was measured at the pavement surface, therefore the rotation of the joint faces played a significant role in the observations.

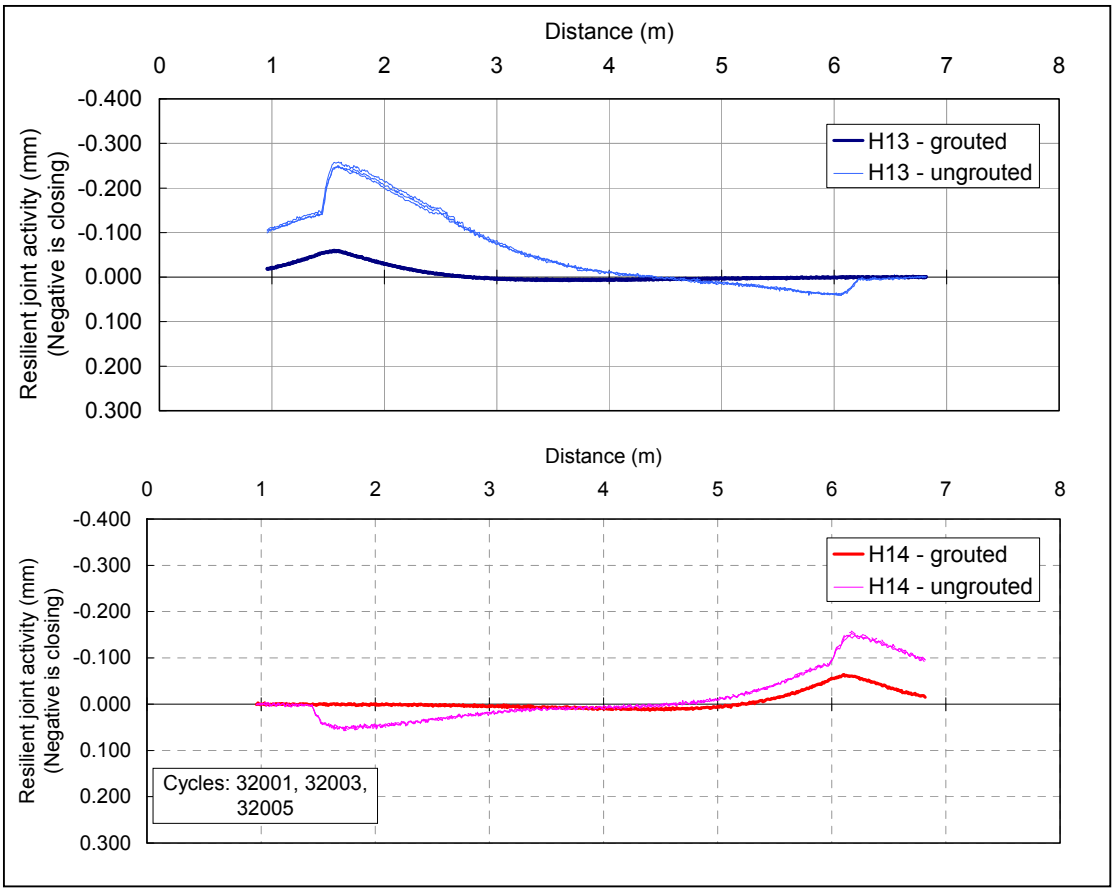

Figure 123. Transverse joint activity change after grouting.

7 CONCLUSIONS

7.1 Subgrade and Base Construction, and Slab Placement

7.1.1 Subgrade Quality

Based on the DCP (Dynamic Cone Penetrometer) analysis, the subgrade is of superior quality in terms of its bearing capacity. CBR (California Bearing Ratio) values for the subgrade derived from DCP analysis are between 45 and 80, which are higher than most subgrades and indicate a granular material. It is concluded that the subgrade has sufficient structural strength to carry the imposed loads. FWD (Falling Weight Deflectometer) analysis revealed a subgrade stiffness value of about 70 MPa.

7.1.2 CTB quality

The backcalculated modulus of the CTB (cement-treated base) presented considerable scatter, but a representative value of 2,200 MPa can be assumed for analysis, which is not very high. Backcalculation from deflections measured directly on the CTB resulted in values between 200 and 600 MPa which was lower than what would be expected from a newly constructed CTB layer, but it was attributed to early age (the layer had been constructed less than 14 days prior to FWD testing and would not yet have reached maximum strength).

7.1.3 Pre-Cast Panel Placement

With regard to the placement of the pre-fabricated slabs, it is concluded that although the process can save total construction time (lane closure time) and seems to offer adequate performance, it is a delicate process and inexperienced contractors should not be allowed to construct pavements of this type. After placement of the 10 slabs was completed it was found that the slabs were not vertically aligned correctly. Grinding the pavement surface solved the problem.

7.2 Effect of Grouting

The pavement responses (deflection and joint opening) were significantly reduced after grouting, and rocking of the slabs disappeared. Load transfer efficiency (LTE) changed from being below 20 percent, and in many cases below 5 percent, to being higher than 90 percent.

7.3 Opening to Traffic in Ungrouted Condition

As described in Chapter 4, two HVS tests were performed on the ungrouted slabs to simulate the exposure of the ungrouted system to traffic from the time of placement to the time of grouting, which normally occurs during the next nighttime closure. Truck traffic on the slow lane on highway I-15 SB (near the project) was used. Approximately 4,200 trucks resulting in

16,000 ESAL were calculated for the 16-hour period of traffic in ungrouted condition. A more demanding traffic total of 86,500 ESALs was applied to each section, using approximately 32 hours of HVS loading with a wheel load of 60kN (13,500 lbs). This exercise indicated that in terms of performance, the Super-Slab® System is able to withstand at least 86,500 ESALS in the ungrouted condition without detrimental effects to the pavement system.

8 REFERENCES

1. Partnered Pavement Research Program (2005). "*HVS Test Plan: Super-Slab® Reconstruction of Rigid Pavement Sections.*" Test plan prepared for the California Department of Transportation (Caltrans) by University of California Pavement Research Center, Dynatest Consulting, and CSIR South Africa.

2. Theyse, H., du Plessis, L., and Kohler, E. (2007). "Interim Assessment of Expected Structural Life of Pre-Cast Concrete Pavement Slabs with HVS Testing." Technical Memorandum prepared for the California Department of Transportation (Caltrans) by the University of California Pavement Research Center (UCPRC-TM-2006-04).

3. First draft submitted by UCPRC to Caltrans on November 1, 2005 under title "Technical Memorandum: HVS Testing of Pre-Cast PCC Panels as an Alternative LLPRS Strategy – Test 597FO" (UCPRC-TM-2007-03).

4. De Beer, M. (1991). "*Use of the Dynamic Cone Penetrometer (DCP) in the design of road structures.*" Proceedings of the 10th Regional Conference in Africa on Soil Mechanics and Foundation Engineering. Maseru, Lesotho.

5. Kleyn, E. G. and Savage, P.F. (1982). "*The application of the pavement DCP to determine the bearing properties and performance of road pavements.*" Proceedings of the International Symposium on Bearing Capacity of Roads and Airfields. Trondheim, Norway, 1982.

6. Harvey, J. T., Ali, A., Hung, D., Uhlmeyer, J., Popescu, L., Bush, D., Grote, K., Lea, J., and Scheffy, C. (2003). "Construction and Test Results from Dowel Bar Retrofit HVS Test Sections 553FD, 554FD and 555FD: US 101, Ukiah, Mendocino County." Report prepared for the California Department of Transportation. Pavement Research Center, Institute of Transportation Studies, University of California (UCPRC-RR-2003-03).

7. Bian, Y., Harvey, J. T., and Ali, A. (2006). "Construction and Test Results on Dowel Bar Retrofit HVS Test Sections 556FD, 557FD, 558FD, and 559FD: State Route 14, Los Angeles County at Palmdale." Report prepared for the California Department of Transportation (Caltrans) by the University of California Pavement Research Center (UCPRC-RR-2006-02).